

PREDICTION OF TURBULENT SWIRLING

REACTING FLOWS

By

MINGCHUN DONG

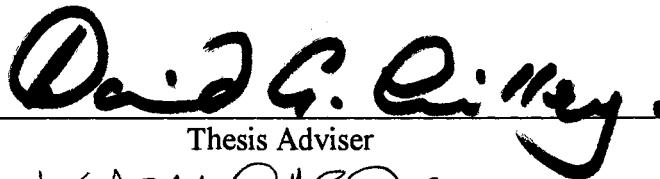
**Bachelor of Science
Harbin Institute of Technology
Harbin, China
1984**

**Master of Science
Oklahoma State University
Stillwater, Oklahoma
1989**

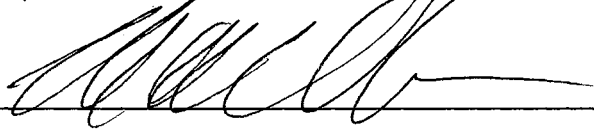
**Submitted to the Faculty of the
Graduate College of the
Oklahoma State University
in partial fulfillment of
the requirements for
the Degree of
DOCTOR OF PHILOSOPHY
July, 1994**

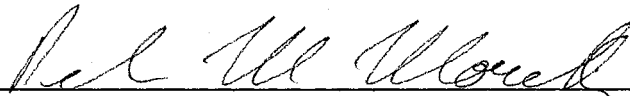
PREDICTION OF TURBULENT SWIRLING
REACTING FLOWS

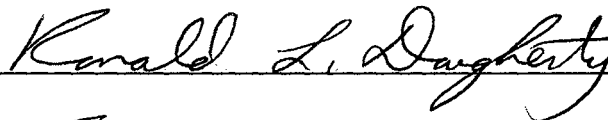
Thesis Approved:


Thesis Adviser











Dean of the Graduate College

ACKNOWLEDGMENTS

I wish to express my sincere appreciation to my major advisor, Dr. David G. Lilley for his intelligent supervision, constructive guidance, inspiration and friendship. My sincere appreciation extends to my other committee members Dr. Frank W. Chambers, Dr. Peter M. Moretti, Dr. Ronald L. Dougherty and Dr. Khaled A. M. Gasem, whose guidance, assistance, encouragement, and friendship are also invaluable.

Moreover, I wish to express my sincere gratitude to my close friends who provided suggestions and assistance for this study: Mr. Tzer-Kun Lin, Mr. Jiaqi Cai, Mr. Tam Lap Mou and Mr. Ye Tian.

I would also like to give my special appreciation to my wife, Mingyan Fan, for her precious suggestions to my research, her strong encouragement at times of difficulty, her love, understanding and countless sacrifices throughout this whole process. Thanks also go to my parents, Fengyun Xu and Guimin Dong, my sister, Mingqiou Dong; and my brothers, Mingdong Dong and Minglin Dong, for their support and encouragement.

Finally, I would like to thank the School of Mechanical and Aerospace Engineering for the financial support during these four and half years of study.

TABLE OF CONTENTS

Chapter	Page
I. INTRODUCTION	1
1.1 Complex Flows.....	1
1.2 Flowfield Predictions of Complex Flows.....	2
1.3 Problem Formulation	3
1.4 Objectives of the Present Study.....	5
1.5 Outline of the Thesis.....	5
II. LITERATURE REVIEW	7
2.1 Experimental Studies for Nonreacting Flows.....	7
2.2 Experimental Studies for Reacting Flows.....	9
2.3 Theoretical Studies for Nonreacting and Reacting Flows.....	11
III. MATHEMATICAL APPROACH.....	14
3.1 Governing Equations	14
3.2 Combustion Simulations	16
3.2.1 One-Step Scheme.....	16
3.2.2 Two-Step Scheme	19
3.2.2.1 Premixed Flames.....	20
3.2.2.2 Diffusion Flames	21
3.2.3 Four-Step Scheme.....	22
3.2.3.1 Premixed Flames.....	26
3.2.3.2 Diffusion Flames	26
3.3 Numerical Formulation	27
3.4 Solution Procedure.....	29
IV. THE "REFINED" COMPUTER CODE.....	32
4.1 Background.....	32
4.2 A Variety of Primary Inlet Velocity Profile Choices	32
4.3 Multi-inlet Capability.....	33
4.4 Inclusion of Two-Step Reaction Scheme.....	34
4.5 Inclusion of Four-Step Reaction Scheme.....	35

Chapter	Page
4.6 Interaction with Flowfield Color Graphic Display.....	36
4.7 Typical Input and Output.....	37
V. APPLICATIONS AND DISCUSSION	39
5.1 Nonreacting Flow Predictions with Various Inlet Velocity Profiles.....	39
5.1.1 Problem Description.....	40
5.1.2 Types of Inlet Velocity Profiles Considered	40
5.1.3 Effects of Inlet Turbulence Quantities on Predicted Results	42
5.1.4 Effects of Inlet Velocity Profiles	42
5.1.5 Effects of Swirl.....	44
5.1.6 Closure.....	45
5.2 Inlet Design Parameter Effects on Nonreacting Flowfields	46
5.2.1 Problem Description.....	46
5.2.2 Secondary to Primary Velocity Ratio Effect.....	47
5.2.3 Primary Swirl Angle Effect	48
5.2.4 Primary Contraction Angle Effect.....	48
5.2.5 Secondary Swirl Angle Effect	49
5.2.6 Secondary Upstream Angle Effect	50
5.2.7 Closure.....	50
5.3 Inlet Design Parameter Effects on Reacting Flowfields.....	51
5.3.1 Problem Description.....	51
5.3.2 Secondary to Primary Velocity Ratio Effect.....	52
5.3.3 Primary Swirl Angle Effect	53
5.3.4 Primary Contraction Angle Effect.....	53
5.3.5 Secondary Swirl Angle Effect	54
5.3.6 Secondary Upstream Angle Effect	54
5.3.7 Closure.....	55
5.4 Reacting Flow Predictions with Three Kinetic Reaction Schemes.....	55
5.4.1 Problem Description.....	56
5.4.2 Results and Discussion	57
5.4.3 Closure.....	59
VI. CLOSURE.....	61
6.1 Conclusions.....	61
6.2 Recommendations for Future Work	62
REFERENCES.....	63
APPENDIXES	70
APPENDIX A - TABLES	71

Chapter	Page
APPENDIX B - FIGURES	79
APPENDIX C - TYPICAL INPUT AND OUTPUT	152

LIST OF TABLES

Table	Page
I. Source Terms and Exchange Coefficients Used in the General Equation of ϕ One-Step Scheme	72
II. Source Terms for Chemical Species - Two-Step Scheme	73
III. Source Terms for Chemical Species - Four-Step Scheme	74
IV. The Form of the Components of the Linearized Source term One-Step Scheme	75
V. Newly Defined FORTRAN Variables	76

LIST OF FIGURES

Figure	Page
1. Schematic of Flow Regions [1].....	80
2. Idealized Axial and Swirl Velocity Profile Cases	81
3. Inflow Parameters To Be Investigated	82
4. Staggered Grid and Notation for the Rectangular Computational Mesh.....	83
5. The Three Control Volumes Associated with the Points of Grids	84
6. Multi-Inlet Grid System.....	85
7. Schematic of The Combustor Domain.....	86
8. Schematic of Nonuniform Rectangular Grid System.....	86
9. Predicted Velocity Profiles for $\theta = 45$ Degrees Using Various Inlet Conditions	87
10. Predicted Streamlines for $\theta = 45$ Degrees Flowfield Using Various Inlet Conditions	89
11. Location of Central Recirculation Zone on x-Axis for Swirl Vane Angle = 45 Degrees.....	90
12. Full-Width of Central Recirculation Zone for Swirl Vane Angle = 45 Degrees.....	90
13. Predicted Velocity Profiles for $\theta = 70$ Degrees Using Various Inlet Conditions	91
14. Predicted Streamlines for $\theta = 70$ Degrees Flowfield Using Various Inlet Conditions	93

Figure	Page
15. Location of Central Recirculation Zone on x-Axis for Swirl Vane Angle = 70 Degrees.....	94
16. Full-Width of Central Recirculation Zone for Swirl Vane Angle = 70 Degrees.....	94
17. Schematic of the Model Combustor Geometry.....	95
18. Effects of Secondary Injection Velocity on Axial Velocity for Nonreacting Flows.....	96
19. Effects of Secondary Injection Velocity on Streamline Patterns for Nonreacting Flows.....	97
20. Effects of Primary Swirl Angle on Axial and Swirl Velocities for Nonreacting Flows.....	98
21. Effects of Primary Swirl Angle on Streamline Patterns for Nonreacting Flows.....	100
22. Effect of Primary Contraction Angle on Axial Velocity for Nonreacting Flows.....	101
23. Effect of Primary Contraction Angle on Streamline Patterns for Nonreacting Flows.....	102
24. Effect of Secondary Swirl Angle on Axial and Swirl Velocities for Nonreacting Flows.....	103
25. Effect of Secondary Swirl Angle on Streamline Patterns for Nonreacting Flows.....	105
26. Effect of Secondary Upstream Angle on Axial Velocity for Nonreacting Flows.....	106
27. Effect of Secondary Upstream Angle on Streamline Patterns for Nonreacting Flows.....	107
28. Effects of Secondary Injection Velocity on Axial Velocity and Temperature for Reacting Flows.....	108
29. Effects of Secondary Injection Velocity on Streamline Patterns for Reacting Flows.....	109

Figure	Page
30. Effects of Primary Swirl Angle on Axial Velocity and Temperature for Reacting Flows.....	110
31. Effects of Primary Swirl Angle on Streamline Patterns for Reacting Flows.....	111
32. Effect of Primary Contraction Angle on Axial Velocity and Temperature for Reacting Flows.....	112
33. Effect of Primary Contraction Angle on Streamline Patterns for Reacting Flows.....	113
34. Effect of Secondary Swirl Angle on Axial Velocity and Temperature for Reacting Flows.....	114
35. Effect of Secondary Swirl Angle on Streamline Patterns for Reacting Flows.....	115
36. Effect of Secondary Upstream Angle on Axial Velocity and Temperature for Reacting Flows.....	116
37. Effect of Secondary Upstream Angle on Streamline Patterns for Reacting Flows.....	117
38. Geometry of Axisymmetric Combustor with Coaxial Fuel and Air Jets [31].....	118
39. Temperature Profiles with Data of Lewis & Smoot [31]	119
40. Unburned Fuel Profiles with Data of Lewis & Smoot [31]	121
41. Oxygen Profiles with Data of Lewis & Smoot [31]	123
42. Water Vapor Profiles with Data of Lewis & Smoot [31].....	125
43. Carbon Dioxide Profiles with Data of Lewis & Smoot [31].....	127
44. Carbon Monoxide Profiles with Data of Lewis & Smoot [31].....	129
45. Hydrogen Profiles with Data of Lewis & Smoot [31].....	131
46. Streamline Patterns with One-Step Scheme.....	133

Figure	Page
47. Streamline Patterns with Two-Step Scheme.....	134
48. Streamline Patterns with Four-Step Scheme.....	135
49. Temperature Contour Map with One-Step Scheme.....	136
50. Temperature Contour Map with Two-Step Scheme.....	137
51. Temperature Contour Map with Four-Step Scheme.....	138
52. Unburned Fuel Mass Fraction Contour Map with One-Step Scheme.....	139
53. Unburned Fuel Mass Fraction Contour Map with Two-Step Scheme.....	140
54. Unburned Fuel Mass Fraction Contour Map with Four-Step Scheme.....	141
55. Oxygen Mass Fraction Contour Map with One-Step Scheme.....	142
56. Oxygen Mass Fraction Contour Map with Two-Step Scheme.....	143
57. Oxygen Mass Fraction Contour Map with Four-Step Scheme.....	144
58. Water Vapor Mass Fraction Contour Map with Two-Step Scheme.....	145
59. Water Vapor Mass Fraction Contour Map with Four-Step Scheme.....	146
60. Carbon Dioxide Mass Fraction Contour Map with Two-Step Scheme.....	147
61. Carbon Dioxide Mass Fraction Contour Map with Four-Step Scheme.....	148
62. Carbon Monoxide Mass Fraction Contour Map with Two-Step Scheme.....	149
63. Carbon Monoxide Mass Fraction Contour Map with Four-Step Scheme.....	150
64. Hydrogen Mass Fraction Contour Map with Four-Step Scheme.....	151

NOMENCLATURE

a	Coupling coefficient
A	Area
C_A	Chemical kinetic reaction constant
C_R	Eddy-Breakup constant
C_μ	Turbulence model constant
C_p	Specific heat of species
E	Eastern neighbor
E/R	Activation energy
f	Mixture fraction of fuel or relaxation factor
f_u	Fuel
h	Stagnation enthalpy
H_{fu}	Heating value of fuel
i	Stoichiometric ratio for one-step scheme
k	Turbulence kinetic energy
m	Species mass fraction
m_{fu}	Fuel mass fraction
N	Northern neighbor
ox	Oxygen
p	Pressure
P	Center point of cell or pre-exponential factor
pr	Product
r	Radial direction

R	Radius of outer wall, or gas constant, or residual
S_ϕ	Mean reaction rate or source term of ϕ variable
S	Southern neighbor or swirl number
S_p, S_u	Components of linearized source term
T	Temperature
u	Axial velocity component
v	Radial velocity component
Vol	Volume of cell
V_T	Total resultant velocity
w	Swirl velocity component
W	Western neighbor or molecular weight
x	Axial direction or carbon composition of hydrocarbon fuel
y	Radial direction or hydrogen composition of hydrocarbon fuel

Greek Letters

ε	Turbulence dissipation rate
Γ	Turbulence exchange coefficient
μ	Effective viscosity
ρ	Time-mean density
ϕ	General dependent variable
σ	Prandtl or Schmidt number

Superscripts

ϕ	General dependent variable
n	Update value of previous iteration
n+1	Update value of current iteration

Subscripts

e, w, n, s	Control volume or cell surface of east, west, north and south
P	Center point of cell
x, r	x- and r-direction
ϕ	General dependent variable

CHAPTER I

INTRODUCTION

Turbulent swirling reacting flows have attracted increasing interest in recent years. The requirements of the increased combustion efficiency and decreased pollutant emission from a variety of devices, from power plants to jet engines, have led to the need for improved methods of prediction and calculation for turbulent swirling flows involving chemical reactions. Such work combines the rapidly developed fields of theoretical combustion aerodynamics and computational fluid dynamics, and their continued improvement and use will significantly reduce the time and cost of combustor development programs.

1.1 Complex Flows

Practical combustion systems often have complex flowfields to enhance flame characteristics due to the introduction of strong swirling inlet flow, laterally induced turbulent jets and contoured boundary geometry. The strong favorable effects of applying swirl are extensively used as an aid to the promotion of rapid mixing. Therefore, combustor flows are highly turbulent, swirling and recirculating, and very complicated. In chemically nonreacting flows, the following different flow regions, see Figure 1, are contained: inviscid core region, recirculation zones, shear region between the inviscid core region and recirculation zones, reattachment region, recovery region, and ordinary boundary layer along the wall [1]. Each of these regions has its particular turbulence characteristics. Any proposed turbulence model has to be general enough to predict all these different regions successfully if it is to be used in combustor flow predictions. In

chemically reacting flows, the flow characteristics in these regions are further complicated by a large number of chemical species participating simultaneously in numerous elementary kinetic steps, and the nonlinear coupling of the fluid mechanics, turbulence, heat transfer and chemical processes involved. The rates of turbulent exchange of various species and the rates of chemical change need to be modeled. Additionally, the presence of liquid sprayed or solid particles, which are subject to intimate interactions within a gaseous flowfield, add another complexity in the prediction and calculation of flow properties [1-5].

This study is concerned with a theoretical prediction technique for gaseous turbulent swirling reacting flowfields in practical combustors.

1.2 Flowfield Predictions of Complex Flows

Computation of complex flows, such as those described above, is very difficult. Mathematical models of turbulence and combustion, and the corresponding solution scheme play an important role in the analysis. Any proposed mathematical model should simulate the flow in all its important aspects (turbulence, combustion, geometry and boundary conditions, etc.), and provide a means whereby the governing equations may be quantitatively solved. Books [3-6] introduce in detail the mathematical models and numerical methods for complex flows.

In numerical predictions, most practical combustion flowfields are described in cylindrical polar coordinates. An axisymmetric flow has been of special interest in the calculation of flow properties because of its geometric simplicity and convenience in mathematical modeling and practical applications to many flow problems. One of the currently available primitive pressure-velocity variable finite difference computer codes, called COSMIC (acronym for Computation Of Swirling Mixing In Combustors) [7], which has been employed as the starting point for the proposed studies, can predict the

distribution of velocities, pressure, species concentrations, turbulence quantities, stagnation enthalpy and temperature for turbulent reacting flows in an axisymmetric domain. This code was developed based on the ideas which had been embodied into the 1974 Imperial College TEACH (acronym for Teaching Elliptic Axisymmetric Characteristics Heuristically) computer program [8]. A further development of the computer code evolved by Lilley and Rhode [9] in the formulation of the STARPIC (acronym for Swirling Turbulent Axisymmetric Recirculating flows in Practical Isothermal Combustor geometries) code, in which chemical reaction was omitted, but several improvements to the original TEACH code were embodied. The well-known SIMPLE (acronym for Semi-Implicit Method for Pressure Linked Equations) solution algorithm [9] was adopted in these codes. Turbulence simulation is by way of the two equation k- ϵ model, and combustion via a simple one-step chemical reaction scheme based on the Arrhenius and Eddy-breakup concepts [10-13].

1.3 Problem Formulation

In practical combustion systems, different types of swirl-generating methods are used, for example, tangential-entry, flat and/or curved blades with/without constant turn angle (that is, twist). These alternate methods produce differing velocity profiles at combustor entrance, which are typified by the cases shown in Figure 2 with profile expressions. However, in combustor flowfield predictions, all the previous studies make gross simplifications with regard to the inlet boundary conditions, especially, the inlet velocity profiles. For example, the inlet radial velocity is often taken to be zero, and the axial and swirl velocity profiles, if not measured, are often assumed to be simple flat profiles, or sometimes a flat axial profile with a solid body rotation swirl profile. These have been shown to be quite unrealistic and lead to considerable errors in flowfield predictions [14,15], because the governing differential equations of swirling recirculating

flows are elliptic, and the numerical solutions depend strongly on the boundary conditions applied around the flow domain. Therefore, the first research need is to investigate the effects of other inlet velocity profiles on flowfield predictions to give a more realistic definition of the inlet boundary conditions.

Additionally, the influential design parameters associated with the inlet flow boundary conditions, which are very important in combustor design program due to their favorable effects on combustor performance, have not been numerically investigated before. These parameters include the secondary to primary inlet velocity ratio (v_0/u_0), primary swirl angle (PSA), primary contraction angle (PCA), secondary swirl angle (SSA), and secondary upstream angle (SUA), see Figure 3 for the schematic.

In combustion simulation, the overall one-step reaction scheme, currently used in the COSMIC code, fails to predict the important characteristics of hydrocarbon oxidation, that is, the formation of intermediates and carbon monoxide, which influence the combustion process considerably. As a result, the one-step combustion model is inadequate for obtaining quantitative predictions. So, another research need is to improve the combustion simulation of the COSMIC code with available higher-order chemical reaction schemes. The two-step scheme proposed by Westbrook and Dryer [16] can provide the prediction of carbon monoxide, which will improve the combustion simulation dramatically, but the formation of intermediate hydrocarbons is ignored. The four-step scheme proposed by Hautmanm et al. [17] describes the transformation mechanism of the hydrocarbon fuel into intermediate hydrocarbons and hydrogen, and the oxidation of intermediates to carbon monoxide, carbon dioxide, and water vapor. These two higher-order reaction schemes should be included in the code to be developed in this study for improved combustion simulation.

1.4 Objectives of the Present Study

The existing problems lead to the need for a general and powerful computer code for turbulent swirling reacting flow predictions. The objectives of the study are identified as:

- (a) To investigate the effects of a variety of inlet velocity profiles on combustor flowfield predictions to give a more realistic definition of the inlet flow boundary conditions
- (b) To develop a solution procedure to study the effects of important and influential design parameters on combustor flowfields with secondary circumferential slot injection
- (c) To develop mathematical models and solution procedures for the two-step and four-step reaction schemes for improved combustion simulation, and provide a means whereby the dominant species, such as the unburned hydrocarbon fuel, intermediate hydrocarbons, carbon monoxide, carbon dioxide, water vapor and hydrogen etc., may be predicted.
- (d) To incorporate (a), (b) and (c) with the updated chemical reaction simulations into a new computer code, named REFINED (acronym for Reacting Elliptic Flows IN Expansion Domains).
- (e) To apply the resulting computer program, REFINED, to practical flow problems. The simulations and accuracy of the code will be assessed via comparison with available experimental data.

1.5 Outline of the Thesis

Chapter I of this six-chapter thesis is the introduction. First, complex flows and their predictions are briefly addressed. Second, the present research problems are formulated. Finally, the objectives of this study are identified in detail.

Both experimental and theoretical studies of other researcher's on turbulent nonreacting and reacting flows are reviewed in Chapter II. The experimental study findings, mathematical modeling efforts and computational methods of turbulent swirling nonreacting and reacting flows are highly summarized.

Chapter III provides the governing equations, combustion simulation, numerical techniques and solution procedure adopted in the resulting computer code.

Computer code developments are described in Chapter IV. First, the background of the original COSMIC code is introduced, and then new developments follow. Finally, typical code input and output are described.

Application and validation of the developed code are addressed in Chapter V. Four applications are presented here. Assessments are conducted by comparing the predicted results with available experimental data for the chosen test cases

Chapter VI is the closure of this study. The conclusions of the present investigation are summarized and the recommendations for future work are briefly stated..

CHAPTER II

LITERATURE REVIEW

The flowfield characteristics of turbulent reacting flows has been an important subject of various experimental and numerical investigations. A brief review of previous studies is given below.

2.1 Experimental Studies for Nonreacting Flows

The velocity characteristics of turbulent confined coaxial jets with and without swirl were studied by Habib and Whitelaw [18,19]. The degree of swirl is characterized by the swirl number S , which is a dimensionless number representing axial flux of swirl momentum divided by axial flux of axial momentum, times the corresponding equivalent nozzle radius. That is:

$$S = \frac{G_{\theta}}{G_x d / 2} \quad (2.1)$$

where G_{θ} is the axial flux of swirl momentum, G_x is the axial flux of axial momentum, and $d/2$ is the nozzle radius, see Gupta et al. [3] for details. Habib and Whitelaw measured the time-mean axial velocity and the RMS (root mean square) axial velocity fluctuations. Their results indicated that central toroidal recirculation zones (CTRZ), see Figure 1 for example, grow with swirl number increasing, and large annular to center jet velocity ratios result in larger central recirculation zones, larger velocity gradients and larger turbulence intensities in the mixing region.

Extensive measurements were made by Vu and Gouldin [20] in a model swirl combustor with two coaxial concentric nozzles (inlets) under coswirl and counterswirl

conditions (both jets are swirling). The secondary annular diameter (outer nozzle) is identical to that of the downstream region, and therefore no expansion chamber exists for this experiment. The measured parameters are the time-mean velocities, turbulence intensities, and turbulence stresses. They reported that secondary jet swirl has a strong influence on the formation of the recirculation zone. High levels of turbulent fluctuations and dissipation rates characterized the central flow region for both coswirl and counterswirl conditions. More turbulence was generated in the interjet shear layer near the nozzles under counterswirl than for coswirl.

Owen [21] made the measurements in the initial mixing length region of free and confined coaxial air jets with recirculation zone to study the time averaged characteristics of the two flowfields. The measurements indicated that there are large differences in the time averaged structure of the two flowfields, the size and recirculating mass flux being significantly larger in the confined flow than in the free expansion. However, the mean radial velocities measured in both initial regions are the same order of magnitude as the mean axial velocities.

The downstream mixing of two coaxial concentric water jets discharging into an expanded duct was studied by Roback and Johnson [22,23]. They employed a visualization technique to qualitatively study the time-dependent flow characteristics and the scale of turbulence. They noted that intensive mixing regions exist at the interface between the near stream and the centerline recirculation, and at the interface between the central and annular jet streams. Mixing for swirling flow was found to complete in one-third of the distance required for nonswirling flow.

Yoon and Lilley [24] employed a five-hole pitot probe to measure time-mean velocity profiles of turbulent swirling jets in suddenly and gradually expanding chambers. The primary concern of this study was to characterize flows of this type in terms of the effects of side wall angle, swirl strength, inlet turbulence intensity, and expansion ratio on the resulting flowfield. They noted that the presence of swirl shortens corner recirculation

zones and generate a CTRZ followed by a precessing vortex core. An increase in swirl seems to, at least initially, expand the CTRZ in width and length, and a further increase causes the length to decrease with significant increase in width. They indicated that a chamber contraction at a downstream location produces a favorable pressure gradient which is superimposed on the adverse pressure gradient promoted by swirl. In certain cases where the contraction is strong enough to influence the upstream field, the size of the recirculation zone is diminished.

2.2 Experimental Studies for Reacting Flows

The flowfield of reactive recirculating jet mixing was investigated by Smith et al. [25] in a dump combustor. They extensively measured the downstream radial distribution of mean axial and radial velocities, turbulent intensity, gas composition, total pressure and static temperature. Their data indicated that turbulent mixing is slower in the chemically reacting flowfield than in the nonreactive one, and the decay of velocity and concentration is less rapid for the reacting case. The large temporal temperature fluctuations implied that any prediction technique must account for the huge fluctuations in temperature and concentration.

The velocity field characteristics of a swirling flow combustor were studied by Gouldin et al. [26] for both reacting and nonreacting cases. The combustor consists of two confined concentric swirling jets. The central jet flow is premixed methane and air, and the annular jet flow is swirling air. They indicated that turbulent transport is not the mechanism for swirl induced recirculation in the flow, and the failure to accurately predict flow recirculation is most likely not the result of a pure turbulence model. In addition, large anisotropic velocity fluctuations were observed in high shear regions.

Three velocity components and the corresponding correlations were measured by Baker et al. [27] for both swirling and nonswirling flows in a model furnace with and

without combustion. They employed a swirl number of 0.52 to study the effect of swirl in a sudden expansion chamber. The comparison revealed larger forward velocities in the combusting flow and correspondingly larger regions of central recirculation zone. The swirl reduced the length of the flow and tended to increase the anisotropic region of the flow.

Measurements of mean and turbulence properties were reported by Owen [28] in the initial mixing region of a confined turbulent diffusion flame burner. The measurements showed that there are large differences in time averaged flowfields with and without inlet swirl, and substantial large-scale contributions to the total RMS turbulent velocity field. These large-scale fluctuations result in significant deviations from isotropy over most initial mixing region. Such large-scale motions indicate that turbulence models based on local equilibrium principles, such as mixing lengths and others which utilized local mean gradient, will not adequately represent the physics of the combusting flows.

The mean and RMS values of axial and swirl velocity components were measured by Bicen and Jones [29] in a non-axisymmetric can-type gas turbine combustor with dilution holes under isothermal and combusting flow conditions. They concluded that the influence of combustion on the velocity field was generally to increase the strength and decrease the width of primary recirculation zone, to accelerate the flow in the axial direction and to increase velocity fluctuations. The effect of air-fuel ratio was small on the primary zone flow, but was more pronounced at downstream regions where the increased temperature and thus reduced densities associated with the lower air-fuel ratio values resulted in higher velocity at exit.

The other significant experimental studies are those of Spadaccini et al. [30], Lewis and Smoot [31], Hasson et al. [32], Larue et al. [33], Ramos and Somer [34], So et al. [35] and Weber et al. [36] on the measurements of mean velocities, gas temperature and species concentrations under different combustor geometries.

2.3 Theoretical Studies for Nonreacting and Reacting Flows

Numerous publications exist to introduce the theoretical approaches to the solution of turbulent swirling flows under reacting or nonreacting conditions. Some significant books, technical reports and research papers about turbulent flows, swirling flows, combustion models and general computational methods are briefly reviewed here.

The nature and theories of turbulence are described mathematically in detail by Hinze [37]. Turbulence analysis for the engineering purpose is well illustrated in Schetz's book [38]. Several important turbulence models have been introduced and assessed by Launder and Spalding [39] based on the engineering calculation of turbulent flows. A comprehensive introduction to the phenomenon of swirl, its occurrence in practical equipment and atmosphere, both with and without combustion, is described by Gupta et al. [3]. The mathematical modeling and solution techniques for the complex turbulent reacting flows, with emphasis placed on the applications of swirling flow combustion, are well addressed by Gupta & Lilley [4]. The prediction methods used in the furnace and combustor modeling approaches are described and assessed in Khalil's book [5]. General computational methods for complex flows are extensively discussed in Patankar's book [6].

The present status and related combustion research needs in the area of modeling and nonintrusive physical diagnostics as applied to combustion systems are reported by Jones and Whitelaw [40], Libby and Williams [41], Spalding [42] and Gupta and Lilley [43]. Different turbulence models are studied and assessed in reports [1,2], books [3-5] and papers [44-50] under various flow conditions, such as swirling, chemically inert or reacting. For nonswirling or moderate swirling flows, the two equation k - ϵ turbulence model is considered to be the simplest and superior to other models having a similar degree of complexity. Studies of turbulent combustion such as diffusion flames, premixed flames, fast chemistry models, finite rate chemistry models, and the nonlinear interaction

between turbulence and combustion in practical combustion systems are well addressed in reports [1,2], books [3-5] and references [51-59]. It is indicated that the turbulent combustion is so complicated that only the PDF (probability density function) model offers the possibility of handling large numbers of reacting species, but in view of computer storage requirements, run times and multidimensionality of the approach, its suitability requires further investigation. To avoid this problem, the gas turbine combustion modeling effort has frequently been simplified by using a global approach that reduces the complex chemistry to the specification of an overall global oxidation scheme (one-step, two-step or four-step mechanism). This can predict quantities of special interest, such as fuel consumption, heat release rates and dominant species concentrations, etc.

Studies of discretization schemes to improve the accuracy of numerical simulations are reported in references [60-69]. In the formulation of the governing equations into the finite difference forms, the spatial differencing of the convective terms often result in numerical diffusions in the solution. The use of a higher order differencing scheme, such as the central-differencing scheme, can eliminate or significantly reduce this diffusion, but produces numerical oscillations that have no physical significance in the solution. The use of an upwind differencing technique eliminates the oscillations but introduces a diffusion-like term into the finite difference equation. The hybrid finite differencing scheme (the combination of the upwind and central differencing schemes), which is currently used in TEACH-type computer code, although yielding physically realistic solutions in all circumstances, introduces excess numerical diffusion for many flows [60]. Therefore, several improved higher order finite differencing schemes [61-69], such as the Third-Order-Accurate Upwind Scheme, Quadratic Upstream Interpolation Scheme, Skew-Upstream Differencing Scheme, Linear Spline Approximation Scheme and Cubic Spline Approximation Scheme etc., were developed to reduce the numerical diffusion. Among those improved schemes, the Bounded Skew Upwind Differencing Scheme (BSUDS) has

been recommended for TEACH-type code to reduce the numerical diffusion in terms of accuracy and stability [67].

CHAPTER III

MATHEMATICAL APPROACH

3.1 Governing Equations

In the modeling and prediction of combustor flowfields, the problem is simulated by a set of simultaneous nonlinear partial differential equations. The turbulent Reynolds equations for conservation of mass, momentum, stagnation enthalpy, chemical species mass fractions, turbulent kinetic energy and turbulence dissipation rate govern the turbulent swirling reacting flows. These transport equations are all similar and contain terms for the convection, diffusion (via effective flux term) and source S_ϕ of a general variable ϕ (which contains terms describing the generation (creation) and consumption (dissipation) of ϕ). Introduction of turbulent exchange coefficients Γ_ϕ and the usual turbulent diffusion-flux laws provides a similarity in the form among all the governing partial differential equations. This similarity allows them to be put in a common form and solve in a similar manner. In fact, for two-dimensional axisymmetric flows, they all conform to (in cylindrical polar coordinates):

$$\frac{1}{r} \left[\frac{\partial}{\partial x} (\rho u r \phi) + \frac{\partial}{\partial r} (\rho v r \phi) - \frac{\partial}{\partial x} \left(r \Gamma_\phi \frac{\partial \phi}{\partial x} \right) - \frac{\partial}{\partial r} \left(r \Gamma_\phi \frac{\partial \phi}{\partial r} \right) \right] = S_\phi \quad (3.1)$$

and the equations differ not only in their effective exchange coefficients Γ_ϕ but also in their final source terms S_ϕ as inspection of the summary Table I reveals, with the simple three component one-step combustion model being used, for example. If they are to be solved, then the turbulent effective exchange coefficients Γ_ϕ , and other thermodynamic unknowns

such as density ρ , stagnation enthalpy h , and fuel consumption rate S_{fu} , must be specified prior to solution to close the problem.

To define the effective exchange coefficients Γ_ϕ , the turbulent or eddy viscosity concept, given in Reynolds transport equations, may be suitably generalized to the multicomponent system equations. The flux-gradient transport laws of Newton, Fourier and Fick for momentum, heat and mass transfer provided most useful unifying assumptions. In the multicomponent flow case, the analogy in the form to the single component flow leads to the effective exchange coefficients μ (effective viscosity) and Γ_ϕ being defined. These effective exchange coefficients are composed of laminar and turbulent parts:

$$\mu = \mu_{lam} + \mu_{turb} \quad (3.2)$$

$$\Gamma_\phi = \Gamma_{\phi lam} + \Gamma_{\phi turb} \quad (3.3)$$

where the turbulent viscosity, μ_{turb} , is calculated from the standard two-equation k - ϵ turbulence model (which is widely used for turbulence prediction because it is moderate in complexity and is considered to be superior to other models having a similar degree of complexity) as:

$$\mu_{turb} = C_\mu \rho k^2 / \epsilon \quad (3.4)$$

If isotropy is assumed, constant Prandtl, Schmidt and $r\theta$ (and other) viscosity numbers relate other effective exchange coefficients to the primary component of effective viscosity $\mu = \mu_{TX}$; these are defined by:

$$\sigma_\phi = \mu / \Gamma_\phi \quad (3.5)$$

$$\sigma_{r\theta} = \mu_{TX} / \mu_{r\theta} \quad (3.6)$$

where often the former are taken near 0.7 and the latter as unity (isotropic) [4]. For the two turbulence quantities k and ϵ , Schmidt numbers for the corresponding equations are taken as: $\sigma_k = 1.0$, $\sigma_\epsilon = 1.21$. The final turbulence constants are taken as: $C_\mu = 0.9$, $C_1 = 1.44$, $C_2 = 1.92$. Other thermodynamic unknowns are discussed and specified in the next section.

3.2 Combustion Simulation

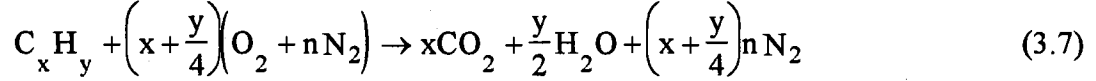
The conservation equations of stagnation enthalpy and chemical species mass fractions are not completely closed since the density and mass rates of creation or consumption of the species are unknowns. These variables must also be specified prior to the solution of the equations. Introducing the chemical reaction model and thermodynamic considerations provide the necessary extra information to close the system.

Usually, a successful modeling of combustion systems depends on an adequate description of the combustion reaction mechanism. For hydrocarbon oxidation, a large number of species participating simultaneously in numerous elementary kinetic steps is required to specify the mechanism. The corresponding governing differential equations are 'stiff' and require special time-consuming integration methods. For a complex three dimensional problem, the computing costs would be prohibitive. Besides the large number of species equations to be solved, the elementary steps and their rate constants are not well known except for the simplest of hydrocarbons (for example, methane). To avoid this problem, the gas turbine combustion modeling effort has frequently been simplified by using a global approach that reduces the complex chemistry to the specification of an overall global oxidation scheme. This can predict quantities of interest, such as fuel consumption, heat release rates and dominant species concentrations, etc.

3.2.1 One-Step Scheme

The simplest global mechanism is the one-step reaction scheme. The advantage of this mechanism is its simplicity; it involves the solution of the conservation equations for stagnation enthalpy, unburned fuel and the mixture fraction (diffusion and premixed flames can be treated in the same way for the one-step scheme). The heat release and the concentrations of other species are then obtained from linear functions of the amount of

fuel consumed. But this model fails to predict the important characteristics of hydrocarbon oxidation, that is, the formation of intermediates and carbon monoxide, which influence the process considerably. As a result, it is inadequate to obtain quantitative predictions. The scheme is described as the following:



where $C_x H_y$ is a typical hydrocarbon fuel, O_2 is oxygen, N_2 is nitrogen, CO_2 is carbon dioxide, and H_2O is water vapor. This scheme assumes that the fuel and oxidant react chemically in a unique proportion, combining with a stoichiometric oxidant/fuel ratio of i to form product plus release of energy (finite rate chemistry is assumed). Furthermore, the effective diffusion (exchange) coefficients Γ_ϕ of all the chemical species are taken to be equal especially when the flow is turbulent, and the reaction is a single step with no intermediate compounds. The thermodynamic considerations give:

$$1 \text{ kg fu} + i \text{ kg ox} \rightarrow (1 + i) \text{ kg pr} + H_{fu} \quad (3.8)$$

$$h = c_p T + H_{fu} m_{fu} + V_T^2/2 \quad (3.9)$$

$$m_{fu} + m_{ox} + m_{pr} = 1 \quad (3.10)$$

$$f = m_{ox} - i m_{fu} \quad (3.11)$$

The model is characterized by differential equations for stagnation h , unburned fuel mass fraction m_{fu} and combined mixture quantity f . The equation for f can be deduced by eliminating the source term from the fuel and oxidant equations. It is convenient to solve the partial differential equations for m_{fu} and f (rather than m_{fu} and m_{ox}), from which m_{ox} can be deduced [4].

The interaction between the turbulence and chemical kinetics is described here simply by the time-averaged Arrhenius model and Eddy-Breakup reaction model [4,60]:

$$S_{fu} = -P p^2 m_{fu} m_{ox} \exp(-E/RT) \quad (3.12)$$

$$S_{fu} = -C_A \rho m_{fu} \frac{\varepsilon}{k} \quad (3.13)$$

$$S_{fu} = - C_A \rho \frac{m_{ox}}{i} \frac{\varepsilon}{k} \quad (3.14)$$

where P , E/R and C_A are constants for turbulent flames of high temperature and high Reynolds numbers. In general and in SI units, $P = 0.5$, $E/R = 20000$ and $C_A = 4.0$. In lean diffusion flames, the rate of reaction is determined by the rate of eddy dissipation. Consequently, there will be a relationship between turbulent fluctuations in the flow and the mean concentration of active species. Accordingly, the volumetric reaction rate of fuel can be expressed by Equation (3.13). In regions of the flame where the time-mean mixture is fuel rich, the oxidant will be the reacting species that shows the greatest intermittency. Hence, in this case it is the dissipation of the oxidant-bearing eddies that limits the reaction rate. So, Equation (3.14) is developed to be used together with Equation (3.13). In general, even diffusion flames will contain some level of premixing, so Equations (3.12) through (3.14) will apply simultaneously. Thus, the reaction will proceed at a rate determined by the lowest of the three rates. S_{fu} works as the source term in the fuel mass fraction equation.

All other properties, which will be used in the calculation at any point in the flowfield, may be deduced from the thermodynamic considerations as:

$$m_{ox} = f + i m_{fu} \quad (3.15)$$

$$m_{pr} = 1 - m_{ox} - m_{fu} \quad (3.16)$$

$$T = (h - \sum_j H_j m_j - V_T^2/2) / c_p \quad (3.17)$$

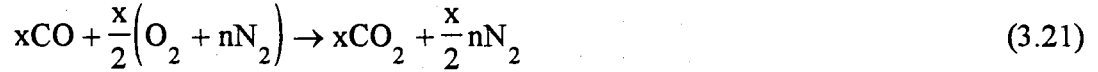
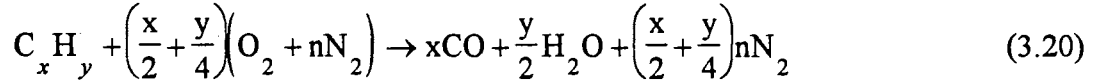
$$\rho = P W / (R T) \quad (3.18)$$

$$1 / W = \sum_j (m_j / W_j) \quad (3.19)$$

where the W 's are the molecular weights of the chemical species. When both the heat of combustion, H_j , and the consumption rate of fuel, S_{fu} , are assigned zero values, a turbulent mixing solution can be obtained.

3.2.2 Two-Step Scheme

A slightly more complex scheme is the two-step mechanism [16]:



Here C_xH_y is a typical hydrocarbon fuel, and the additional species (which did not occur in the one-step scheme) is carbon monoxide CO. This scheme involves the solution of one additional equation for the concentration of carbon monoxide. However, premixed flames and diffusion flames are treated differently as described in the following paragraphs.

Although the two-step scheme has been widely used, it is deficient in that the formation of intermediates is ignored. The derivation of the pertinent equations is given below. For the first reaction, let:

$$r_1 = (\text{mass of } O_2)/(\text{mass of fuel}) \quad (3.22)$$

$$r_2 = (\text{mass of CO})/(\text{mass of fuel}) \quad (3.23)$$

$$r_3 = (\text{mass of } H_2O)/(\text{mass of fuel}) \quad (3.24)$$

For the second reaction, let:

$$r_4 = (\text{mass of } O_2)/(\text{mass of CO}) \quad (3.25)$$

$$r_5 = (\text{mass of } CO_2)/(\text{mass of CO}) \quad (3.26)$$

The values of these ratios can be calculated in a straight-forward manner:

$$r_1 = (x/2 + y/4) W_{O_2}/W_{fu} \quad (3.27)$$

$$r_2 = x W_{CO}/W_{fu} \quad (3.28)$$

$$r_3 = (y/2) W_{H_2O}/W_{fu} \quad (3.29)$$

$$r_4 = (1/2) W_{O_2}/W_{CO} \quad (3.30)$$

$$r_5 = W_{CO_2}/W_{CO} \quad (3.31)$$

Here the W's are the molecular weights of the chemical species.

The mass fractions of all chemical species obey the general differential equation (3.1) with source term S_ϕ as defined in Table II. Further, the effective diffusion coefficient Γ_ϕ can be taken to be the same for all species, especially when the flow is turbulent. The value of Γ_ϕ is then μ_t/σ_t , where σ_t is the turbulent Prandtl or Schmidt number. The source terms for various species are related via the ratios defined in Equations (3.27) through (3.31). In Table II, S_{fu} denotes the mean reaction rate for fuel due to the first reaction, while S_{CO} stands for the rate of consumption of carbon monoxide in the second reaction. They are modeled based on the Arrhenius and Eddy-Breakup concepts as followings [1,2]. For the first reaction, we have:

$$S_{fu} = - (\text{The smallest of } S_1, S_2 \text{ and } S_3) \quad (3.32)$$

$$S_1 = F_1 \rho^{1.5} m_{fu}^{0.5} m_{ox} \exp(-E_1/RT) \quad (3.33)$$

$$S_2 = C_{R,1} \rho m_{fu} \frac{\varepsilon}{k} \quad (3.34)$$

$$S_3 = C_{R,1} \rho \frac{m_{ox}}{r_1} \frac{\varepsilon}{k} \quad (3.35)$$

For the second reaction:

$$S_{CO} = - (\text{The smallest of } S_4, S_5 \text{ and } S_6) \quad (3.36)$$

$$S_4 = F_2 \rho^2 m_{CO} m_{ox} \exp(-E_2/RT) \quad (3.37)$$

$$S_5 = C_{R,2} \rho m_{CO} \frac{\varepsilon}{k} \quad (3.38)$$

$$S_6 = C_{R,2} \rho \frac{m_{ox}}{r_4} \frac{\varepsilon}{k} \quad (3.39)$$

The constants in the above expressions are given the following values in S.I. units [2]:

$$F_1 = 3.3 \times 10^{14}, \quad E_1/R = 27000, \quad C_{R,1} = 3$$

$$F_2 = 6.0 \times 10^8, \quad E_2/R = 12500, \quad C_{R,2} = 4$$

3.2.2.1 Premixed Flames

For turbulent premixed flames, the mass fractions m_{fu} and m_{CO} are used as the dependent variables of the differential equations for chemical species. The consumption

rates for m_{fu} and m_{CO} are calculated from Equations (3.32) and (3.36). The values of m_{OX} , m_{CO_2} , m_{H_2O} and m_{N_2} are then obtained from the following algebraic relations:

$$m_{OX} = m_{OX,p} - r_1 (m_{fu,p} - m_{fu}) - r_4 (r_2(m_{fu,p} - m_{fu}) - m_{CO}) \quad (3.40)$$

$$m_{H_2O} = r_3 (m_{fu,p} - m_{fu}) \quad (3.41)$$

$$m_{CO_2} = r_5 (r_2(m_{fu,p} - m_{fu}) - m_{CO}) \quad (3.42)$$

$$m_{N_2} = 1 - (m_{fu} + m_{CO} + m_{OX} + m_{H_2O} + m_{CO_2}) \quad (3.43)$$

Here $m_{fu,p}$ and $m_{OX,p}$ are the mass fractions of fuel and oxidant respectively at the primary inlet, and m_{N_2} is calculated from the fact that all mass fractions should add up to unity.

3.2.2.2 Diffusion Flames

For diffusion flames, one more differential equation needs to be solved due to fuel and oxidant mixing compared with premixed flames. First of all, the mass fractions of the species are added in certain proportions to yield zero source terms. This is shown in the last three entries of Table II as ϕ_A , ϕ_B and ϕ_C . For these three entries, because their source term is zero, a single solution for them would suffice provided their boundary conditions are the same. This condition can be ensured by normalizing the ϕ 's with reference to their values in the air and fuel streams. Thus a single variable f with a zero source term and with values 0 and 1 in the air and fuel streams respectively can be regarded as providing the solutions for ϕ_A , ϕ_B and ϕ_C via the following relationships:

$$f = \frac{\phi_A - \phi_{A,air}}{\phi_{A,fuel} - \phi_{A,air}} = \frac{\phi_B - \phi_{B,air}}{\phi_{B,fuel} - \phi_{B,air}} = \frac{\phi_C - \phi_{C,air}}{\phi_{C,fuel} - \phi_{C,air}} \quad (3.44)$$

Further, let:

$$(m_{fu})_{fuel} = 1 \quad (3.45)$$

$$(m_{OX})_{air} = R \quad (3.46)$$

$$(m_{N_2})_{air} = 1 - R \quad (3.47)$$

where R is the oxygen mass fraction in the air stream. Combining Equations (3.44) through (3.47) and the definitions of ϕ_A , ϕ_B and ϕ_C , we have:

$$m_{\text{OX}} = R (1 - f) + r_4 m_{\text{CO}} + (r_1 + r_2 r_4) (m_{\text{fu}} - f) \quad (3.48)$$

$$m_{\text{CO}_2} = r_2 r_5 (f - m_{\text{fu}}) - r_5 m_{\text{CO}} \quad (3.49)$$

$$m_{\text{H}_2\text{O}} = r_3 (f - m_{\text{fu}}) \quad (3.50)$$

$$m_{\text{N}_2} = 1 - (m_{\text{fu}} + m_{\text{CO}} + m_{\text{OX}} + m_{\text{H}_2\text{O}} + m_{\text{CO}_2}) \quad (3.51)$$

Incidentally, f can be considered as the mass fraction of "total fuel" that would prevail if the fuel did not react at all.

To summarize, the mass fractions m_{fu} , m_{CO} and f are used as the dependent variables of the differential equations for chemical species. The reaction rates for m_{fu} and m_{CO} are calculated from Equations (3.32) and (3.36), while the source for f is zero. The values of m_{OX} , m_{CO_2} , $m_{\text{H}_2\text{O}}$ and m_{N_2} are then obtained from Equations (3.48) through (3.51).

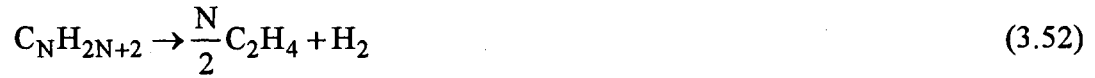
3.2.3 Four-Step Scheme

The complete oxidation of the hydrocarbon fuel can be described by the following steps:

- (a) Transformation of the hydrocarbon fuel into intermediate hydrocarbons and hydrogen with little release of energy
- (b) Oxidation of intermediates to carbon monoxide and hydrogen
- (c) Oxidation of carbon monoxide to carbon dioxide
- (d) Oxidation of hydrogen to water vapor

Steps (b) through (d) are exothermic and are responsible for the release of energy and associated temperature rise. A reaction scheme, which is designed to model correctly the oxidation process, must include a description of these steps. The newly introduced species are intermediate hydrocarbons and hydrogen H_2 , in addition to those of the one-step and two-step schemes.

The simplest mechanism that accounts for the essential features of the hydrocarbon oxidation is the following four-step scheme proposed by Hautman, et al. [17]:



which is valid only for aliphatic hydrocarbons (of the type $C_N H_{2N+2}$). To accommodate a general hydrocarbon $C_x H_y$, the first two steps have been modified by Srinivasan et al. [2] as followings:



This scheme involves the solution of two more transport equations for the mass fractions of intermediate hydrocarbons ($C_x H_{y-2}$) and hydrogen, comparing with transport operations for unburned hydrocarbon fuel, carbon monoxide, and "total fuel" as outlined in the two-step scheme.

The derivation of the pertinent equations is given below similar to the two-step scheme. For the first reaction, let:

$$r_1 = (\text{mass of } C_x H_{y-2}) / (\text{mass of fuel}) \quad (3.58)$$

$$r_2 = (\text{mass of } H_2) / (\text{mass of fuel}) \quad (3.59)$$

For the second reaction, let:

$$r_3 = (\text{mass of } O_2) / (\text{mass of } C_x H_{y-2}) \quad (3.60)$$

$$r_4 = (\text{mass of } CO) / (\text{mass of } C_x H_{y-2}) \quad (3.61)$$

$$r_5 = (\text{mass of } H_2) / (\text{mass of } C_x H_{y-2}) \quad (3.62)$$

For the third reaction, let:

$$r_6 = (\text{mass of } O_2) / (\text{mass of } CO) \quad (3.63)$$

$$r_7 = (\text{mass of CO}_2)/(\text{mass of CO}) \quad (3.64)$$

For the fourth reaction, let:

$$r_8 = (\text{mass of O}_2)/(\text{mass of H}_2) \quad (3.65)$$

$$r_9 = (\text{mass of H}_2\text{O})/(\text{mass of H}_2) \quad (3.66)$$

The values of these ratios can be calculated in a straight-forward manner:

$$r_1 = W_{C_xH_{y-2}}/W_{fu} \quad (3.67)$$

$$r_2 = W_{H_2}/W_{fu} \quad (3.68)$$

$$r_3 = \frac{x}{2} W_{O_2}/W_{C_xH_{y-2}} \quad (3.69)$$

$$r_4 = x W_{CO}/W_{C_xH_{y-2}} \quad (3.70)$$

$$r_5 = \frac{y-2}{2} W_{H_2}/W_{C_xH_{y-2}} \quad (3.71)$$

$$r_6 = (1/2) W_{O_2}/W_{CO} \quad (3.72)$$

$$r_7 = W_{CO_2}/W_{CO} \quad (3.73)$$

$$r_8 = (1/2) W_{O_2}/W_{H_2} \quad (3.74)$$

$$r_9 = W_{H_2O}/W_{H_2} \quad (3.75)$$

Here the W's are the molecular weights of the chemical species.

The source term S_ϕ of different species is defined in Table III, where S_{fu} denotes the reaction rate for fuel in the first reaction, $S_{C_xH_{y-2}}$ the rate of consumption for intermediate hydrocarbons in the second reaction, S_{CO} the rate of consumption of carbon monoxide in the third reaction, and S_{H_2} the rate of consumption of hydrogen in the fourth reaction.

They are modeled based on the Arrhenius and Eddy-Breakup concepts as followings

[2,17]. For the first reaction, we have:

$$S_{fu} = - (\text{The smaller of } S_1, S_2 \text{ and } S_3) \quad (3.76)$$

$$S_1 = F_1 \rho^2 m_{fu}^{0.5} m_{OX}^{1.07} m_{C_xH_{y-2}}^{0.43} \exp(-E_1 / RT) \quad (3.77)$$

$$S_2 = C_{R,1} \rho m_{fu} \frac{\epsilon}{k} \quad (3.78)$$

$$S_3 = C_{R,1} \rho \frac{m_{OX}}{r_x} \frac{\epsilon}{k} \quad (3.79)$$

(where r_x is the stoichiometric ratio of mass fraction of O_2/C_xH_y)

For the second reaction:

$$S_{C_xH_{y-2}} = - \text{(The smallest of } S_4, S_5 \text{ and } S_6) \quad (3.80)$$

$$S_4 = F_2 \rho^{1.71} m_{C_xH_{y-2}}^{0.9} m_{OX}^{1.18} m_{fu}^{-0.37} \exp(-E_2 / RT) \quad (3.81)$$

$$S_5 = C_{R,2} \rho m_{C_xH_{y-2}} \frac{\varepsilon}{k} \quad (3.82)$$

$$S_6 = C_{R,2} \rho \frac{m_{OX}}{r_3} \frac{\varepsilon}{k} \quad (3.83)$$

For the third reaction:

$$S_{CO} = - \text{(The smallest of } S_7, S_8 \text{ and } S_9) \quad (3.84)$$

$$S_7 = F_3 \rho^{1.75} m_{CO} m_{OX}^{0.25} m_{H_2O}^{0.5} \exp(-E_3 / RT) \quad (3.85)$$

$$S_8 = C_{R,3} \rho m_{CO} \frac{\varepsilon}{k} \quad (3.86)$$

$$S_9 = C_{R,3} \rho \frac{m_{OX}}{r_6} \frac{\varepsilon}{k} \quad (3.87)$$

Finally, for the fourth reaction, we have:

$$S_{H_2} = - \text{(The smallest of } S_{10}, S_{11} \text{ and } S_{12}) \quad (3.88)$$

$$S_{10} = F_4 \rho^{1.71} m_{H_2}^{0.85} m_{OX}^{1.42} m_{C_xH_{y-2}}^{-0.57} \exp(-E_4 / RT) \quad (3.89)$$

$$S_{11} = C_{R,4} \rho m_{H_2} \frac{\varepsilon}{k} \quad (3.90)$$

$$S_{12} = C_{R,4} \rho \frac{m_{OX}}{r_8} \frac{\varepsilon}{k} \quad (3.91)$$

The constants in the above expressions are given the following values all in S.I. units [2]:

$$F_1 = 2.0893 \times 10^{22}, \quad E_1/R = 24800, \quad C_{R,1} = 3.0$$

$$F_2 = 5.0117 \times 10^{21}, \quad E_2/R = 25000, \quad C_{R,2} = 3.0$$

$$F_3 = 3.9811 \times 10^{19}, \quad E_3/R = 20000, \quad C_{R,3} = 3.0$$

$$F_4 = 3.3113 \times 10^{18}, \quad E_4/R = 20500, \quad C_{R,4} = 3.0$$

3.2.3.1 Premixed Flames

For turbulent premixed flames, similar to the two-step scheme, the mass fractions m_{fu} , $m_{C_xH_y-2}$, m_{CO} and m_{H_2} are used as the dependent variables of the differential equations for chemical species. The consumption rates for m_{fu} , $m_{C_xH_y-2}$, m_{CO} and m_{H_2} are calculated from Equations (3.76), (3.80), (3.84) and (3.88), respectively. The values of m_{OX} , m_{CO_2} , m_{H_2O} and m_{N_2} are then obtained from the following algebraic relations:

$$m_{OX} = m_{OX,p} - (r_1r_3 + r_1r_4r_6 + r_2r_8 + r_1r_5r_8)(m_{fu,p} - m_{fu}) + (r_3 + r_4r_6 + r_5r_8) m_{C_xH_y-2} + r_6 m_{CO} + r_8 m_{H_2} \quad (3.92)$$

$$m_{H_2O} = (r_2r_9 + r_1r_5r_9)(m_{fu,p} - m_{fu}) - r_5r_9 m_{C_xH_y-2} - r_9 m_{H_2} \quad (3.93)$$

$$m_{CO_2} = r_1r_4r_7(m_{fu,p} - m_{fu}) - r_4r_7 m_{C_xH_y-2} - r_7 m_{CO} \quad (3.94)$$

$$m_{N_2} = 1 - (m_{fu} + m_{CO} + m_{OX} + m_{H_2O} + m_{CO_2}) \quad (3.95)$$

Here $m_{fu,p}$ and $m_{OX,p}$ are the mass fractions of fuel and oxidant respectively at the primary inlet, and m_{N_2} is calculated from the fact that all mass fractions should add up to unity.

3.2.3.2 Diffusion Flames

For diffusion flames, similar to the two-step scheme, the mass fractions of the species are added in certain proportions to yield zero source terms. This is shown in the last three entries of Table III as ϕ_A , ϕ_B and ϕ_C . For these three entries, because their source term is zero, a single solution for them would suffice provided their boundary conditions are the same. This condition can be ensured by normalizing the ϕ 's with reference to their values in the air and fuel streams. Thus a single variable f (defined the same as that for the two-step scheme) with a zero source term and with values 0 and 1 in the air and fuel streams respectively can be regarded as providing the solutions for ϕ_A , ϕ_B and ϕ_C . Follow the same procedure applied for the two-step scheme, finally we have:

$$m_{OX} = R(1 - f) + (r_1r_3 + r_1r_4r_6 + r_2r_8 + r_1r_5r_8)(m_{fu} - f) + (r_3 + r_4r_6 + r_5r_8) m_{C_xH_y-2} + r_6 m_{CO} + r_8 m_{H_2} \quad (3.96)$$

$$m_{H_2O} = (r_2 r_9 + r_1 r_5 r_9)(f - m_{fu}) - r_5 r_9 m_{C_x H_y - 2} - r_9 m_{H_2} \quad (3.97)$$

$$m_{CO_2} = r_1 r_4 r_7 (f - m_{fu}) - r_4 r_7 m_{C_x H_y - 2} - r_7 m_{CO} \quad (3.98)$$

$$m_{N_2} = 1 - (m_{fu} + m_{CO} + m_{OX} + m_{H_2O} + m_{CO_2}) \quad (3.99)$$

To summarize, the mass fractions m_{fu} , $m_{C_x H_y - 2}$, m_{CO} , m_{H_2} and f are used as the dependent variables of the differential equations for chemical species. The consumption rates for m_{fu} , $m_{C_x H_y - 2}$, m_{CO} and m_{H_2} are calculated from Equations (3.76), (3.80), (3.84) and (3.88), respectively, while the source for f is zero. The values of m_{OX} , m_{CO_2} , m_{H_2O} and m_{N_2} are then obtained from Equations (3.96) through (3.99), and m_{N_2} is calculated from the fact that all mass fractions should add up to unity.

3.3 Numerical Formulation

The governing partial differential equations described in Sections 3.1 and 3.2 are nonlinear and strongly coupled. Since it is impossible to obtain analytical solutions to those equations, some numerical techniques have to be used to solve them.

Solution of hydrodynamics may be via the well-known stream function-vorticity approach or the primitive pressure-velocity variable approach, which are the two common numerical methods in the field of computational fluid mechanics. The former approach reduces the number of equations by one through automatic satisfaction of the conservation of mass (continuity equation), and eliminates the troublesome pressure term at the expense of trouble with the vorticity equation and specification of boundary conditions. The preferred approach now is the primitive pressure-velocity variable approach with SIMPLE algorithm being used. This approach possesses many advantages: (a) it can be used for two-dimensional as well as three-dimensional problems; (b) it can handle compressible transient problems as well as incompressible steady ones; (c) the boundary conditions and variable properties are more accurately and realistically handled.

To formulate the governing partial differential equations into the finite difference equations, the staggered grid system [6] was used, see Figure 4. All variables except u and v velocities are stored at the central grid nodes (intersections of the grid lines), while the u and v velocities are stored at the points which are denoted by arrows (and labeled w and s respectively) located midway between the grid intersections. The boomerang-shape envelope encloses a triad of points with the reference location P at (I,J) . The advantages of this staggered grid system are: first, it places the u and v velocities between the pressure nodes which drive them; and second, the velocities are directly available for the calculation of the convective fluxes across the boundaries of the control volume surrounding the central node. Figure 5 shows three types of the control volumes C , U and V which are appropriate for the P , w and s locations respectively.

The finite difference equations for each ϕ are constructed by integrating Equation (3.1) over the appropriate control volume (centered about the location of ϕ) and expressing the result in terms of the values at neighboring grid nodes. The convection and diffusion terms become surface integrals of the convection and diffusion fluxes, while the source term becomes volume integral of the source. The source, which is a function of the dependent variables, can be expressed in a linear form. Because first the nominally linear frame work would allow only a formally linear dependence, and second the incorporation of linear dependence is better than treating the source as a constant [6]. The resulting equation is:

$$\begin{aligned} & \left[\rho u \phi - \Gamma_{\phi} \frac{\partial \phi}{\partial x} \right]_e A_e - \left[\rho u \phi - \Gamma_{\phi} \frac{\partial \phi}{\partial x} \right]_w A_w + \\ & \left[\rho v \phi - \Gamma_{\phi} \frac{\partial \phi}{\partial r} \right]_n A_n - \left[\rho v \phi - \Gamma_{\phi} \frac{\partial \phi}{\partial r} \right]_s A_s = \left[S_p^{\phi} \phi_p + S_u^{\phi} \right] \bullet \text{Vol} \end{aligned} \quad (3.100)$$

where S_p^{ϕ} and S_u^{ϕ} are tabulated in Table IV with the one-step reaction scheme being used, for example, and subscripts n , s , e and w refer to the north, south, east and west control

volume surfaces. Equation (3.100) is discretized by using the hybrid scheme which is a combination of the so-called central and upwind finite differences. The details of the discretization procedure are given in the report [9]. The final finite difference equations all conform to:

$$a_p^\phi \phi_p = \sum_j a_j^\phi \phi_j + S_u^\phi \quad (3.101)$$

$$a_p^\phi = \sum_j a_j^\phi - S_p^\phi \quad (3.102)$$

\sum_j = sum over the N, S, E and W neighbors.

3.4 Solution Procedure

The method of solution differs for different flows. Marching methods are appropriate for parabolic flows (boundary-layer type) and relaxation methods are appropriate for elliptic flows (recirculating type). Since combustor flows are elliptic, relaxation methods of solution are necessary. The preferred approach is to use the SIMPLE relaxation algorithm. The basic features of SIMPLE are as follows:

- (a) a finite difference procedure is used in which the dependent variables are the velocity components and pressure;
- (b) the pressure is deduced from an equation which is obtained by the combinations of the continuity equation and momentum equation;
- (c) the idea is present at each iteration of a first approximation of u , v and p followed by a succeeding correction;
- (d) the procedure incorporates displaced grids for the axial and radial velocities u and v , which are placed between the nodes where pressure, p , and other variables are stored;
- (e) an implicit line-by-line relaxation technique is employed in the solution procedure.

The finite difference equations (3.101) result in a system of strongly coupled simultaneous algebraic equations. Although they appear linear they are not since the coefficients and source terms are themselves function of the variables, and the velocity equations are strongly linked through the pressure. The solution of coupled nonlinear equations proceeds using an iterative scheme. The iteration technique greatly simplifies the construction of the numerical method and provides a way in which, in principle, one can handle any non-linearity and coupled partial differential equations. In the iteration solution of the algebraic equations or in the overall iterative scheme employed for handling non-linearity, it is often desirable to speed up or to slow down the changes, from iteration to iteration, in the values of the dependent variable. This process is called over-relaxation or under-relaxation depending on whether the variable changes are accelerated or reduced. Over-relaxation is often used in conjunction with the Gauss-Seidel Method, the resulting scheme being known as Successive Over-Relaxation (SOR). Under-relaxation is often employed to avoid divergence in the iterative solution procedure of strongly nonlinear equations. The over-relaxation factor is a value between 1 and 2, but the under-relaxation factor is a value between 0 and 1. There are no general rules for choosing the best value of the factor, f_ϕ . The optimum value depends on a number of factors, such as the nature of the problem, the number of grid points, the grid spacing, the particular variable and the iterative procedure used. Usually a suitable value of f_ϕ can be found by experience and from exploratory computations for a given problem.

In the code, a certain degree of under-relaxation is used to enhance convergence. The under-relaxation factor f_ϕ ($0 < f_\phi < 1$) is applied directly to the dependent variable ϕ_p^{n+1} via

$$\left(\frac{a_p^\phi}{f_\phi} \right) \phi_p^{n+1} = \sum_j a_j^\phi \phi_j^n + S_u^\phi + (1 - f_\phi) \frac{a_p^\phi}{f_\phi} \phi_p^n \quad (3.103)$$

In addition to the dependent variables, other quantities can be under-relaxed with advantage. The density ρ is often the main link between the equations for momentum,

temperature and species concentration. An under-relaxation of ρ would cause the velocity field to respond rather slowly to the changes in temperature and species concentration. A diffusion coefficient Γ_ϕ can be under-relaxed to restrain the influence of the turbulence quantities on the velocity field. To enhance convergence, the density and diffusion coefficient are under-relaxed via

$$\rho = f_\rho \rho_{\text{new}} + (1 - f_\rho) \rho_{\text{old}} \quad (3.104)$$

$$\Gamma_\phi = f_{\Gamma_\phi} \Gamma_{\phi_{\text{new}}} + (1 - f_{\Gamma_\phi}) \Gamma_{\phi_{\text{old}}} \quad (3.105)$$

The well-known tridiagonal matrix algorithm (TDMA) is used to solve the algebraic equations for each dependent variable. Since TDMA can be applied along a grid line, in the two dimensional problem one applies the TDMA along each vertical grid line from left to right sequentially in the solution domain for each iteration step (line-by-line method). The values at grid points along a vertical grid line are considered to be unknown (values at P, N and S for a typical point P), and the most recent values at E and W neighbor points are considered known and stored in a column vector. The coefficients and source terms of Equation (3.100) are updated prior to each iteration because previous ones are only tentative.

The method of monitoring convergence is to examine how perfectly the discretized equations are satisfied by the current values of the dependent variables. For each grid point, a residual, R_p^ϕ , is defined by:

$$R_p^\phi = \sum_j a_j^\phi \phi_j + S_u^\phi - a_p^\phi \phi_p \quad (3.106)$$

When the summation of $|R_p^\phi|$ all over the flow domain becomes smaller than a predetermined value, the computed solution is considered converged.

CHAPTER IV

THE "REFINED" COMPUTER CODE

4.1 Background

The COSMIC code has been employed and suitably modified for the proposed studies identified in Chapter I. In its original form, it can predict the distribution of velocities, pressure, species (unburned fuel, oxygen and products only) concentrations, turbulence quantities, stagnation enthalpy and temperature for turbulent reacting flows in an axisymmetric domain. This code was developed based on the ideas which had been embodied into the 1974 Imperial College TEACH computer program with the SIMPLE solution algorithm adopted. Turbulence simulation is by way of a two equation $k-\epsilon$ model, and combustion via a simple one-step chemical reaction scheme based on the Arrhenius and Eddy-breakup concepts. In addition to the incorporation of swirl, some special numerical features were included in the code, such as: (a) a generalized stair-step simulation of the sloping wall boundary, (b) an advanced non-uniform grid system, and (c) the wall functions derived from a recent experiment [9].

The new computer code, REFINED (acronym for Reacting Elliptic Flows IN Expansion Domains) developed in this study, started with the original COSMIC code. Some new developments are highlighted in the following sections.

4.2 A Variety of Primary Inlet Velocity Profile Choices

In practical systems, different types of swirl-generating methods are used, for example, tangential-entry, flat and/or curved blades with/without constant turn angle (that

is, twist). These alternate methods produce differing velocity profiles at the combustor entrance, which are typified by the cases shown in Figure 2. When measured inlet data are not available, great care should be taken in selecting these profiles, since some of them may be inappropriate and lead to poor predictions on the resulting flowfield. To handle different flow systems and investigate the effects of different inlet velocity profiles on flowfield predictions, the cases shown in Figure 2 are included in the new code. Further discussion is give in Section 5.1.

4.3 Multi-Inlet Capability

To handle more realistic combustor flows, the capability of treating multi-inlets must be ready in the new code. Figure 6 shows the schematic of a grid system used to cover the combustor domain with a secondary circumferential slot injection. The two side concentric inlets and one top inlet can be specified using control parameters as follows:

IGCS (side inlet control code)	= 1 -- one axisymmetric central inlet (A)
	= 2 -- two concentric inlets (A and B)
IGCT (top inlet control code)	= 0 -- no top inlet
	= 1 -- one top inlet

The sizes and locations of each inlet can be assigned with the following gridline values:

Side inlet A:	JINAS (inlet south J)
	JINAN (inlet north J)
Side inlet B:	JINBS (inlet south J)
	JINBN (inlet north J)
Top inlet:	IINW (inlet west I)
	IINE (inlet east I)

At each inlet, inlet conditions can be specified with the following variables:

Side inlet A:	UIN (u velocity, m/sec)
---------------	-------------------------

VIN (v velocity, m/sec)

WIN (w velocity, m/sec)

FUIN (fuel mass fraction)

OXIN (oxygen mass fraction)

OFIN (mixture mass fraction)

PRIN (product or nitrogen mass fraction)

HIN (inlet stagnation enthalpy, J/kg)

TIN (inlet temperature, °K)

Side inlet B: UINB, VINB, WINB, FUINB, OXINB, PRINB, OFINB, HINB
and TINB

Top inlet: UIN2, VIN2, WIN2, FUIN2, OXIN2, PRIN2, OFIN2, HIN2, and
TIN2

Here, to calculate VINB and WINB, two primary inflow parameters are used, and they are PCA (primary contraction angle) for VINB and PSA (primary swirl angle) for WINB, respectively. To calculate UIN2 and WIN2, two secondary inflow parameters are used, and they are SUA (secondary upstream angle of injection) for UIN2 and SSA (secondary swirl angle of injection) for WIN2, respectively.

4.4 Inclusion of Two-Step Reaction Scheme

For improved combustion simulation, the two-step reaction scheme and the corresponding solution procedure developed in Section 3.2.2 have been incorporated into the new code for both premixed and diffusion-controlled flames. First, S_{fu} (Equations (3.32) through (3.35)) are added to the m_{fu} solver subroutine CALCFU as the source term of m_{fu} for the two-step scheme. Then, a new solver subroutine called CALCCO is developed for m_{CO} . S_{CO} (Equations (3.36) through (3.39)) combined with S_{fu} , as given in Table II for m_{CO} , are used as the source term of m_{CO} in CALCCO. Species mass fractions

m_{OX} , $m_{\text{H}_2\text{O}}$, m_{CO_2} , and m_{N_2} from Equations (3.40) through (3.43) for premixed flames, Equations (3.48) through (3.51) for diffusion flames, respectively, are included in subroutine PROPS. Some other modifications associated with the two-step scheme are also added to the code, such as the initializations of newly introduced variables in subroutine INIT, thermodynamic calculations of mixture properties in MAIN and subroutine PROPS, and problem modifications at boundary node points in subroutine PROMOD. Newly introduced FORTRAN variables associated with the inclusion of the two-step scheme are listed in Table V. With control parameter $\text{IMODEL} = 2$, the two-step scheme is selected for combustion simulation.

4.5 Inclusion of Four-Step Reaction Scheme

The four-step reaction scheme and the corresponding solution procedure developed in Section 3.2.3 have also been incorporated into the new code for both premixed and diffusion controlled flames. First, S_{fu} (Equations (3.76) through (3.79)) are added to the m_{fu} solver subroutine CACLFU as the source term of m_{fu} for the four-step scheme. Second, S_{CO} (Equations (3.84) through (3.87)) combined with $S_{\text{C}_x\text{H}_y-2}$ (Equations (3.80) through (3.83)), as given in Table III for m_{CO} , are added to the m_{CO} solver subroutine CALCCO as the source term of m_{CO} for the four-step scheme. Then two new solver subroutines called CALCF2 and CALCH2 are developed for $m_{\text{C}_x\text{H}_y-2}$ and m_{H_2} , respectively. $S_{\text{C}_x\text{H}_y-2}$ combined with S_{fu} , as given in Table III for $m_{\text{C}_x\text{H}_y-2}$, are used as the source term of $m_{\text{C}_x\text{H}_y-2}$ in CALCF2, and S_{H_2} (Equations (3.88) through (3.91)) combined with S_{fu} and $S_{\text{C}_x\text{H}_y-2}$, as given in Table III for m_{H_2} , are used as the source term of m_{H_2} in CALCH2. Species mass fractions m_{OX} , $m_{\text{H}_2\text{O}}$, m_{CO_2} , and m_{N_2} from Equations (3.92) through (3.95) for premixed flames, Equations (3.96) through (3.99) for diffusion flames, respectively, are included in subroutine PROPS. Some other modifications associated with the four-step scheme are also added to the code, such as the initializations

of newly introduced variables in subroutine INIT, thermodynamic calculations of mixture properties in MAIN and subroutine PROPS, and problem modifications at boundary node points in subroutine PROMOD. Newly introduced FORTRAN variables associated with the inclusion of the four-step scheme are listed in Table V. With control parameter IMODEL = 4, the four-step scheme is selected for combustion simulation.

4.6 Interaction with Flowfield Color Graphic Display

A user-friendly computer program CFCD (Combustor Flowfield Color Display) [70] is being developed for the color graphic display of combustor flowfields. Any user selected variable can be plotted in the form of contour lines or shaded maps throughout the entire domain. Graphs of the radial profile of the chosen variable at five user-selected axial stations (labeled A, B, C, D and E with different colors) are also displayed. For the contour lines or shaded maps, CFCD internally assigns ten different colors to represent ten different magnitude ranges of the chosen variable. The magnitude subrange is a constant selected by the user. For the values of the chosen variable below zero, or above ten times this subrange magnitude, the color display outlined above is automatically repeated. The plot can be captured and processed further with any image processing software from the user's convenience. All the user needs to do is to prepare a data file in the format that the CFCD reads in. The data file must provide information of geometry (width and length of the domain), rectangular grid system (NI, NJ), coordinates (x, r) of each node, name of variable, and values of the variable at each node. A definite form of the data file is required for reading into the color graphic program CFCD. To interact with the CFCD program, a subroutine, called GRAPH5, has been developed and incorporated into the REFINED code.

4.7 Typical Input and Output

The REFINED code is very friendly. Users have a variety of choices for a problem to be simulated. The flow system may have one axisymmetric side inlet, two concentric side inlets and/or one top circumferential inlet. The flow may be nonreacting or reacting. For a reacting flow, the fuel may be methane, propane or a general hydrocarbon fuel C_xH_y with the user's choices of x and y . The flame may be premixed or diffusion-controlled. Three kinetic schemes are available for the combustion simulation, and they are one-step, two-step and four-step by the user's choice. The inlet velocity profiles may be flat, linear, parabolic or a combination of these. The inlet flow parameters such as u_0/v_0 , PSA, PCA, SSA and SUA can be selected by the user.

The REFINED code generates automatically two data files with names specified by the user. One of them is the data file prepared for the color graphic display program, CFCD, for the post-processing. The other provides the iterative information, input data, and matrix printouts for each dependent variable such as axial velocity u , radial velocity v , and temperature T etc. The grid number (I, J) and coordinates (x, r) at each node are also printed.

Sample input and output for the REFINED code are given in Appendix C. For the output, only five dependent variables are attached here for the illustration purpose, and they are the axial velocity u (m/sec), radial velocity v (m/sec), temperature (K), unburned fuel mass fraction, and oxygen mass fraction. In this sample computation, the reacting flow system has only two concentric side inlets A and B, see Figure 6 for the schematic. The radius of the outer wall (adiabatic) is 0.1016 m, and the length of the combustion chamber is 1.524 m. Air enters the main chamber through the annular inlet B (radii of 0.0111 m and 0.0286 m) with a uniform axial velocity of $U_{INB} = 49$ m/sec at 300 K. Fuel (methane) enters through the central pipe inlet A (radius of 0.008 m) with a uniform axial velocity of $U_{IN} = 22.3$ m/sec at 589 K. The overall equivalence ratio of the fuel/oxygen is

1.18 on the mass basis. In the computation, a grid of 40x15 ($NI = 40$, $NJ = 15$) is used, and the combustion simulation is given via the one-step reaction scheme.

CHAPTER V

APPLICATIONS AND DISCUSSION

In order to demonstrate the capability of the developed computer code described in Chapters III and IV, several applications are considered. For each case, turbulence simulation is given via the use of the standard two-equation k - ϵ model. Both nonreacting and reacting flows are considered. For reacting flows, the combustion simulation is given via the use of one-step, two-step or four-step schemes based on Arrhenius and Eddy-Breakup concepts for premixed or diffusion situations. As a special application of the developed code, the impinging combustion flowfield predictions for CVD (chemical vapor deposition) diamond synthesis are not included here, and the complete presentations are given in Refs. [71] and [72].

5.1 Nonreacting Flow Predictions with Various Inlet Velocity Profiles

This application is concerned with the axisymmetric modeling approach with emphasis placed on various inlet velocity profile effects on the nonreacting flowfield. The well-known k - ϵ turbulence model is used. It is conceded that more advanced models might be more accurate, but even this relatively simple model illustrates the dramatic effects of inlet profiles on the predictions, the main emphasis of this study. When a verified more advanced model is available, it may be included. However, the present model serves to illustrate the main points of the study. The validity of the predictions is assessed via available experimental data [73], and the complete presentations of this study are given in Refs. [74] and [75].

5.1.1 Problem Description

The problem schematic is given in Figure 7 for a model combustor domain. Air enters the prechamber from the left, and then encounters a sudden expansion into the main chamber. The flow domain has a nozzle radius of 0.075 m, chamber radius 0.15 m and length 1.2 m. The domain is covered with a nonuniform rectangular grid system as illustrated in Figure 8, where NI and NJ are taken as 21 and 22, respectively. The r-direction is equally subdivided, but the x-direction is covered with a gradually expanding mesh system.

5.1.2 Types of Inlet Velocity Profiles Considered

Seven possible specifications of the inlet velocities are considered, and the idealized axial and swirl velocity profile cases 1 through 5 are shown in Figure 2 in the form of profile expressions. Parameters, swirl numbers and discussions associated with these profiles are deduced in References [14,76]. In each case, the magnitude of u_{mo} and w_{mo} (identified below) are chosen to conform to the same swirl number consistent with the appropriate swirl vane angle. The equations given in Reference [77] are used for this. In all cases considered, the kinetic energy k of turbulence and its dissipation rate ϵ are specified as in general accepted ways [9,60,78]. First, the kinetic energy k is specified as a function of radial location by means of a constant multiplied by local mean axial velocity squared. The constant is taken as 0.03, which is consistent with isotropic turbulence intensity of 14%. Second, the turbulence length scale is taken as 3% of the radius of the flow passage. Then ϵ is deduced locally from k and the length scale. An indication of the effect of these choices on the results is given in Section 5.1.3.

Case 1 Flat inlet axial and swirl velocities with radial velocity zero are assumed.

That is, both u and w are constant valued:

$$u_0 = \text{constant}$$

$$w_0 = u_0 \tan\theta$$

where θ is the swirl vane angle.

Case 2 As in Case 1, except that the inlet swirl velocity profile is assumed to be that of solid body rotation:

$$u_0 = \text{constant}$$

$$w_0 = w_{mo} r/R$$

where w_{mo} is the maximum orifice value of w which occurs at the outer edge $r = R$ of the inlet. The value of w_{mo} is so chosen as to ensure the swirl number the same as in Case 1.

Case 3 Linear axial and swirl velocities with radial velocity zero are assumed:

$$u_0 = u_{mo} r/R$$

$$w_0 = w_{mo} r/R$$

where u_{mo} is the maximum orifice value of u which occurs at the outer edge $r = R$ of the inlet. The values of u_{mo} and w_{mo} are so chosen as to ensure the swirl number the same as in Case 1.

Case 4 Parabolic axial and linear swirl profiles with radial velocity zero are assumed:

$$u_0 = u_{mo} (r/R)^2$$

$$w_0 = w_{mo} r/R$$

Case 5 Parabolic axial and swirl profiles with radial velocity zero are assumed:

$$u_0 = u_{mo} (r/R)^2$$

$$w_0 = w_{mo} (r/R)^2$$

where the values of u_{mo} and w_{mo} , as Case 4, are so chosen as to ensure the swirl number as in Case 1.

Case 6 Measured inlet axial and swirl velocities are used [24] with radial velocity assumed to be zero.

Case 7 Measured inlet axial, radial and swirl velocity values are used [24].

5.1.3 Effects of Inlet Turbulence Quantities on Predicted Results

Taking measured inlet velocity components u , v and w (Case 7) with length scale specified as 3% of the characteristic dimension (radius) of the flow passage, predictions were made for swirl vane angle $\theta = 45$ and 70 degrees with turbulence intensities of 8, 14 and 26%, respectively. Over this range of variance of turbulence intensity, predicted axial and swirl velocity profiles did not change much further downstream. However, the (small) magnitude of negative axial velocity in the central recirculation zone approximately doubled. Other predictions were made with turbulence intensity held at 14%, while the length scale varied over the range 1, 3 and 10% of the radius of the flow passage. Over this range of variance of length scale, profiles of axial and swirl velocities did not change much. Again, the most dramatic effect was seen in the magnitude of the negative axial velocity in the central recirculation zone, which approximately halved. In the following analysis, the turbulence intensity is specified as 14%, and length scale as 3% of the characteristic dimension of the flow passage.

5.1.4 Effects of Inlet Velocity Profiles

Swirl Vane Angle $\theta = 45$ degrees Consider first the flowfield resulting when the inlet swirl vane angle is 45 degrees. Figure 9 shows predicted axial and swirl velocity profiles at various downstream axial stations, $x/D = 0.5, 1.0, 1.5$ and 2.0 , obtained when the inlet velocity profiles are specified by the seven cases discussed above. The flowfield structure for these cases is further illustrated via streamline shady plots, which are computer calculated and drawn, in Figure 10. The figure is stretched in the radial direction by 50 percent to aid observation. This same streamline stretch is retained in all subsequent streamline plots. Inspection of these figures is quite revealing and may be assessed in the light of pitot probe experimental data [24]. Figure 11 shows the starting and terminating locations of the central toroidal recirculation zones (CTRZ) for seven

different test cases and the corresponding experimental measurements. The starting and terminating locations of the CTRZ are specified as s and $(s + l)$, respectively, where s is the distance from the inlet and l is the length of the CTRZ. The blockage ratio, W/D , or the width (W) of the CTRZ is shown in Figure 12 for seven different test cases and the corresponding measurements.

Cases 3 through 7 covered in Figures 9 through 12 give central recirculation zones terminating at about $x/D = 1.5$, similar to that found in practice in length and width. But initial spreading rates vary considerably: only in Cases 6 and 7 does the central recirculation zone begin immediately on entry to the large chamber, with Case 7 spreading most rapidly in the initial region. Cases 1 and 2 do not possess enough centrifugal effect because of their unrealistic inlet swirl velocity profiles, resulting in predictions of short and narrow central recirculation zones. Also, Cases 1 through 6 do not have a radial component of velocity to encourage inlet radial spreading of the streamlines. These inlet flow ideas may be confirmed by observing the size of the corner recirculation zones. Cases 2, 5 and 7 exhibit short corner recirculation zones, with only Case 7 also possessing the correct central activity near the inlet - rapid spreading with a central recirculation flow beginning immediately. None of the predictions match the precessing vortex core details found in flow visualization studies [3] or the negative axial velocities measured by pitot probe experimentation near the facility axis, $r/D < 0.1$, extending all the way to test section exit. Nevertheless, comparison of the prediction with the gross features of the corresponding experimental data clearly indicates that the inlet conditions of Case 7 are superior in allowing realistic flowfield prediction.

Swirl Vane Angle $\theta = 70$ Degrees Figures 13 and 14 correspond to Figures 9 and 10, and Figures 15 and 16 correspond to Figures 11 and 12, with the swirl vane angle increased to 70 degrees. Now the strong centrifugal forces present in the incoming flow play their part. Initial spreading rates are very high with very small corner recirculation zones in all cases, except that of Cases 6 and 7 seen in Figure 14. All central recirculation

zones, except Case 2, begin immediately at the inlet and are much wider and longer than the measurements indicate, see Figures 14 through 16. This results from unrealistically large swirl velocity magnitudes. With zero inlet radial velocity, Case 6 does not spread rapidly enough at the inlet and a long central recirculation zone extending to $x/D = 1.9$ is predicted. With the inclusion of the correct inlet radial velocity, a recirculation zone much more like that found experimentally results in Case 7. None of the cases predict swirl velocity profiles very accurately, with w -profiles more like solid body rotation soon developing in the downstream direction, in contrast to the more free-forced vortex profiles found in the experiments. Maybe part of the reasons is that the two-equation k - ϵ model is not appropriate for strong swirling flows. When significant streamline curvatures are introduced into the flowfield, such as strong recirculation zones or swirl, the k - ϵ model does not adequately account for the enhanced turbulence diffusion caused by the extra strain rates associated with streamline curvature. For analyzing such flowfields, the k - ϵ model should be modified with the Richardson number, which is a measure of the extra strain rate due to the streamline curvature [2].

5.1.5 Effects of Swirl

Predicted streamline patterns for swirl vane angles of 45 and 70 degrees for Cases 1-7 are shown in Figures 10 and 14, parts a-g, respectively. The predicted effects of swirl shown in these figures confirm in general the well-known ideas about swirl effects on axisymmetric turbulent confined jet flows. Under nonswirling conditions, a large corner recirculation zone exists and the centerline axial velocity changes gradually from its inlet value as downstream development occurs. However, as the degree of inlet swirl is 45 degrees, axial velocity profiles change dramatically. Near the inlet, a central toroidal recirculation zone appears and the corner recirculation zone shortens considerably. Under strong swirl conditions of θ equal to 70 degrees, a much wider central recirculation region

is established. It promotes a very large forward velocity near the confining walls rather than a corner recirculation region.

These predicted effects generally agree with the experimental data, except that precessing vortex core regions of solid body rotation back flow, which occur downstream of central recirculation regions in the swirl flow cases investigated [3], are not well predicted. Only the 70-degree case predicts almost zero axial velocity on the centerline extending to $x/D = 4$. The central recirculation zone is predicted to be longer than found in practice. Also, swirl velocity profiles do not match well the experimental data - the radial location of the swirl velocity maximum value occurs too close to the confining chamber walls rather than occurring abruptly at the edge of a vortex core region. The observed discrepancies may be because of poor probe sensitivity in turbulent low velocity regions, and/or poor turbulence model performance in these regions. Only further detailed hot-wire and/or laser Doppler anemometer measurements and turbulence model development will resolve the inconsistencies. Clearly, measured inlet profiles must be used in future turbulence modeling development studies for improved simulation of this flowfield.

5.1.6 Closure

A numerical prediction using the standard two-equation $k-\epsilon$ model and different inlet flow boundary condition assumptions has been applied to a confined turbulent swirling flow. The $k-\epsilon$ model has been illustrated to be inappropriate for swirling flow predictions, and the inlet flow boundary conditions have been demonstrated to be extremely important in simulating a flowfield via numerical calculations. Predictions with flat, linear or parabolic inlet axial and swirl velocity profiles, or a combination of these profiles with zero radial velocity, are shown to be inappropriate. Realistic predictions are forthcoming only from the inclusions of realistic axial, radial and swirl velocity profiles as

inlet conditions. Clearly, measured inlet profiles must be used in future turbulence modeling development studies for improved simulation of flowfields.

5.2 Inlet Design Parameter Effects on Nonreacting Flowfields

This application is concerned with the axisymmetric modeling approach with emphasis placed on the application of the code to nonreacting combustor flowfields so as to assist in combustion system design and development. Here, application of the code is stressed, and consideration is given to the relative effect of certain important and influential design parameters. Discussion is primarily aimed to guide designers in judiciously deciding where experimental emphasis should be placed and/or in interpolating results from a limited amount of experimental data. Complete presentations of this study are given in Refs. [79] and [80].

5.2.1 Problem Description

The combustor schematic is illustrated in Figure 17. Ambient air enters the prechamber from the left, and then encounters a sudden expansion into the main chamber. Additionally, a top wall secondary circumferential inlet is permitted, through which secondary ambient air flows. The flow domain has a nozzle radius of 0.04 m, chamber radius 0.1 m and length 0.5 m (equal to 5 radii), with secondary inlet starting location being one chamber radius downstream of the primary inlet, and secondary to primary inlet area ratio equal to 1.25. The domain is covered with a nonuniform rectangular grid system as illustrated in Figure 6, where NI and NJ are taken as 40 and 12. The r-direction is equally subdivided, but the x-direction is covered with a gradually expanding mesh system. The west wall and top wall are adiabatic and isothermal (ambient temperature), respectively. The five influential inlet design parameters of special interest, shown schematically in Figure 3, are:

v_0/u_0 = secondary to primary velocity ratio

PSA = primary swirl angle (degrees) giving flat swirl velocity at primary inlet

PCA = primary contraction angle (degrees) giving radial velocity at primary inlet

SSA = secondary swirl angle (degrees) giving swirl velocity at secondary inlet

SUA = secondary upstream angle (degrees) giving axial velocity at secondary inlet

The standard conditions (with $u_0 = 10$ m/s) for the discussions in Sections 5.2.2 through 5.2.6 are defined as:

$$v_0/u_0 = 0.1 \quad \text{PSA} = 0 \quad \text{PCA} = 0 \quad \text{SSA} = 0 \quad \text{SUA} = 0$$

5.2.2 Secondary to Primary Velocity Ratio Effect

Production runs of the computer code were required to illustrate the effect of secondary air inlet velocity on the flowfield patterns, velocities, and turbulence levels. Figure 18 illustrates the effect of a range of four values given to $v_0/u_0 = 0.1, 0.2, 0.4$ and 0.8 ($v_0 = 1, 2, 4$ and 8 m/s with $u_0 = 10$ m/s). Radial profiles of normalized axial velocity are given at the axial stations $x/D = 0.25, 0.5, 1.0$ and 2.5 , and for interpretive purposes it may be noted that the secondary inlet begins at $x/D = 0.5$ and that the combustor exit is at $x/D = 2.5$. It is observed that at $x/D = 1$ and 2.5 , downstream of the secondary inlet, the axial velocity increases with the increasing of the secondary air inflows. The radial profiles of the axial velocity are flatter at the further downstream location because of further downstream development. The corresponding shady plot streamline patterns, which are stretched in the radial direction by 43 percent to aid observation, are given in Figure 19, where the penetration of the secondary jet is clearly seen to increase as the injected velocity increases. This same streamline stretch is retained in all subsequent streamline plots. A secondary recirculation zone is seen downstream of the secondary inlet, its size increasing with the injection velocity. When the secondary injection velocity (v_0) increases to 4 m/s, a corner recirculation zone is observed upstream of the secondary

inlet, its size increasing with the injection velocity. The observed secondary recirculation zone and corner recirculation zone are substantiated by the strong penetration effect and momentum conservation.

5.2.3 Primary Swirl Angle Effect

The effect of varying the primary swirl angle through the range of 0, 30, 45 and 60 degrees is seen in Figures 20 and 21, for the axial and swirl velocity profiles at four axial stations $x/D = 0.25, 0.5, 1.0$ and 2.5 , and streamline patterns for $PSA = 0, 30, 45$ and 60 degrees, respectively. As the swirl strength increases, centrifugal effects increase. At large swirl angle, a dramatic reduction of the axial velocity near the centerline is observed, which is substantiated by the momentum conservation, see Figure 20. When PSA increases to 45 degrees, a wide central recirculation zone and a small corner recirculation zone are observed. The size of the central recirculation zone increases with swirl strength, but the size of the corner recirculation zone decreases with the swirl strength, see Figure 21. When $PSA = 60$ degrees, no corner recirculation zone is observed, but a much wider and longer central recirculation zone is observed, which results in the large forward axial velocity near the top wall at $x/D = 0.25$ in Figure 20.

5.2.4 Primary Contraction Angle Effect

When the primary air inflow is not directly in the axial direction, it may be anticipated that aerodynamic influences on the central, corner and secondary recirculation zones will be seen. With $PCA = -60$ degrees there is a strong positive radial outflow velocity component, and with $PCA = +60$ degrees there is a strong negative radial velocity component representing inflow toward the centerline. The former (to some extent) occurs automatically as the inlet flow is swirled through a vane swirler; the latter may occur deliberately via the use of a conical contraction in the inlet passage. Radial profiles of

axial velocity are given at four axial stations $x/D = 0.25, 0.5, 1.0$ and 2.5 in Figure 22, and streamline patterns for $PCA = -60, 0$ and $+60$ degrees are given in Figure 23. Compared with the axial inflow case, a very wide central recirculation zone and a more compact secondary recirculation zone are observed with the diverging inflow of $PCA = -60$ degrees, and much larger a secondary recirculation zone and a corner recirculation zone are observed with the contracting inflow of $PCA = +60$ degrees. The diverging inflow case has much flatter radial profiles of axial velocity than standard inflow and contracting inflow cases have with further downstream development. At $x/D = 0.5$, an expected spike is seen in the axial velocity profile near the top wall for diverging inflow case because of the wide central recirculation zone established there, which is not observed for standard inflow and contracting inflow cases. Dramatic effects of the secondary inflow parameters on the flowfield are discussed in the following sections.

5.2.5 Secondary Swirl Angle Effect

For the following two cases, the secondary inlet velocity is increased to 4 m/s, giving $v_0/u_0 = 0.4$. This is because the swirl and upstream angles given to this secondary inflow lead to a lack of penetration into the main flow at the lower velocity and the observed effects would then be minimal. The more interesting case of $v_0 = 4$ m/s permits useful observations and deductions about the effects of the secondary swirl angle (SSA) and secondary upstream angle (SUA) of the secondary flow into the main flow. Figure 24 gives the radial profiles of axial velocity and swirl velocity at four axial stations $x/D = 0.25, 0.5, 1.0$ and 2.5 ; Figure 25 gives the corresponding streamline patterns for $SSA = 0, 30, 45,$ and 60 degrees. A secondary inlet recirculation zone and a corner recirculation zone are clearly seen (from the streamline patterns) and their sizes decrease as the secondary swirl angle increase. The radial profiles of the axial velocity have trends to be flatter as the secondary swirl strength increases, but this trend is not dramatic.

5.2.6 Secondary Upstream Angle Effect

When the secondary air inflow is not directly inward from boundary, the aerodynamic influences on recirculation zones will be seen. With secondary upstream angle $SUA = -60$ degrees, there is a strong positive axial velocity component with the secondary flow in the downstream direction to the right, and with $SUA = +60$ degrees, there is a strong negative axial velocity component representing inflow with a velocity component upstream toward the west wall - the upstream dome end of the combustor. Radial profiles of axial velocity are given at four axial stations $x/D = 0.25, 0.5, 1.0$ and 2.5 in Figure 26; the corresponding streamline patterns for $SUA = -60, 0$ and $+60$ degrees are given in Figure 27. Compared with the normally injected secondary flow, a larger corner recirculation zone and a smaller secondary recirculation zone are clearly seen when the injected flow has a downstream axial velocity component ($SUA = -60$ degrees), but only one much larger secondary recirculation zone is seen when the injected flow has an upstream axial velocity component ($SUA = 60$ degrees). An expected spike is seen in the axial velocity profile near the top wall in the case of a downstream injection velocity component. Downstream and upstream injections trend to make the radial profiles of axial velocity at exit flatter compared with the normal injections.

5.2.7 Closure

The developed computer code has been applied to the turbulent swirling nonreacting flows in a typical combustor. Parameters of special interest include the secondary to primary velocity ratio, primary swirl angle, primary contraction angle, secondary swirl angle, and secondary upstream angle. Numerical predictions were given to illustrate the dramatic effects of these parameters on the nonreacting flowfields via radial profiles and streamline patterns.

5.3 Inlet Design Parameter Effects on Reacting Flowfields

This application is concerned with the axisymmetric modeling approach with emphasis placed on the application of the code to reacting flowfields so as to assist in combustion system design and development. Here, application of the code is stressed, and consideration is given to the relative effect of certain important and influential inlet design parameters. Turbulence simulation is given by the standard two-equation $k-\epsilon$ model, and combustion simulation is given via the one-step kinetic reaction scheme based on the Arrhenius and Eddy-Breakup concepts. Discussion is primarily aimed to guide combustor designers in judiciously deciding where experimental emphasis should be placed and/or in interpolating results from a limited amount of experimental data. The selected combustor geometry is the same as described in Section 5.2 for nonreacting flows, and the complete presentations of this study are given in Refs. [81] and [82].

5.3.1 Problem Description

The combustor schematic is illustrated in Figure 17 for reacting flows. With ambient temperature, stoichiometrically premixed fuel and air enters the prechamber from the left, and then encounters a sudden expansion into the main chamber. Additionally, a top wall secondary circumferential inlet is permitted, through which secondary ambient air flows. The flow domain has a nozzle radius of 0.04 m, chamber radius of 0.1 m and length of 0.5 m (equal to 5 radii), with the secondary inlet starting location being one chamber radius downstream of the primary inlet, and secondary to primary inlet area ratio equal to 1.25. The domain is covered with a nonuniform rectangular grid system as illustrated in Figure 6, where N_I and N_J are taken as 40 and 12. The r -direction is equally subdivided, but the x -direction is covered with a gradually expanding mesh system. The west wall and top wall are adiabatic and isothermal (ambient temperature), respectively. The five inlet flow parameters of special interest, shown schematically in Figure 3, are:

v_0/u_0 = secondary to primary velocity ratio

PSA = primary swirl angle (degrees) giving flat swirl velocity at primary inlet

PCA = primary contraction angle (degrees) giving radial velocity at primary inlet

SSA = secondary swirl angle (degrees) giving swirl velocity at secondary inlet

SUA = secondary upstream angle (degrees) giving axial velocity at secondary inlet

The standard conditions (with $u_0 = 10$ m/s) are:

$v_0/u_0 = 0.1$ PSA = 0 PCA = 0 SSA = 0 SUA = 0

5.3.2 Secondary to Primary Velocity Ratio Effect

As described in Section 5.2.2, production runs of the computer code were required to illustrate the effect of secondary air inlet velocity on the flowfield patterns, velocities and temperature levels. Figure 28 illustrates the effect of a range of four values given to $v_0/u_0 = 0.1, 0.2, 0.4$ and 0.8 ($v_0 = 1, 2, 4$ and 8 m/s with $u_0 = 10$ m/s), corresponding to the overall air/fuel ratio (on the volume basis) AFR = 2.375, 2.75, 3.5 and 5.0, with stoichiometry at the primary inlet. Radial profiles of normalized axial velocity and temperature are given at the axial stations $x/D = 1.0$ and 2.5 . It is observed that at $x/D = 1$ and 2.5 , downstream of the secondary inlet, the axial velocity increases and the temperature level reduces with the increase of the secondary cooling dilution air inflows. The radial profiles of the axial velocity and temperature are flatter at the downstream location because of further downstream development. The corresponding shady plot streamline patterns are given in Figure 29, where the penetration of the secondary jet is clearly seen to increase as the injected velocity increases. A secondary recirculation zone is seen downstream of the secondary inlet, its size increasing with the injection velocity.

5.3.3 Primary Swirl Angle Effect

The effect of varying the primary swirl angle through the range of 0, 30, 45 and 60 degrees is seen in Figures 30 and 31, for the axial velocity and temperature profiles at axial stations $x/D = 1.0$ and 2.5, and streamline patterns for PSA = 0, 30, 45 and 60 degrees, respectively. As the swirl strength increases, centrifugal effects increase, and a wider more compact reaction zone is observed, but no central recirculation zone was observed for the most strongly swirling case of the premixed fuel and air at primary inlet. The radial profiles of the axial velocity and temperature at $x/D = 1$ and 2.5 get more smooth when the swirl angle increases. At large swirl angle, a dramatic reduction of the axial velocity near the centerline is observed, which is substantiated by the momentum conservation. There is no dramatic effect on the profiles of temperature when swirl angle increases

5.3.4 Primary Contraction Angle Effect

When the primary inflow of premixed fuel and air is not directly in the axial direction, it may be anticipated that aerodynamic influences on the burning zone will be seen. With PCA = -60 degrees there is a strong positive radial outflow velocity component, and with PCA = +60 degrees there is a strong negative radial velocity component representing inflow toward the centerline. The former (to some extent) occurs automatically as the inlet flow is swirled through a vane swirler; the latter may occur deliberately via the use of a conical contraction in the inlet passage. Radial profiles of axial velocity and temperature are given at two axial stations $x/D = 1.0$ and 2.5 in Figure 32; streamline patterns for PCA = -60, 0 and +60 degrees are given in Figure 33. Compared with the axial inflow case, a wider reaction zone is observed with the diverging inflow of PCA = -60 degrees, and a narrower reaction zone is observed with the contracting inflow of PCA = +60 degrees, which is substantiated by the momentum conservation. Therefore, the diverging inflow case has much flatter radial profiles of axial

velocity further downstream, and a higher flatter temperature distribution, but the contracting inflow case exhibits even lower temperature than the standard axial inflow case.

5.3.5 Secondary Swirl Angle Effect

For the following two cases, the secondary inlet velocity is increased to 4 m/s, giving $v_0/u_0 = 0.4$. This is because the swirl and upstream angles given to this secondary inflow lead to a lack of penetration into the main flow at the lower velocity and the observed effects would then be minimal. The more interesting case of $v_0 = 4$ m/s permits useful observations and deductions about the effects of the secondary swirl angle (SSA) and secondary upstream angle (SUA) of the secondary flow into the main flow. Figure 34 gives the radial profiles of axial velocity and temperature at axial stations $x/D = 1.0$ and 2.5; Figure 35 gives the corresponding streamline patterns for SSA = 0, 30, 45, and 60 degrees. A secondary inlet recirculation zone is clearly seen (from the streamline patterns - just to the right of the injection location) and its size decreases as the secondary swirl angle increase. The radial profiles of the axial velocity and temperature have trends to be flatter as the secondary swirl strength increases, but this trend is not dramatic. The flatter radial profiles of the axial velocity are substantiated by the conservation of momentum, the flatter radial profiles of the temperature are due to the enhanced mixing and combustion of the secondary injection.

5.3.6 Secondary Upstream Angle Effect

When the secondary air inflow is not directly inward from boundary, the aerodynamic influences on the burning zone will be seen. With secondary upstream angle $SUA = -60$ degrees, there is a strong positive axial velocity component with the secondary flow in the downstream direction to the right, and with $SUA = +60$ degrees,

there is a strong negative axial velocity component representing inflow with a velocity component upstream toward the west wall - the upstream dome end of the combustor. Radial profiles of axial velocity and temperature are given at axial stations $x/D = 1.0$ and 2.5 in Figure 36; the corresponding streamline patterns for $SUA = -60, 0$ and $+60$ degrees are given in Figure 37. Compared with the normally injected secondary flow, a wider and longer reaction zone is clearly seen when the injected flow has a downstream axial velocity component ($SUA = -60$ degrees), and a narrower and shorter reaction zone is seen when the injected flow has an upstream axial velocity component ($SUA = 60$ degrees). An expected spike is seen in the axial velocity profile near the top wall in the case of a downstream injection velocity component. Downstream injection tends to make temperature levels much higher due to the enhanced mixing and combustion in the wider and longer reaction zone established upstream, whereas the upstream injection dilutes the primary reaction zone yielding lower reaction rates and temperature levels.

5.3.7 Closure

The developed computer code has been applied to the turbulent swirling reacting flows in a typical combustor. Parameters of special interest include the secondary to primary velocity ratio, primary swirl angle, primary contraction angle, secondary swirl angle, and secondary upstream angle. Numerical predictions were given to illustrate the dramatic effects of these parameters on the reacting flowfields via radial profiles and streamline patterns.

5.4 Reacting Flow Predictions with Three Kinetic Reaction Schemes

This application is concerned with the axisymmetric modeling approach with emphasis placed on the turbulent nonswirling reacting flow predictions. Swirl flow predictions have already been addressed in Sections 5.1 through 5.3, with and without

combustion. Here, the assessment of different combustion simulation schemes is stressed. Turbulence is simulated with the standard two-equation k- ϵ model, and combustion is simulated with one-step, two-step and four-step schemes based on the Arrhenius and Eddy-Breakup concepts. Dramatic effects are illustrated via contour maps and radial profiles of temperature and dominant species concentrations such as unburned hydrocarbon fuel, intermediate hydrocarbons, oxygen, carbon monoxide, carbon dioxide, water vapor, hydrogen and nitrogen. The validity of flowfield predictions is assessed by comparison with available experimental data.

5.4.1 Problem Description

In this application, the geometry of Lewis and Smoot [31], simulating an industrial furnace, is selected as the test case. In the experiment, coaxial streams of fuel (town gas) and air are injected into a suddenly-expanded combustion chamber, see Figure 38. The flame is stabilized at the dividing lip between the two streams. Measurements have been made of the temperature and time-mean species concentrations. The parameters and test conditions of the combustor are summarized as follows:

Air velocity, $U_{\text{air}} = 34.3$ m/sec

Air temperature, $T_{\text{air}} = 589$ ° K

Fuel velocity, $U_{\text{fuel}} = 21.3$ m/sec

Fuel temperature, $T_{\text{fuel}} = 300$ ° K

Inlet pressure, $P = 94$ kPa

Overall equivalence ratio (CH_4/O_2), OER = 1.18.

In the predictions, a non-uniform grid of 40x15 is used (NI = 40, NJ = 15). Uniform axial velocity and temperature profiles are prescribed for the fuel and air stream as given above, respectively. The inlet turbulence intensities for air and fuel are given in the measurements as 6%, and the length scales are assumed to be 0.0057 m for the air jet

and 0.0016 m for fuel jet, respectively [1]. The walls are taken to be adiabatic, and the wall function treatment is employed in the momentum equations for wall drag calculations. The fuel mixture fraction is set equal to one in the fuel stream and zero in the air stream.

5.4.2 Results and Discussion

Predictions of temperature, unburned fuel, oxygen, water vapor, carbon dioxide, carbon monoxide and hydrogen using three kinetic schemes, respectively, are presented in Figures 39 through 45 with the available experimental measurements. The time-mean reaction rate constants given in Section 3.2 are used for the predictions. Figure 39 shows the comparison between the data and the predictions for the temperature. Near the inlet (at $x/D = 0.06$), the predicted temperature profiles are in good agreement with the data. However, in the developing and middle regions (up to $x/D = 2.34$), all three models over-predict the temperature level because of the over-estimated reaction rates given by the recommended rate constants of Srinivasan et al. [2]. Generally, the higher-order scheme shows better agreement with the data than the lower-order results due to the relatively slow reaction rate. The unburned fuel mole fractions are presented in Figure 40. These profiles are in good agreement with the measurements. However, the one-step and two-step schemes over-predict the unburned fuel, and the four-step scheme under-predicts the unburned fuel due to the overly-fast estimate of the pyrolysis rate transforming into the intermediate hydrocarbons and hydrogen with little release of energy. This conclusion is substantiated by the predicted temperature levels and oxygen concentrations shown in Figure 39 and 41, respectively. For water vapor and carbon dioxide, the predicted concentrations are lower compared to the data initially (up to $x/D = 1.21$), but beyond $x/D = 2.34$, the predicted concentrations are higher due to the overly-fast estimate of the reaction rate, as seen in Figures 42 and 43. Qualitatively, the trends of these predicted profiles are in good agreement with that of the data. Figure 44 shows the carbon

monoxide mole fractions predicted by the two-step and four-step schemes, and they are significantly smaller than the measured values, especially in regions close to the axis of the combustor. Similarly, the concentration of hydrogen is under-predicted by the four-step model initially at $x/D = 2.34$, and beyond that station, it is significantly over-predicted in the regions close to the axis of the combustor, see Figure 45. All the results discussed above show good agreement with those obtained by Nikjooy et al. [1] and Srinivasan et al. [2].

Streamline patterns and contour plots of temperature and species mass fractions are presented in Figures 46 through 64, which further illustrate and complement the results discussed above. All these figures are stretched in the radial direction by 200 percent to aid observation. First, a large corner recirculation zone (due to the sudden expansion) is observed in the streamline pattern plots shown in Figures 46 through 48 with three different schemes, and approximately the same reattachment length of $x/D = 2$ is predicted. Second, the predicted flame zones are clearly delineated by the temperature contours as shown in Figures 49 through 51. Although they all look similar, the predicted maximum temperatures (given in the plots), which are used in scaling for each plot, are dramatically different. Additionally, contour maps for unburned fuel mass fractions in Figures 52 through 54, oxygen in Figures 55 through 57, water vapor in Figures 58 and 59, carbon dioxide in Figures 60 and 61, carbon monoxide in Figures 62 and 63, and hydrogen in Figure 64, further illustrate the other kinetic facets of the entire reacting flowfield. Most of the hydrocarbon fuel are consumed in the reaction zone to produce intermediate hydrocarbons, carbon monoxide, hydrogen, water vapor and carbon dioxide. Large amount of intermediate hydrocarbons, carbon monoxide and hydrogen are predicted in the reaction region, which is substantiated by the experimental measurements. The four-step scheme predicts a wider and longer carbon monoxide zone due to the relatively estimated slow reaction rate compared with the two-step scheme.

All results above are obtained by using a constant turbulent Prandtl number of 0.9 as recommended in reference [1]. Generally, they are qualitatively correct. Actually in the fully developed region, the agreement is observed to be quite good. This suggests that a good prediction of unburned fuel fraction in the reaction zone (middle region) requires a lower turbulent Prandtl number. A large number of computer runs were given to investigate the effect of turbulent Prandtl number on the flowfield prediction. It was found that in the region near the inlet, since the convection is dominant, the change of the Prandtl number over the range of 0.5 to 0.9 does not have any effect on the prediction of unburned fuel fraction. In the developing region, since the absolute levels of unburned fuel fraction are low, the difference caused by changing the Prandtl number is not significant. The middle zone is the region of very steep variation in unburned fuel fraction, and a lower Prandtl number (0.5) dramatically improved the prediction of the unburned fuel fraction in this region. Furthermore, the predicted results above are based on the assumption of equal diffusivity for all species and enthalpy. It is obvious that the values of turbulent Prandtl number are not necessarily the same for all species and may not even be uniform over the whole flowfield. Therefore, further investigation regarding the scalar transport model is required. A more realistic approach would be to abandon the constant Prandtl number assumption and proceed to evaluate the turbulent fluxes by their own transport equations.

5.4.3 Closure

The main conclusions emerging from this study can be summarized as follows:

1. The two-step and four-step schemes both show promise for application in gas turbine combustors, because more kinetic information can be qualitatively calculated with these two schemes.

2. The mechanism of the four-step scheme is valid, but needs to be further validated with simple flames (plug flow reactor, diffusion and premixed laminar, and turbulent jet flames) to establish rate constants and model constants, so that major species, such as unburned fuel, carbon monoxide and hydrogen etc., can be accurately predicted.

3. Qualitatively, satisfactory prediction of species concentrations can be obtained by using a turbulent Prandtl number that is constant over the flowfield. However, in the developing region, the isotropic diffusion model is not valid and a more realistic approach is to evaluate the turbulent fluxes by their respective transport equations.

CHAPTER VI

CLOSURE

6.1 Conclusions

A general computer code has been developed for turbulent swirling reacting flow predictions. The new code is named REFINED (acronym for Reacting Elliptic Flows IN Expansion Domains). A variety of user's choices, such as inlet velocity profiles, inlet flow parameters, chemical reaction schemes from user-oriented accuracy and complexity requirements, and interaction with flowfield color graphic display utility are included. Predicted results exhibit qualitatively good agreement with available experimental data. Important specific conclusions for each application in Chapter V are provided at the end of each section. This chapter, therefore, presents general conclusions and makes recommendations for future work. Major conclusions are:

1. Flat inlet profile assumptions, such as uniform axial and swirl velocities, produce poor predictions near the inlet region, but these assumptions do not influence greatly the flowfield calculation at further downstream locations.
2. The standard two equation k - ϵ turbulence model, although being capable of working well in many situations, is not completely satisfactory for strongly swirling flows
3. Measured inlet velocity components should be used to obtain most realistic predictions of combustor flowfields.
4. Measured inlet velocity components should be used in turbulence modeling development, in order that errors arising from incorrect inlet flow specification do not lead to erroneous conclusions.

5. Both two-step and four-step reaction schemes show promise for application in gas turbine combustors. However, they need to be further validated with simple flames to establish universal model constants and rate constants, so that major species, such as unburned fuel, carbon monoxide and hydrogen etc., can be accurately predicted.

6. In the reaction region, the isotropic diffusion model is not precisely valid and a more realistic approach is to evaluate the turbulent fluxes by their respective transport equations.

6.2. Recommendations for Future Work

Further fundamental research should be extended in several areas to develop a more powerful and accurate simulation tool for combustor flowfields. They are briefly identified as follows:

1. An advanced turbulence model such as an algebraic differential Reynolds stress model should be incorporated into the code for strong swirl flow predictions.
2. Further application about the effects of inlet flow parameters on combustor flowfields can be continued and assessed versus experimental data.
3. An intensive submodel validation and development effort, especially for the scalar transport model in high shear layer region, and the two-step and four-step chemical kinetic schemes, should be continued.
4. Radiation heat transfer should be included for improved predictions of high temperature turbulent reacting flows
5. Inclusion of a quasi-global kinetic scheme would make it possible to study the dissociation effects of important species in combustion flowfields.
6. A more accurate and stable discretization scheme should be developed and incorporated into the computer code to reduce the numerical diffusion resulting from the hybrid scheme currently used in the newly developed REFINED computer code.

REFERENCES

1. Nikjooy, Mohammad and So, Ronald M.C., "On the Modeling of Non- Reactive and Reactive Turbulent Combustor Flows," NASA CR-4041, Grants NAG3-167 and NAG3-260, April 1987.
2. Srinivasan, R., Reynolds, R., Ball, I., Berry, R., Johnson, K., and Mongia, H., "Aerothermal Modeling Program, Phase I - Final Report," NASA CR-168243, Vol. 1, August 1983.
3. Gupta, A.K., Lilley, D.G., and Syred, N., Swirl Flows, Abacus Press, Tunbridge Wells, England, 1984.
4. Gupta, A.K. and Lilley, D.G., Flowfield Modeling and Diagnostics, Abacus Press, Tunbridge Wells, England, 1985.
5. Khalil, E.E., Modeling of Furnaces and Combustors, Abacus Press, Tunbridge Wells, England, 1982.
6. Patankar, S.V., Numerical Heat Transfer and Fluid Flow, Hemisphere Publishing Corporation, London, 1980.
7. Novick, A.S., Miles, G.A., and Lilley, D.G., "Numerical Simulation of Combustor flowfields," AIAA/SAE 14th Joint Propulsion Conference, July 25-27, 1978, Las Vegas, Nevada.
8. Gosman, A.D. and Pun, W.M., "Calculation of Recirculating Flows," Report No. HTS/74/2, Department of Mechanical Engineering, Imperial College, London, England, 1974.
9. Lilley, D.G. and Rhode, D.L., "STARPIC - A Computer Code for Swirling Turbulent Axisymmetric Recirculating Flows in Practical Isothermal Combustor Geometries," NASA CR-3442, June 1981.
10. Lilley, D.G., "Primitive Pressure-Velocity Code for the Computation of Strongly Swirling Flows," AIAA Journal, Vol. 14, No. 6, June 1976.
11. Lilley, D.G., "Turbulent Swirling Flame Prediction," AIAA Journal, Vol. 12, No. 2, February 1974.

12. Khalil, E.E., Spalding, D.B., and Whitelaw, J.H., "The Calculation of Local Flow Properties in Two-Dimensional Furnaces," International Journal of Heat and Mass Transfer, Vol. 18, 1975.
13. Patankar, S.V. and Spalding, D.B., "A Computer Model for Three-Dimensional Flow in Furnaces," 14th Symposium (International) on Combustion, The Combustion Institute, Pittsburgh, Pa., 1973.
14. Abujelala, M.T. and Lilley, D.G., "Confined Swirling Flow Predictions," AIAA 21st Aerospace Sciences Meeting, AIAA-83-0316, January 10-13, 1983, Reno, Nevada.
15. Ha, S. and Lilley, D.G., "Turbulent Swirling Combustion Flow Computations Using a Boundary-Fitted Non-Orthogonal Grid System," AIAA/ASME/SAE/ASEE 25th Joint Propulsion Conference, July 10-12, 1989, Monterey, California.
16. Westbrook, C.K. and Dryer, F.L., "Simplified Reaction Mechanisms for the Oxidation of Hydrocarbon Fuels in Flames," Combustion Science and Technology, Vol. 27, 1981, pp. 31-43.
17. Hautmann D.J., Dryer, F.L., Schug, K.P. and Glassman, I., "A Multi-step Overall Kinetic Mechanism for the Oxidation of Hydrocarbons," Combustion Science and Technology, Vol. 25, 1980, pp. 219-225.
18. Habib, M.A. and Whitelaw, J.H., "Velocity Characteristics of Confined Coaxial Jets with and without Swirl," Journal of Fluid Engineering, Vol. 102, March 1980, pp. 47-53.
19. Habib, M.A. and Whitelaw, J.H., "Velocity Characteristics of a Confined Coaxial Jet," Journal of Fluid Engineering, Vol. 103, December 1979, pp. 521-529.
20. Vu, B.T. and Gouldin, F.C., "Flow Measurements in a Model Swirl Combustor," AIAA Journal, Vol. 20, No. 5, May 1982, pp. 642-651.
21. Owen, F.K., "Measurements and Observations of Turbulent Recirculation Jet Flows," AIAA Journal, Vol. 14, No. 11, November 1976, pp. 1556-1562.
22. Johnson, B.V. and Roback, R., "Mass and Momentum Turbulent Transport Experiments with Confined Swirling Coaxial Jets - Part I," AIAA/SAE/ASME 20th Joint Propulsion Conference, AIAA-84-1380, June 11-13, 1984, Cincinnati, Ohio.
23. Roback, R. and Johnson, B.V., "Mass and Momentum Turbulent Transport Experiments with Confined Swirling Coaxial Jets - Part II,"

AIAA/ASME/SAE/ASEE 22nd Joint Propulsion Conference, AIAA-86-1665,
June 16-18, 1986, Huntsville, Alabama.

24. Yoon, H.K. and Lilley, D.G., "Five-Hole Pitot Probe Time Mean Velocity Measurements in Confined Swirling Flows," AIAA Paper 83-0313, January 1983.
25. Smith, G.D., Giel, T.V., and Catalano, C.G., "Measurements of Reactive Recirculating Jet Mixing in a Combustor," AIAA Journal, Vol. 21, No. 2, 1983, pp. 270-276.
26. Gouldin, F.C., Depsky, J.S., and Lee, S.L., "Velocity Field Characteristics of a Swirling Flow Combustor," AIAA 21st Aerospace Sciences Meeting, AIAA-83-0314, January 10-13, 1983, Reno, Nevada.
27. Bake, R.J., Hutchinson, P., Khalil, E.E., and Whitelaw, J.H., "Measurements of Three Velocity Components in a Model Furnace with and without Combustion," Proceedings 15th Symposium on Combustion, 1974, pp. 553-559.
28. Owen, F.K., "Laser Velocity Measurements of a Confined Turbulent Diffusion Flame Burner," AIAA 14th Aerospace Sciences Meeting, AIAA-76-33, January 26-28, 1976, Washington, D.C.
29. Bicen, A.F. and Jones, W.P., "Velocity Characteristics of Isothermal and Combusting Flows in a Model Combustor," Combustion and Flame, Vol. 49, 1986, pp. 1-15.
30. Spadaccini, L.J., Owen, F.K., and Bowman, C.F., "Influence of Aerodynamic Phenomena on Pollutant Formation in Combustion," Environmental Protection Agency Report, EPA 600/2-76-2470, 1976.
31. Lewis, M.H. and Smoot, L.D., "Turbulent Gaseous Combustion, Part I: Local Species Concentration Measurements," Combustion and Flame, Vol. 42, 1981, pp. 183-196.
32. Hassan, M.M., Lockwood, F.C., and Moneib, H.A., "Measurements in Gas-Fired Cylindrical Furnace," Combustion and Flame, Vol. 51, 1983, pp. 249-261.
33. Larue, J.C., Samuelsen, G.S., and Seiler, E.T., "Momentum and Heat Flux in a Swirl-Stabilized Combustor," 20th Symposium (International) on Combustion, The Combustion Institute, Pittsburgh, Pa, 1984, pp. 277-285.
34. Ramos, J.I. and Somer, H.T., "Swirling Flow in Research Combustor," AIAA Journal, Vol. 23, No. 2, 1985, pp. 241-248.
35. So, R.M., Ahmed, S.A., and Mongia, H.C., "An Experimental Investigation of Gas Jets in Confined Swirling Air Flow," NASA CR-3832, 1984.

36. Weber, R., Visser, B.M., and Boysan, F., "Assessment of Turbulence Modeling for Engineering Prediction of Swirling Vortices in the Near Burner Zone," International Journal of Heat and Fluid Flow, Vol. 11, No. 3, 1990, pp. 225-235.
37. Hinze, J.O., Turbulence, McGraw-Hill, New York, 1959.
38. Schetz, J.A., Foundations of Boundary Layer Theory for Momentum, Heat and Mass Transfer, Prentice-Hall, Inc., Englewood Cliffs, New Jersey, 1984.
39. Launder, B.E. and Spalding, D.B., Mathematical Models of Turbulence, Academic Press, New York, 1972.
40. Jones, W.P. and Whitelaw, J.H., "Calculation Methods for Reacting Turbulent Flows: A Review," Combustion and Flame, Vol. 48, 1982, pp. 1-26.
41. Libby, P.A. and Williams, F.A., Turbulent Reacting Flows, Springer-Verlag, Berlin Heidelberg, New York, 1980.
42. Spalding, D.B., "Mathematical Models of Turbulent Flames: A Review," Combustion Science and Technology, Vol. 13, 1976, pp. 3-25.
43. Gupta, A.K. and Lilley, D.G., "The Gray Areas in Combustion Research," AIAA/ASME/SAE/ASEE 22nd Joint Propulsion Conference, AIAA-86-1663, June 16-18, 1986, Huntsville, Alabama.
44. Launder, B.E. and Spalding, D.B., "The Numerical Computation of Turbulent Flows," Computer Methods in Applied Mechanics and Engineering, Vol. 3, 1974, pp. 269-289.
45. Peck, R.E. and Samuelsen, G.S., "Eddy Viscosity Modeling in the Prediction of Turbulent, Backmixed Combustion Performance," Sixteenth Symposium (International) on Combustion, The Combustion Institute, Pittsburgh, Pa, 1978, pp. 1675-1687.
46. Abujelala, M.T. and Lilley, D.G., "Limitations and Empirical Extensions of the k- ϵ Model as Applied to Turbulent Confined Swirling Flows," AIAA 22nd Aerospace Sciences Meeting, AIAA-84-0441, January 9-12, 1984, Reno, Nevada.
47. Abujelala, M.T., Jackson, T.W., and Lilley, D.G., "Swirl Flow Turbulence Modeling," AIAA/SAE/ASME 20th Joint Propulsion Conference, AIAA-84-1376, June 11-13, 1984, Cincinnati, Ohio.

48. Rhode, D.L. and Stowers, S.T., "Turbulence Model Assessment for the Confined Mixing of Co-Swirling Concentric Jets," AIAA/SAE/ASME/ASEE, 21st Joint Propulsion Conference, AIAA-85-1269, July 8-10, 1985, Monterey, California.
49. Amano, R.S., "Development of a Turbulence Near-Wall Model and Its Application to Separated and Reattached Flows," Numerical Heat Transfer, Vol. 7, 1984, pp. 59-75.
50. Jennings, M.J. and Morel, T., "Observations on the Application of the k- ϵ Model to Internal Combustion Engine Flows," Combustion Science and Technology, Vol. 58, 1988, pp. 177-193.
51. Libby, P.A., Bray, K.N.C. and Moss, J.B., "Effects of Finite Reaction Rate and Molecular Transport in Premixed Turbulent Combustion," Combustion and Flame, Vol. 34, 1979, pp. 285-301.
52. Libby, P.A. and Bray, K.N.C., "Counter-Gradient Diffusion in Premixed Turbulent Flames," AIAA 18th Aerospace Sciences Meeting, AIAA-80-0013, January 14-16, 1980, Pasadena, California.
53. Libby, P.A. and Bray, K.N.C., "Implications of the Laminar Flamelet Model in Premixed Turbulent Combustion," Combustion and Flame, Vol. 39, 1980, pp. 33-42.
54. Libby, P.A. and Bray, K.N.C., "Variable Density Effects in Premixed Turbulent Flames," AIAA Journal, Vol. 15, No. 8, 1977, pp. 1186-1193.
55. Pope, S.B., "The Probability Approach to the Modelling of Turbulent Reacting Flows," Combustion and Flame, Vol. 27, 1976, pp. 299-312.
56. Bray, K.N.C., "The Interaction between Turbulence and Combustion," 17th Symposium (International) on Combustion, The Combustion Institute, Pittsburgh, Pa, 1979, pp. 223-233.
57. Ballal, D.R. and Chent, T.H., "Turbulence-Combustion Interaction in Practical Combustion Systems," AIAA/ASME/SAE/ASEE 22nd Joint Propulsion Conference, AIAA-86-1607, June 16-18, 1986, Huntsville, Alabama.
58. Ballal, D.R., "Studies of Turbulent Flow-Interaction," AIAA Journal, Vol. 24, No. 7, 1986, pp. 1148-1154.
59. Chomiak, J., "Dissipation Fluctuations and the Structure and Propagation of Turbulent Flames Premixed Gases at High Reynolds Numbers," 16th Symposium (International) on Combustion, The Combustion Institute, Pittsburgh, PA, 1978, pp. 1665-1673.

60. Sturgess, G.J., "Aerothermal Modeling, Phase I - Final Report," NASA CR-168202, May 27, 1983.
61. Agarwal, R.K., "A Third-Order-Accurate Upwind Scheme for Navier-Stokes Solutions at High Reynolds Numbers," AIAA 19th Aerospace Sciences Meeting, AIAA-81-0112, January 12-15, 1981, St. Louis, Missouri.
62. Leonard, B.P., "A Stable and Accurate Convective Modeling Procedure Based on Quadratic Upstream Interpolation," Computer Methods in Applied Mechanics and Engineering, Vol. 19, 1979, pp. 59-98.
63. Raithby, G.D., "Skew-Upstream Differencing Scheme for Problems Involving Fluid Flow," Computer Methods in Applied Mechanics and Engineering, Vol. 9, 1976.
64. Rubin, S.G. and Graves Jr., R.A., "Viscous Flow Solutions with a Cubic Spline Approximation," Computers and Fluids, Vol. 3, 1975, pp. 1-36.
65. Glas, J. and Rodi, W., "A Higher Order Numerical Scheme for Scalar Transport," Computer Methods in Applied Mechanics and Engineering, Vol. 31, 1982, pp. 337-358.
66. Boris, J.P. and Book, D.L., "Flux-Corrected Transport I: Shasta - A Fluid Transport Algorithm That Works," Journal of Computational Physics, Vol. 11, 1973.
67. Syed, S.A., Pratt & Whitney, and Chiappetta, L., "Finite Difference Methods for Reducing Numerical Diffusion in TEACH-type Calculations," AIAA 23rd Aerospace Sciences Meeting, AIAA--85-0057, January 14-17, 1985, Reno, Nevada.
68. Syed, S.A., Chiappetta, L.M., and Gosman, A.D., "Error Reduction Program, Final Report," NASA CR-174776, January 1985.
69. Syed, S.A., Pratt & Whitney, Gosman, A.D., and Peric, M., "Assessment of Discretization Schemes to Reduce Numerical Diffusion in the Calculation of Complex Flows," AIAA 23rd Aerospace Sciences Meeting, AIAA-85-0441, January 14-17, 1985, Reno, Nevada.
70. Lin, T.K., "Combustor Flowfield Color Display," Work in Progress, School of Mechanical and Aerospace Engineering, Oklahoma State University, Stillwater, Oklahoma, 1994.
71. Dong, M.C. and Lilley, D.G., "Combustion Flowfield Prediction for CVD Diamond Synthesis," ASME International Computer in Engineering Conference, San Francisco, CA, August 2-6, 1992.

72. Dong, M.C. and Lilley, D.G., "Impinging Flame Prediction for CVD Diamond Synthesis," ASME International Computer in Engineering Conference, San Diego, CA, August 9-11, 1993.
73. Yoon, H.K. and Lilley, D.G., "Five-Hole Pitot Probe Time-Mean Velocity Measurements in Confined Swirling Flows," Paper AIAA-83-0315, Reno, Nevada, January 10-13, 1983.
74. Dong, M.C. and Lilley, D.G., "Inlet Velocity Profile Effects on Turbulent Swirling Flow Predictions," Journal of Propulsion and Power, Vol. 10, No. 2, pp. 155-160, March-April 1994.
75. Dong, M.C. and Lilley, D.G., "Effect of Inlet Velocity Profiles on Downstream Flow Development of Turbulent Swirling Flows," 28th Annual Intersociety Energy Conversion Engineering Conference, Atlanta, GA, August 8-13, 1993.
76. Sander, G.F., "Axial Vane-Type Swirling Performance Characteristics," M.S. Thesis, School of Mechanical and Aerospace Engineering, Oklahoma State University, Stillwater, Oklahoma, May 1983.
77. Sander, G.F. and Lilley, D.G., "The Performance of an Annular Vane Swirler," Paper AIAA-83-1326, Seattle, Washington, June 27-29, 1983.
78. Launder, B.E. and Spalding, D.B., "The Numerical Computation of Turbulent Flows," Comp. Methods in Applied Mechanical and Engineering, Vol. 3, March 1974, pp. 269-289.
79. Dong, M.C. and Lilley, D.G., "Effect of Inlet Flow Parameters on Confined Turbulent Swirling Flow," ASME International Computers in Engineering Conference, San Diego, CA, August 3-5, 1993.
80. Dong, M.C. and Lilley, D.G., "Parameter Effects on Flow Patterns in Confined Turbulent Swirling Flows," International Joint Power Generation Conference, Kansas City, MI, October 17-21, 1993.
81. Dong, M.C. and Lilley, D.G., "A PC-Based Computer Code for Axisymmetric Turbulent Swirling Reacting Flows," International Joint Power Generation Conference, Atlanta, GA, October 18-22, 1992.
82. Dong, M.C. and Lilley, D.G., "Parameter Effects on Turbulent Swirling Flames in Combustors," 27th Annual Intersociety Energy Conversion Engineering Conference, San Diego, CA, August 3-7, 1992.

APPENDIXES

APPENDIX A

TABLES

TABLE I
SOURCE TERMS AND EXCHANGE COEFFICIENTS
USED IN THE GENERAL EQUATION OF ϕ
ONE-STEP SCHEME

ϕ	Γ_ϕ	S_ϕ
1	0	0
u	μ	$-\frac{\partial p}{\partial x} + S^u$
v	μ	$-\frac{\partial p}{\partial r} + \frac{\rho w^2}{r} - \frac{2v}{r^2} + S^v$
w	μ	$-\frac{\rho v w}{r} - \frac{w}{r^2} \frac{\partial}{\partial r}(r\mu) + S^w$
h	μ/σ_h	0
m_{fu}	μ/σ_{fu}	S_{fu}
$m_{ox} - im_{fu}$	μ/σ_f	0
k	μ/σ_k	$G - C_d \rho \varepsilon$
ε	μ/σ_ε	$(C_1 \varepsilon G - C_2 \rho \varepsilon^2) / k$
$S^u = \frac{\partial}{\partial x} \left(\mu \frac{\partial u}{\partial x} \right) + \frac{1}{r} \frac{\partial}{\partial r} \left(r \mu \frac{\partial v}{\partial x} \right)$ $S^v = \frac{\partial}{\partial x} \left(\mu \frac{\partial u}{\partial r} \right) + \frac{1}{r} \frac{\partial}{\partial r} \left(r \mu \frac{\partial v}{\partial r} \right)$ $S^w = 0$ $G = \mu \left\{ 2 \left[\left(\frac{\partial u}{\partial x} \right)^2 + \left(\frac{\partial v}{\partial r} \right)^2 + \left(\frac{v}{r} \right)^2 \right] + \left(\frac{\partial u}{\partial r} + \frac{\partial v}{\partial x} \right)^2 + \left[r \frac{\partial}{\partial r} \left(\frac{w}{r} \right) \right]^2 + \left(\frac{\partial w}{\partial x} \right)^2 \right\}$		

TABLE II
SOURCE TERMS FOR CHEMICAL SPECIES
TWO - STEP SCHEME

ϕ	S_ϕ
m_{fu}	S_{fu}
m_{CO}	$S_{CO} - r_2 S_{fu}$
m_{OX}	$r_1 S_{fu} + r_4 S_{CO}$
m_{CO_2}	$-r_5 S_{CO}$
m_{H_2O}	$-r_3 S_{fu}$
$\phi_A = m_{OX} - (r_1 + r_2 r_4) m_{fu} - r_4 m_{CO}$	0
$\phi_B = m_{CO_2} + r_5 m_{CO} + r_2 r_5 m_{fu}$	0
$\phi_C = m_{H_2O} + r_3 m_{fu}$	0

TABLE III
SOURCE TERMS FOR CHEMICAL SPECIES
FOUR - STEP SCHEME

ϕ	S_ϕ
m_{fu}	S_{fu}
$m_{C_xH_{y-2}}$	$S_{C_xH_{y-2}} - r_1 S_{fu}$
m_{CO}	$S_{CO} - r_4 S_{C_xH_{y-2}}$
m_{H_2}	$S_{H_2} - r_2 S_{fu} - r_5 S_{C_xH_{y-2}}$
m_{O_2}	$r_3 S_{C_xH_{y-2}} + r_6 S_{CO} + r_8 S_{H_2}$
m_{CO_2}	$-r_7 S_{CO}$
m_{H_2O}	$-r_9 S_{H_2}$
$\phi_A = m_{O_2} - (r_3 + r_4 r_6 + r_5 r_8) m_{C_xH_{y-2}} - r_6 m_{CO} - r_8 m_{H_2} - (r_1 r_3 + r_1 r_4 r_6 + r_1 r_5 r_8 + r_2 r_8) m_{fu}$	0
$\phi_B = m_{CO} + r_7 m_{CO} + r_4 r_7 m_{C_xH_{y-2}} + r_1 r_4 r_7 m_{fu}$	0
$\phi_C = m_{H_2O} + r_9 m_{H_2} + (r_2 r_9 + r_1 r_5 r_9) m_{fu} + r_5 r_9 m_{C_xH_{y-2}}$	0

TABLE IV

THE FORM OF THE COMPONENTS OF
THE LINEARIZED SOURCE TERMS
ONE - STEP SCHEME

ϕ	Γ_ϕ	S_p^ϕ	S_u^ϕ / V
1	0	0	0
u	μ	0	$S^u - \frac{\partial p}{\partial x}$
v	μ	$-2 \frac{\mu}{r^2}$	$S^v + \frac{\rho w^2}{r} - \frac{\partial p}{\partial r}$
w	μ	0	$-\frac{\rho v w}{r} - \frac{w}{r^2} \frac{\partial}{\partial r}(r\mu)$
h	μ / σ_h	0	0
m_{fu}	μ / σ_m	$-S_{fu} / m_{fu}$	0
$m_{ox} - im_{fu}$	μ / σ_f	0	0
k	μ / σ_k	$-C_\mu C_D \rho^2 k / \mu$	G
ε	μ / σ_ε	$-C_2 \rho \varepsilon / k$	$C_1 C_\mu G \rho k / \mu$

S^u , S^v and G are as in Table I

TABLE V
NEWLY DEFINED FORTRAN VARIABLES

Variables	Definitions
AN2(I,J)	Nitrogen mass fraction
AX	Carbon composition of hydrocarbon fuel
AY	Hydrogen composition of hydrocarbon fuel
CALCF2	New solver subroutine for intermediate hydrocarbon fuels
CALCCO	New solver subroutine for carbon monoxide
CALCH2	New solver subroutine for hydrogen
CFU	Specific heat of hydrocarbon fuel
CH2	Specific heat of hydrogen
CN2	Specific heat of nitrogen
CPR	Specific heat of product
CCO2	Specific heat of carbon dioxide
CH2O	Specific heat of water vapor
COX	Specific heat of oxygen
CFU2	Specific heat of intermediate hydrocarbons
CCO	Specific heat of carbon monoxide
CO(I,J)	Carbon monoxide mass fraction
CO2(I,J)	Carbon dioxide mass fraction

TABLE V Continued

Variables	Definitions
FU(I,J)	Unburned fuel mass fraction
FU2(I,J)	Intermediate hydrocarbon fuel mass fraction
GRAPHS	Subroutine to generate data file for color graphic display utility
H2(I,J)	Hydrogen mass fraction
H2O(I,J)	Water vapor mass fraction
HFU	Heat of combustion for hydrocarbon fuel
HCO	Heat of combustion for carbon monoxide
HH2	Heat of combustion for hydrogen
HFU2	Heat of combustion for intermediate hydrocarbons
IMODEL	Control parameter for kinetic schemes
IINE	East grid number of secondary top circumferential inlet
IINW	West grid number of secondary top circumferential inlet
JINAN	North grid number of central pipe inlet
JINAS	South grid number of central pipe inlet
JINBN	North grid number of central annular inlet
JINBS	South grid number of central annular inlet
OX(I,J)	Oxygen mass fraction
PCA	Primary contraction angle

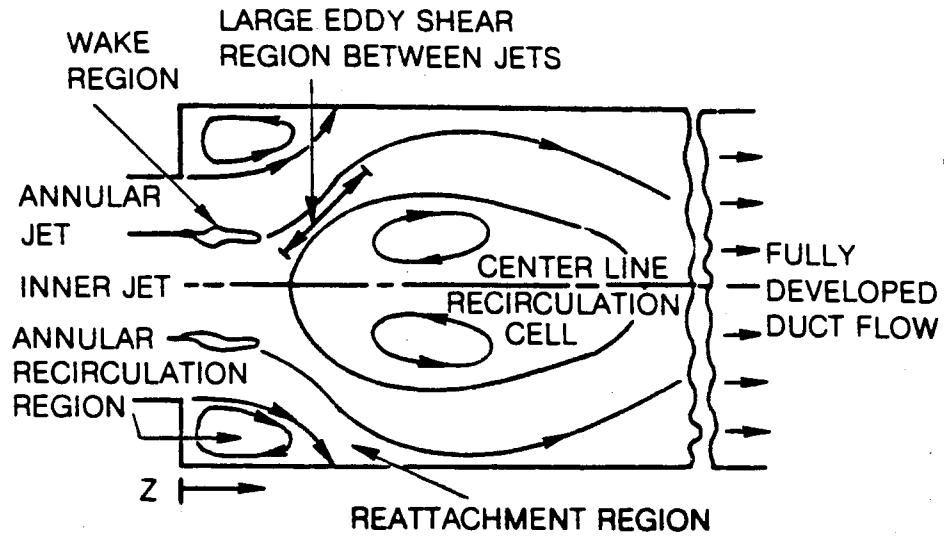
TABLE V Continued

Variables	Definitions
PSA	Primary swirl angle
PR(I,J)	Product mass fraction
RATIO(s)	Mass ratios based on different kinetic steps
SSA	Secondary swirl angle
SUA	Secondary upstream angle
URFF	Underrelaxation factor for hydrocarbon fuel mass fraction
URFF2	Underrelaxation factor for intermediate fuel mass fraction
URFCO	Underrelaxation factor for carbon monoxide mass fraction
URFH2	Underrelaxation factor for hydrogen mass fraction
WFU	Molecular weight of hydrocarbon fuel
WFU2	Molecular weight of intermediate hydrocarbon fuel
WOX	Molecular weight of oxygen
WH2O	Molecular weight of water
WCO2	Molecular weight of carbon dioxide
WCO	Molecular weight of carbon monoxide
WH2	Molecular weight of hydrogen
WPR	Molecular weight of product
WN2	Molecular weight of nitrogen

APPENDIX B

FIGURES

(a) Swirling flow



(b) Non-swirling flow

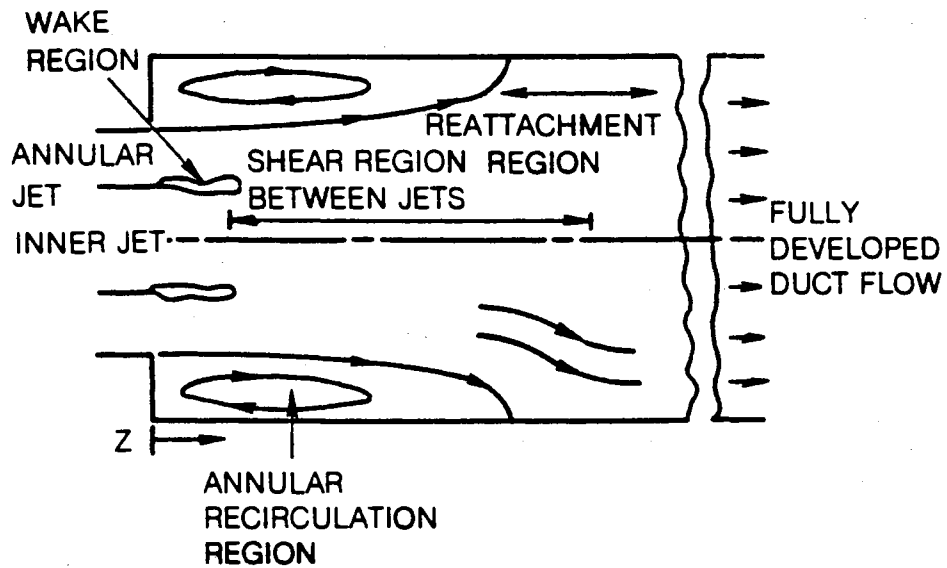
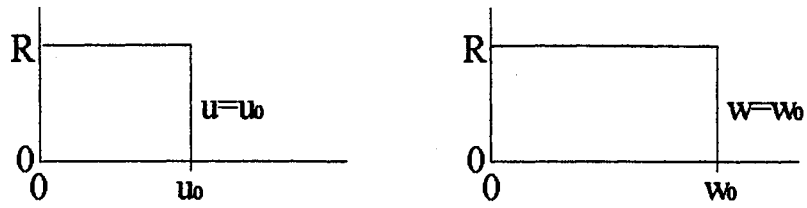
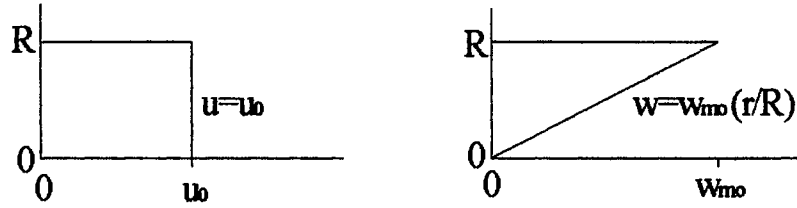


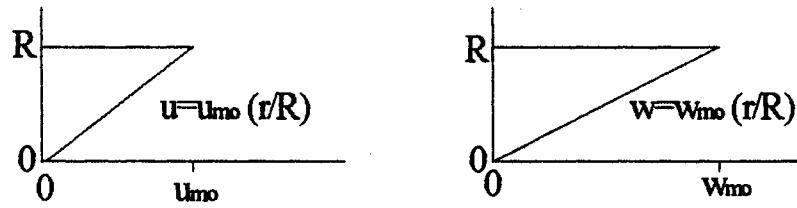
Figure 1. Schematic of Flow Regions [1]



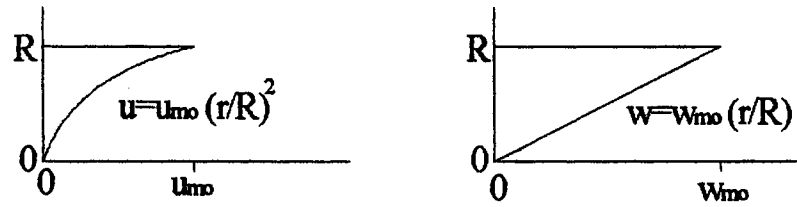
(a) Case 1 - Flat axial and swirl profiles



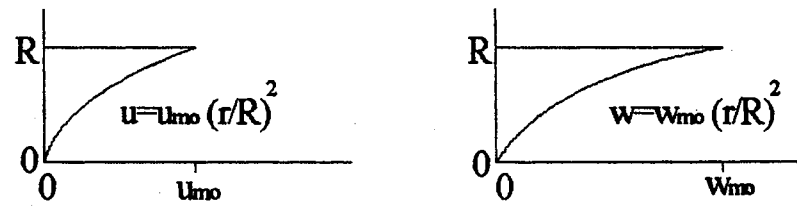
(b) Case 2 - Flat axial and linear swirl profiles



(c) Case 3 - Linear axial and swirl profiles



(d) Case 4 - Parabolic axial and linear swirl profiles



(e) Case 5 - Parabolic axial and swirl profiles

Figure 2. Idealized Axial and Swirl Velocity Profile Cases

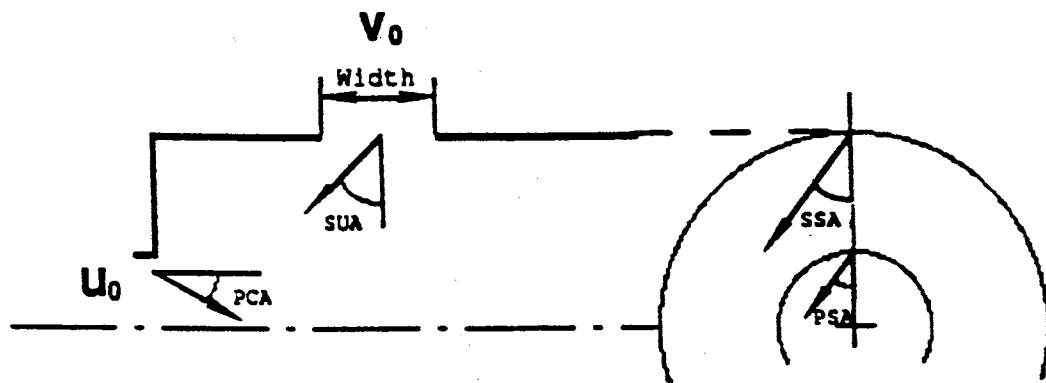
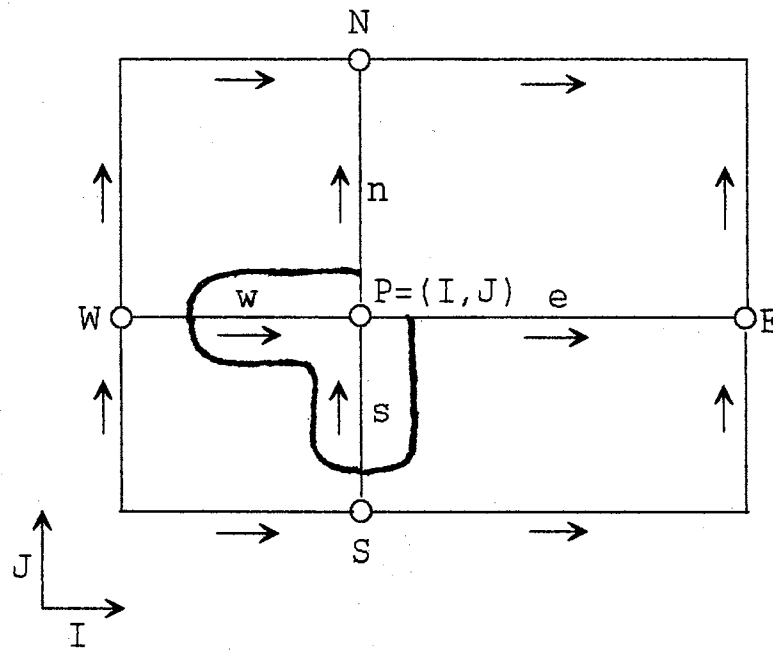


Figure 3. Inflow Parameters To Be Investigated



THREE GRIDS:

For p , w etc. - at position marked (\circ)

For u velocity - at position marked (\rightarrow)

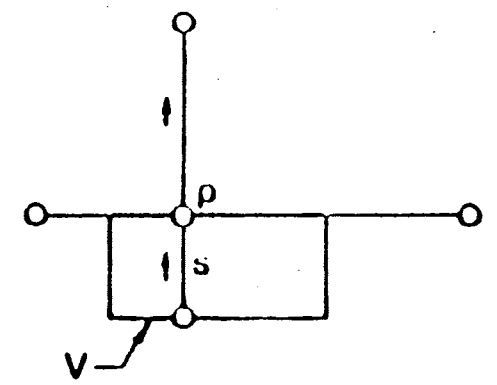
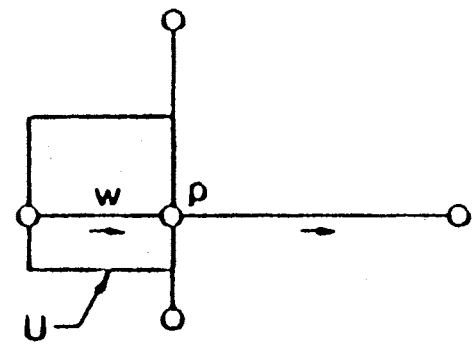
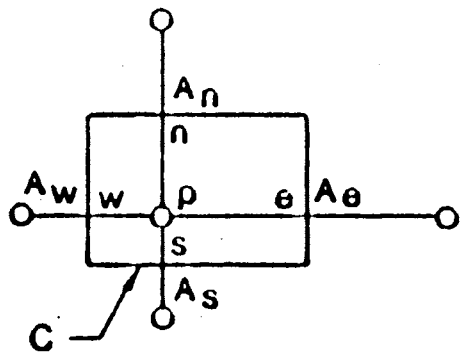
For v velocity - at position marked (\uparrow)

Figure 4. Staggered Grid and Notation for the Rectangular Computational Mesh

ρ, w ETC.
○

u
→

v
↑



**CONTROL VOLUMES C, U, V FACE
AREAS A_n, A_s, A_e AND A_w FOR C, SIMILAR FOR U AND V**

Figure 5. The Three Control Volumes Associated with the Points of Grids

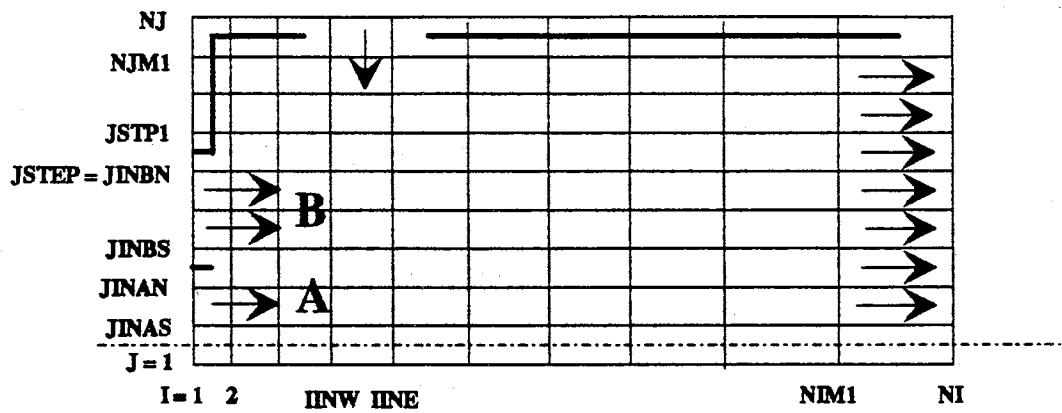


Figure 6. Multi-Inlet Grid System

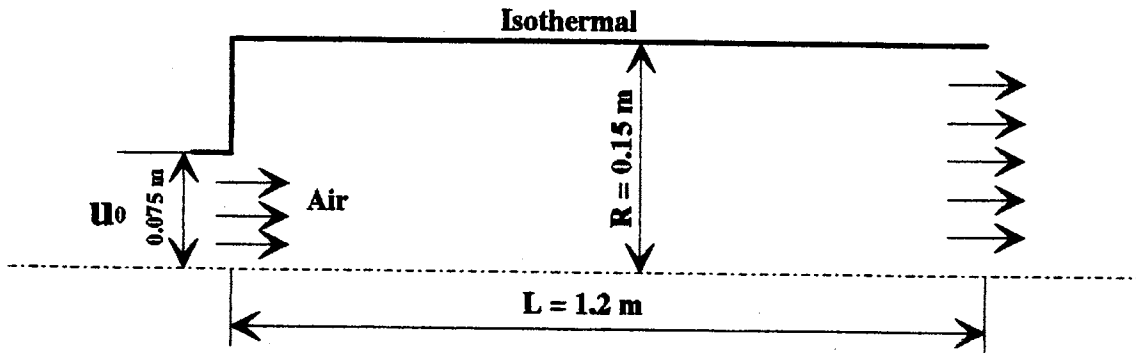


Figure 7. Schematic of The Combustor Domain

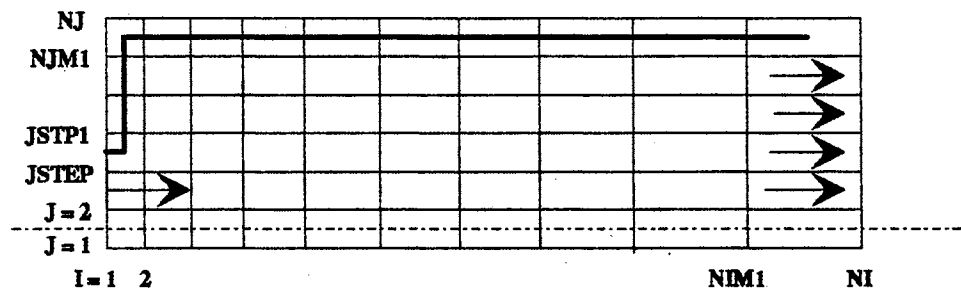


Figure 8. Schematic of Non-Uniform Rectangular Grid System

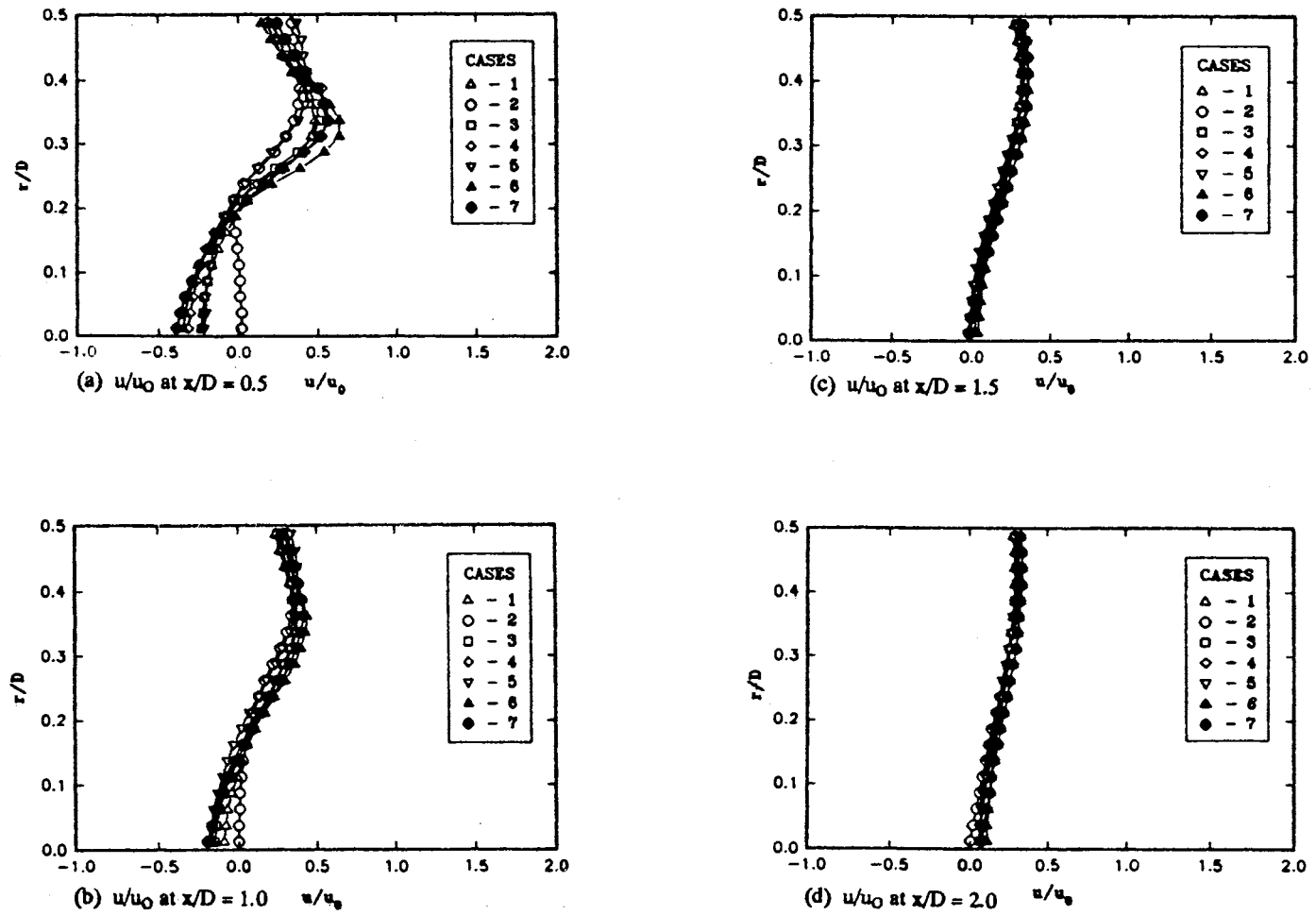


Figure 9. Predicted Velocity Profiles for $\theta = 45$ Degrees
Using Various Inlet Conditions

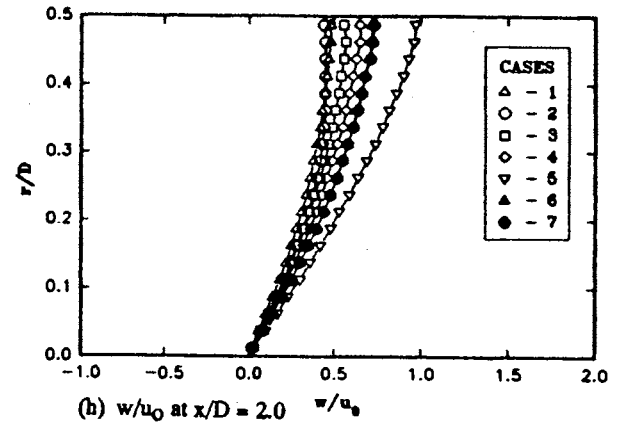
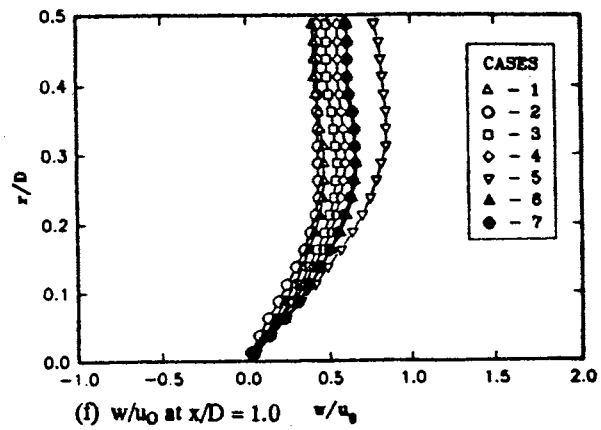
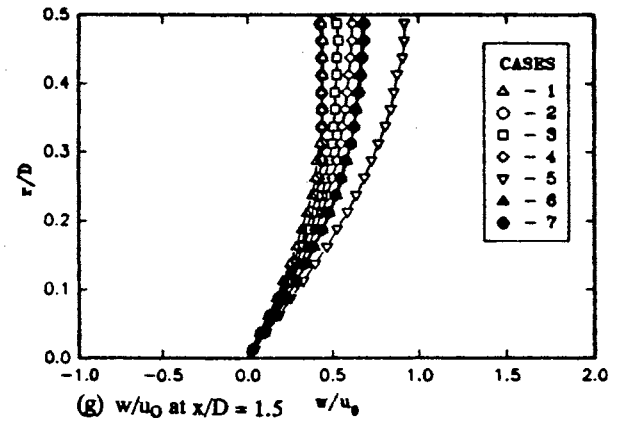
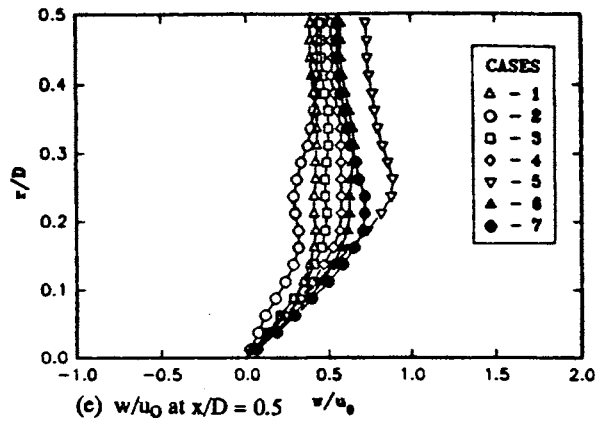
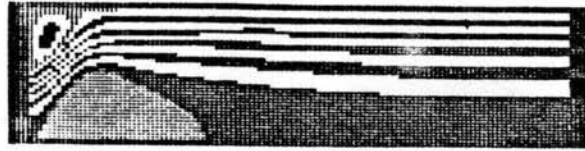


Figure 9. Continued



(a) Case 1 - Flat axial and swirl profiles



(b) Case 2 - Flat axial and linear swirl profiles



(c) Case 3 - Linear axial and swirl profiles



(d) Case 4 - Parabolic axial and linear swirl profiles



(e) Case 5 - Parabolic axial and swirl profiles



(f) Case 6 - Measured inlet axial and swirl velocities



(g) Case 7 - Measured inlet axial, radial and swirl velocities

Figure 10. Predicted Streamlines for $\theta = 45$ Degrees Flowfield Using Various Inlet Conditions

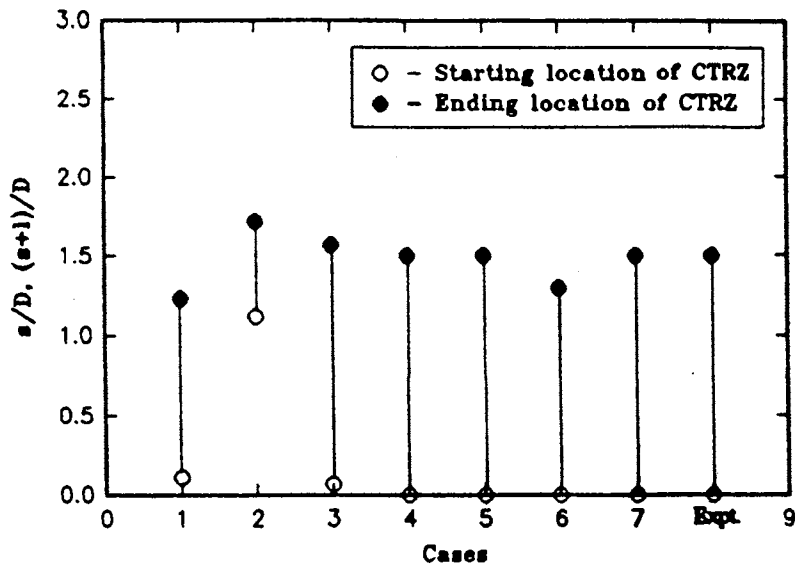


Figure 11. Location of Central Recirculation Zone on x-Axis for Swirl Vane Angle = 45 Degrees

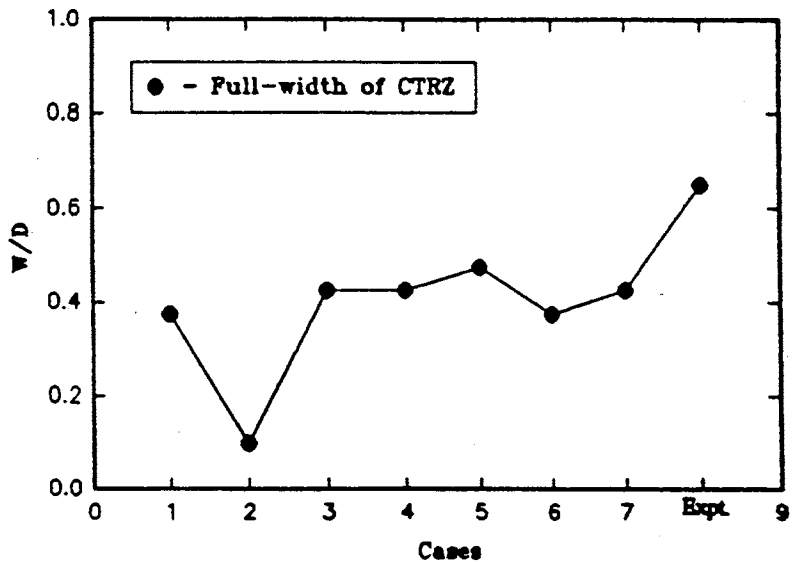


Figure 12. Full-Width of Central Recirculation Zone for Swirl Vane Angle = 45 Degrees

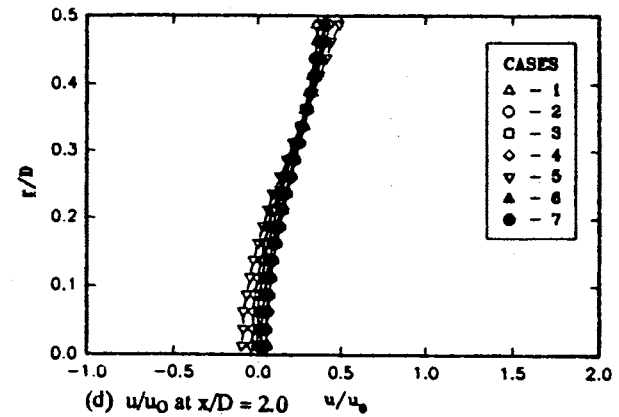
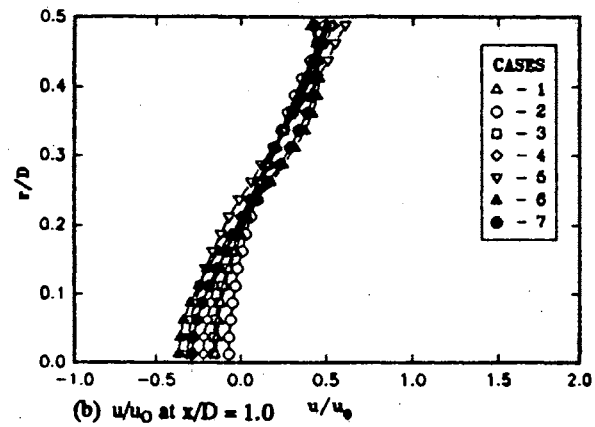
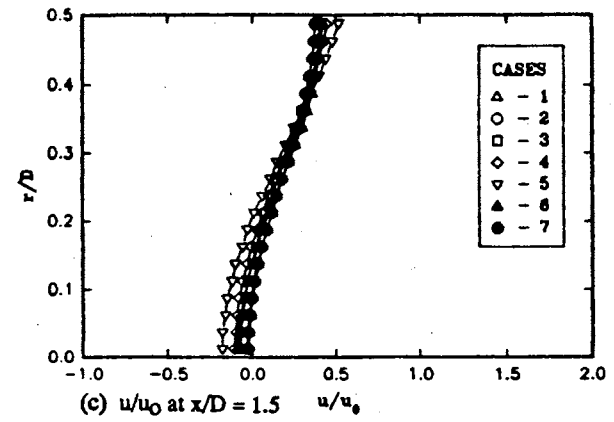
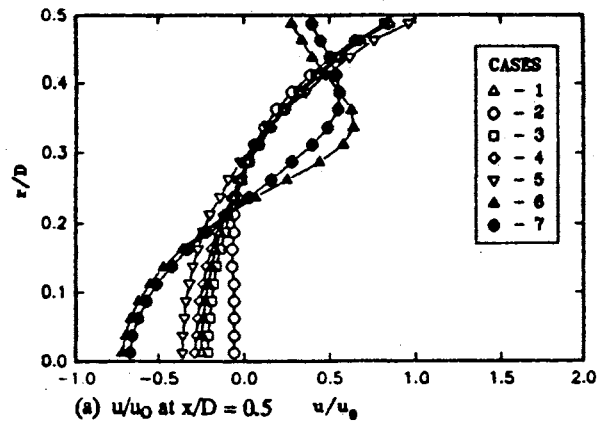


Figure 13. Predicted Velocity Profiles for $\theta = 70$ Degrees
Using Various Inlet Conditions

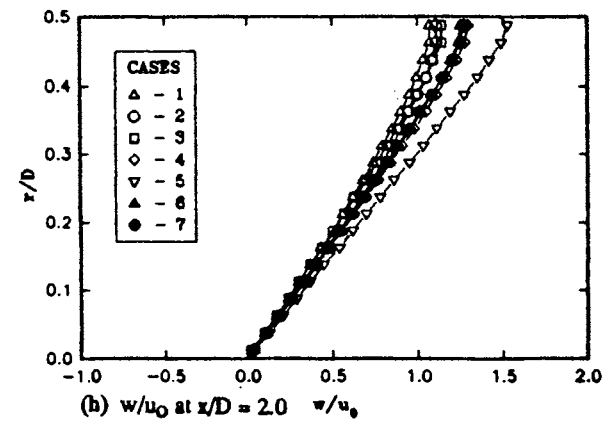
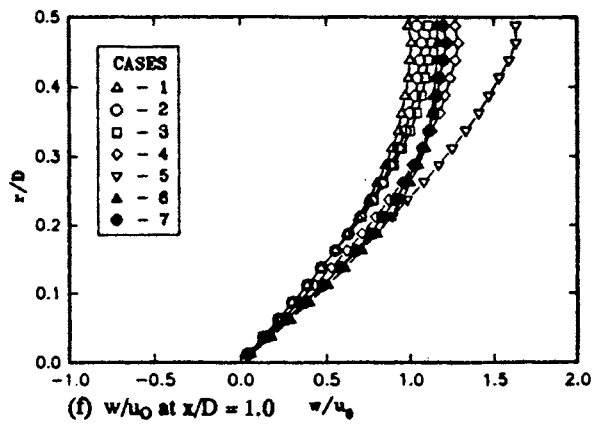
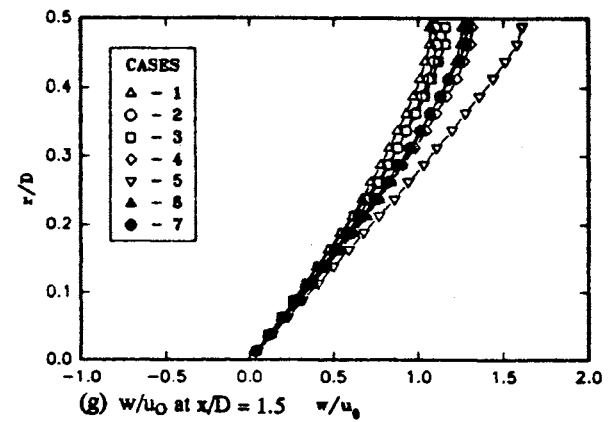
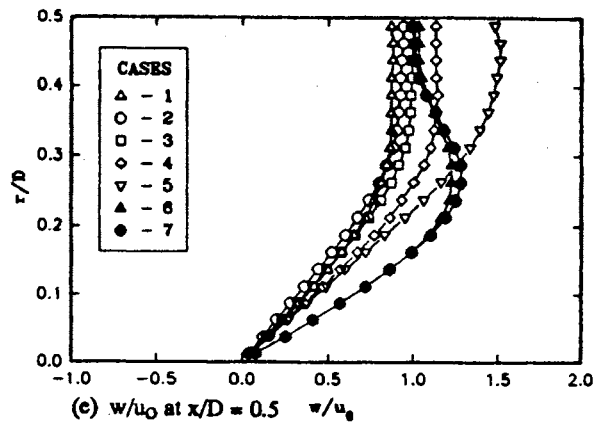


Figure 13. Continued



(a) Case 1 - Flat axial and swirl profiles



(b) Case 2 - Flat axial and linear swirl profiles



(c) Case 3 - Linear axial and swirl profiles



(d) Case 4 - Parabolic axial and linear swirl profiles



(e) Case 5 - Parabolic axial and swirl profiles



(f) Case 6 - Measured inlet axial and swirl velocities



(g) Case 7 - Measured inlet axial, radial and swirl velocities

Figure 14. Predicted Streamlines for $\theta = 70$ Degrees Flowfield Using Various Inlet Conditions

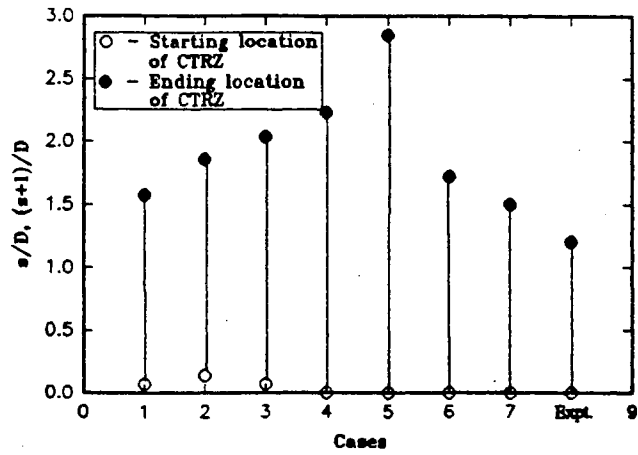


Figure 15. Location of Central Recirculation Zone on x-Axis or Swirl Vane Angle = 70 Degrees

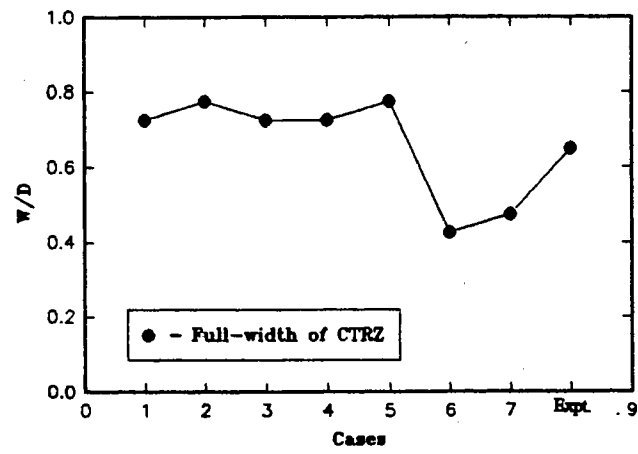


Figure 16. Full-Width of Central Recirculation Zone for Swirl Vane Angle = 70 Degrees

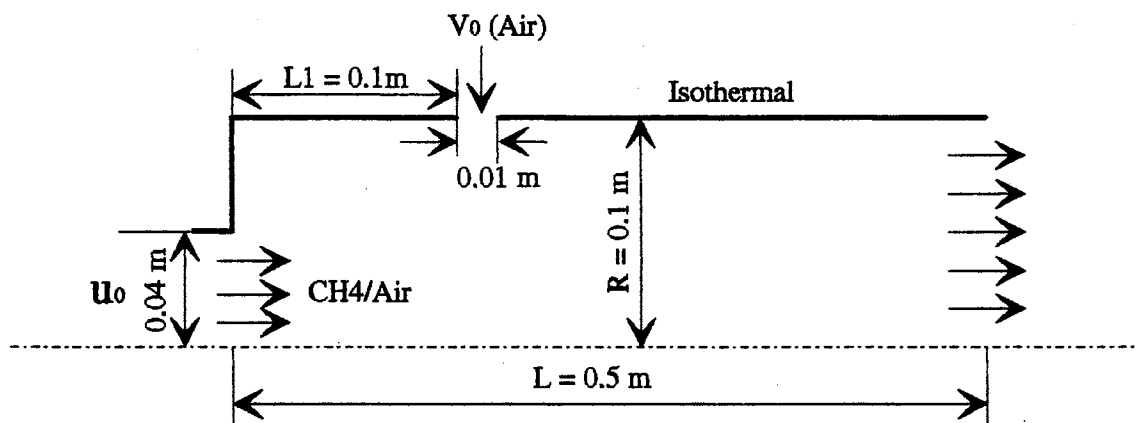


Figure 17. Schematic of the Model Combustor Geometry

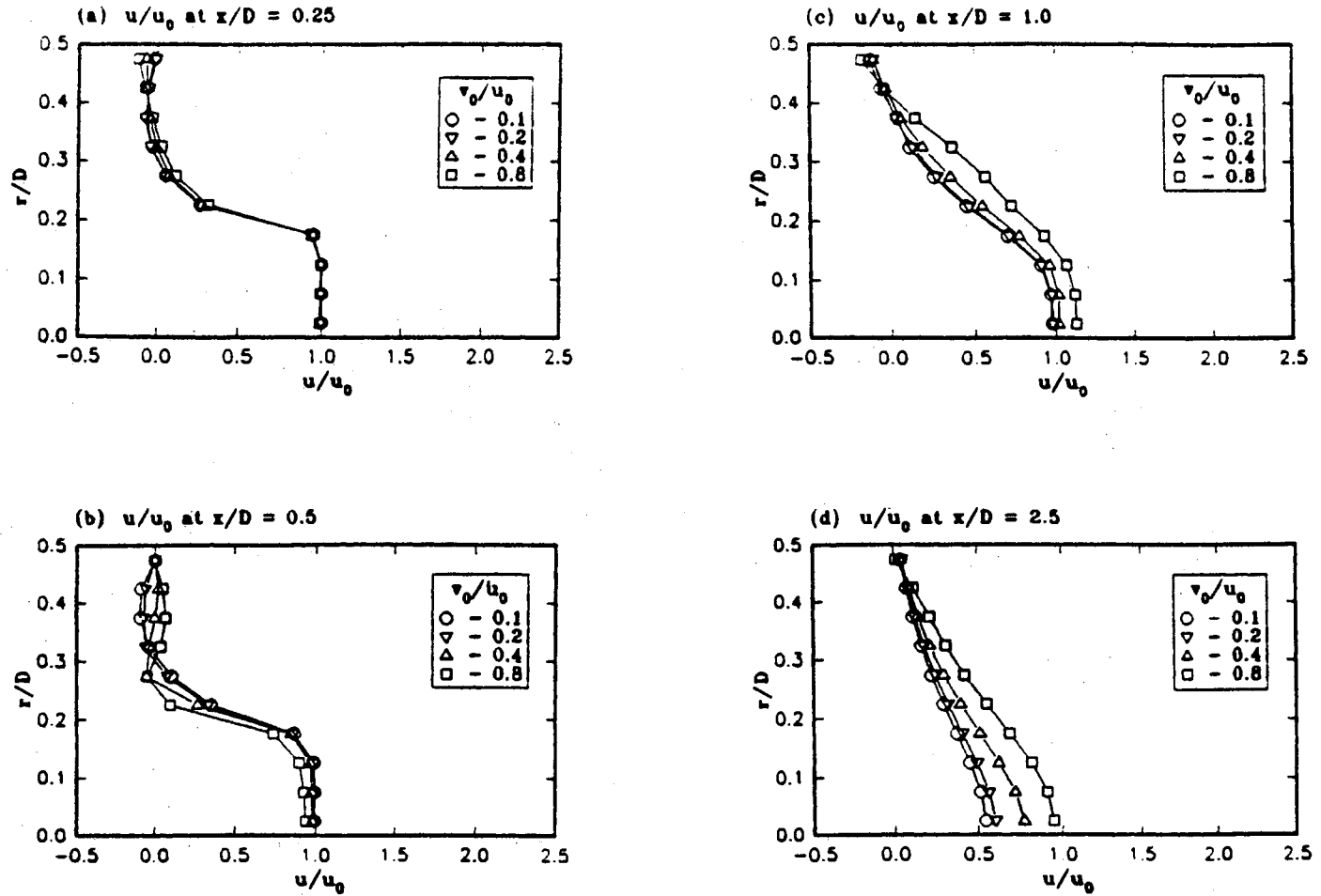


Figure 18. Effects of Secondary Injection Velocity on Axial Velocity for Nonreacting Flows

(a) $v_0/u_0 = 0.1$



(b) $v_0/u_0 = 0.2$



(c) $v_0/u_0 = 0.4$



(d) $v_0/u_0 = 0.8$



Figure 19. Effects of Secondary Injection Velocity on Streamline Patterns for Nonreacting Flows

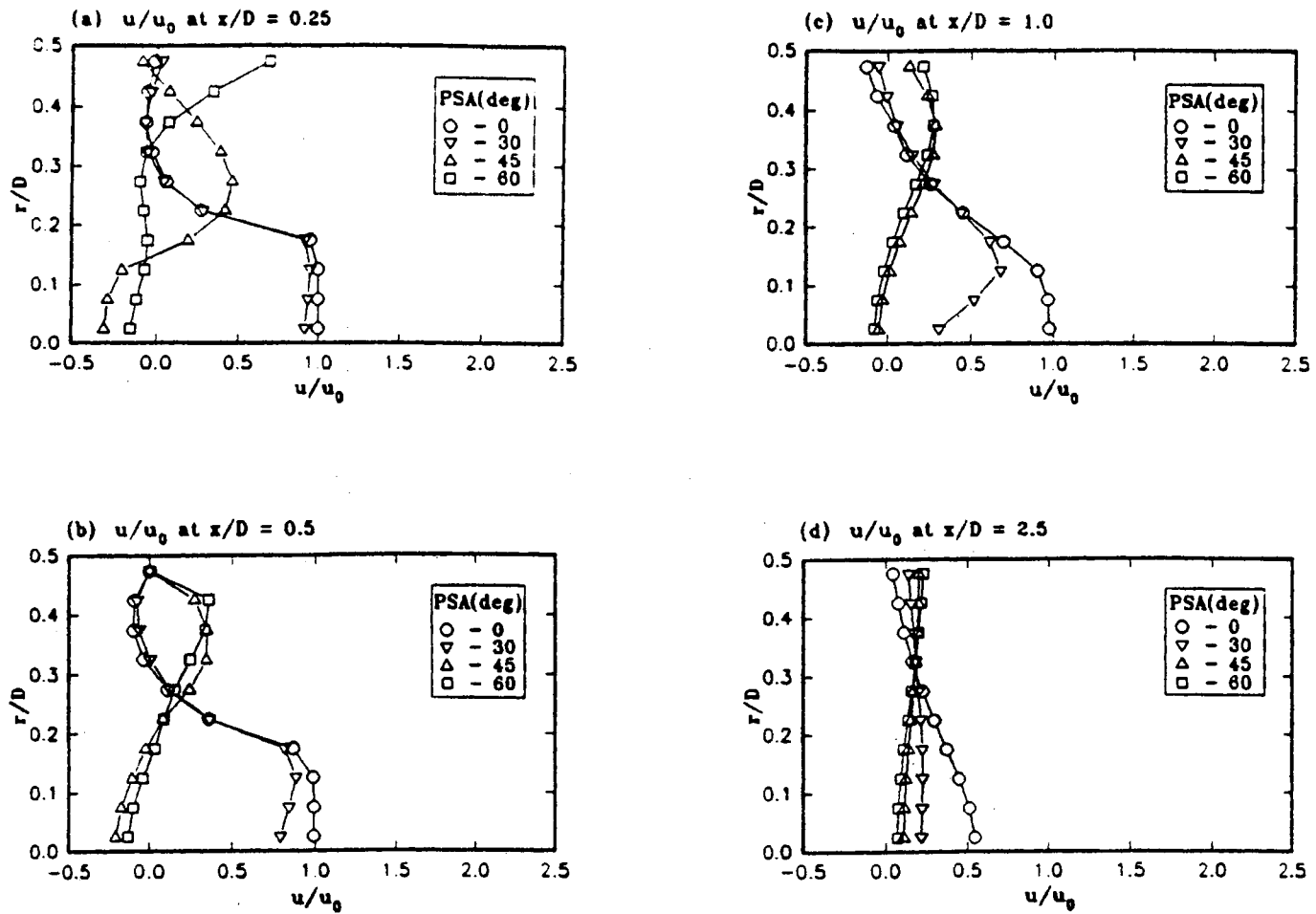


Figure 20. Effects of Primary Swirl Angle on Axial and Swirl Velocities for Nonreacting Flows

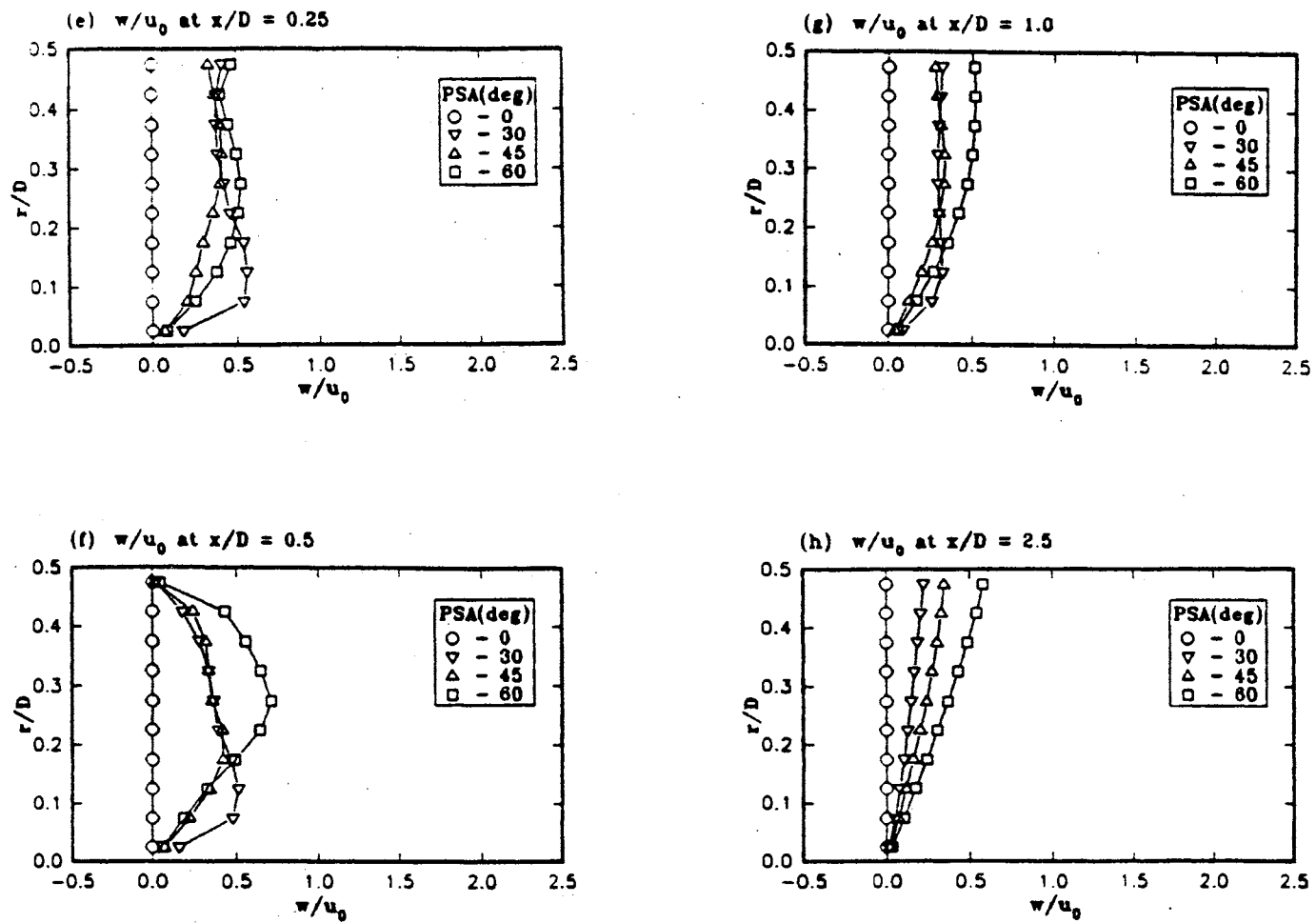


Figure 20. Continued

(a) PSA = 0 degrees



(b) PSA = 30 degrees



(c) PSA = 45 degrees



(d) PSA = 60 degrees



Figure 21. Effects of Primary Swirl Angle on Streamline Patterns for Nonreacting Flows

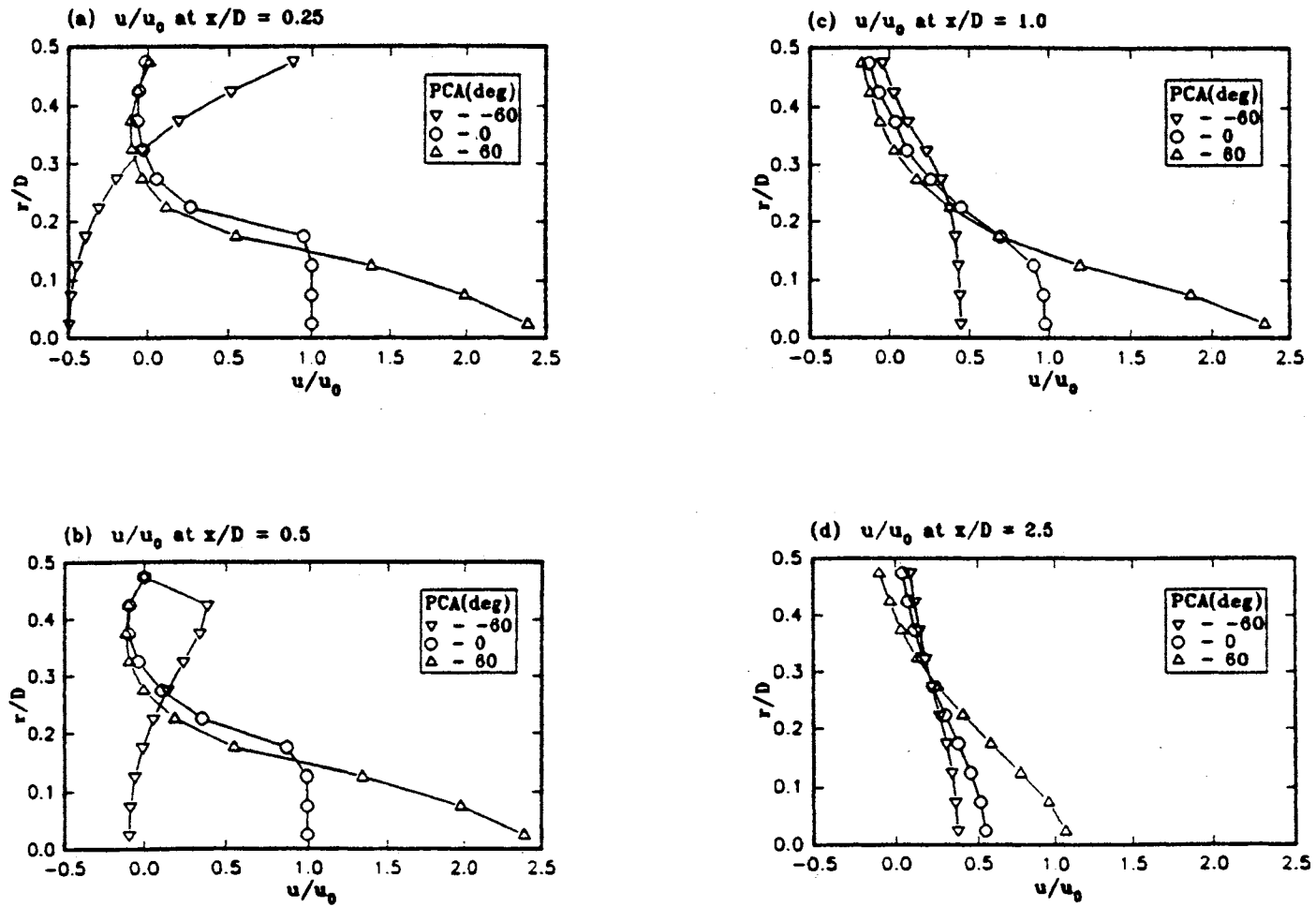
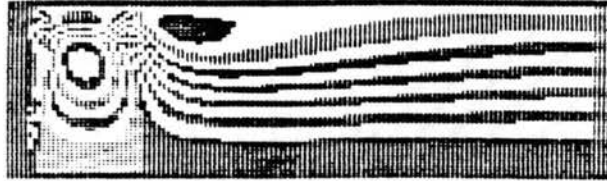


Figure 22. Effect of Primary Contraction Angle on Axial Velocity for Nonreacting Flows

(a) PCA = -60 degrees



(b) PCA = 0 degrees



(c) PCA = 60 degrees



Figure 23. Effect of Primary Contraction Angle on Streamline Patterns for Nonreacting Flows

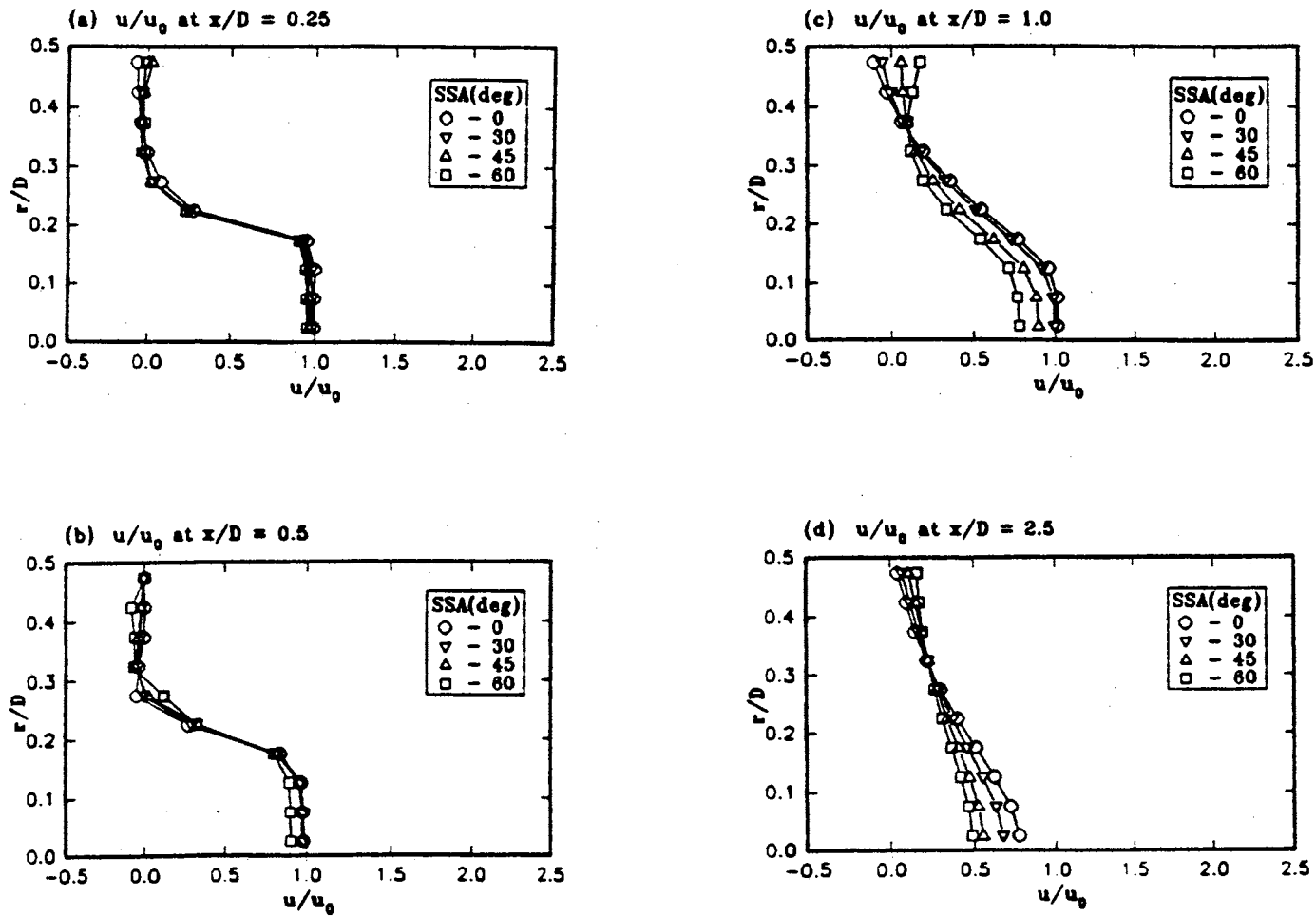


Figure 24. Effect of Secondary Swirl Angle on Axial and Swirl Velocities for Nonreacting Flows

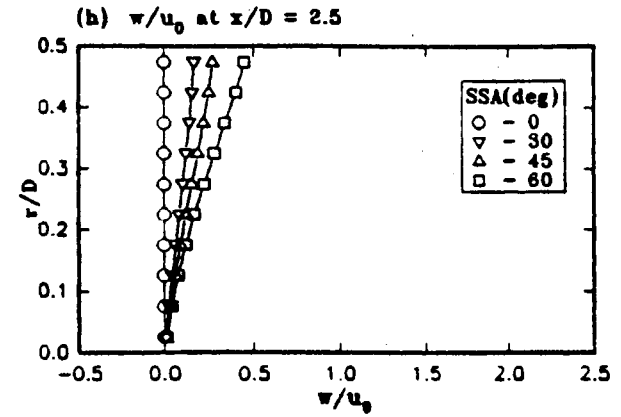
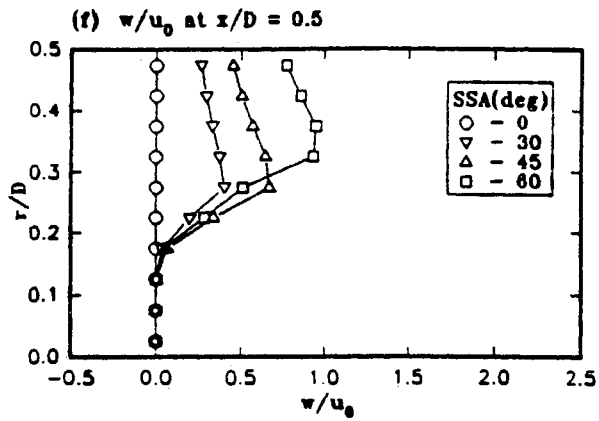
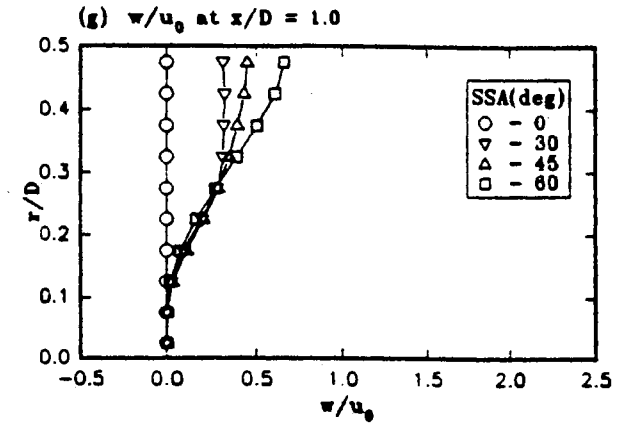
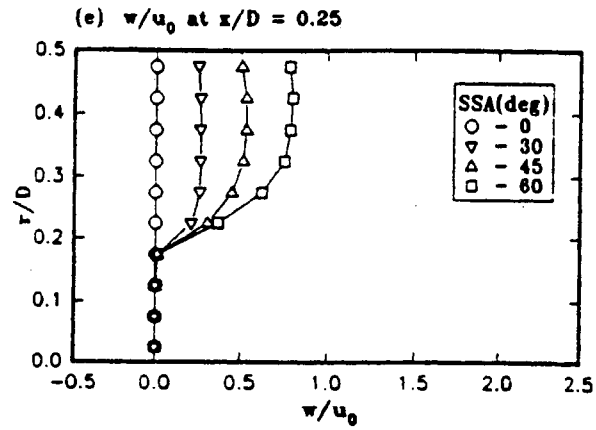
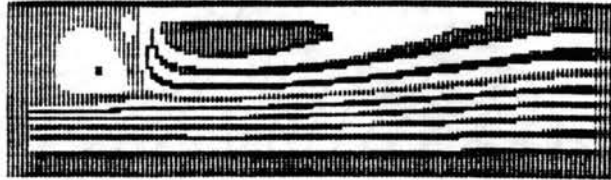
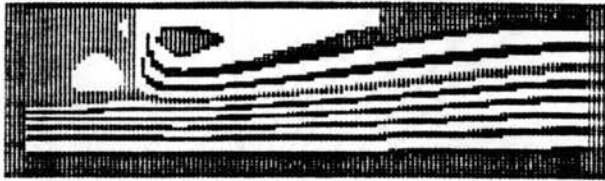


Figure 24. Continued

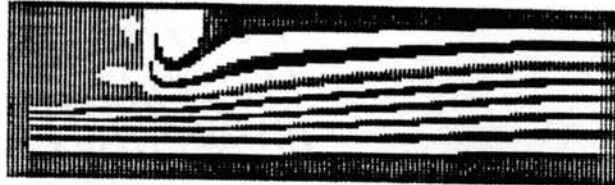
(a) SSA = 0 degrees



(b) SSA = 30 degrees



(c) SSA = 45 degrees



(d) SSA = 60 degrees

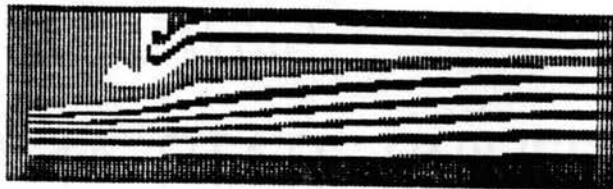


Figure 25. Effect of Secondary Swirl Angle on Streamline Patterns for Nonreacting Flows

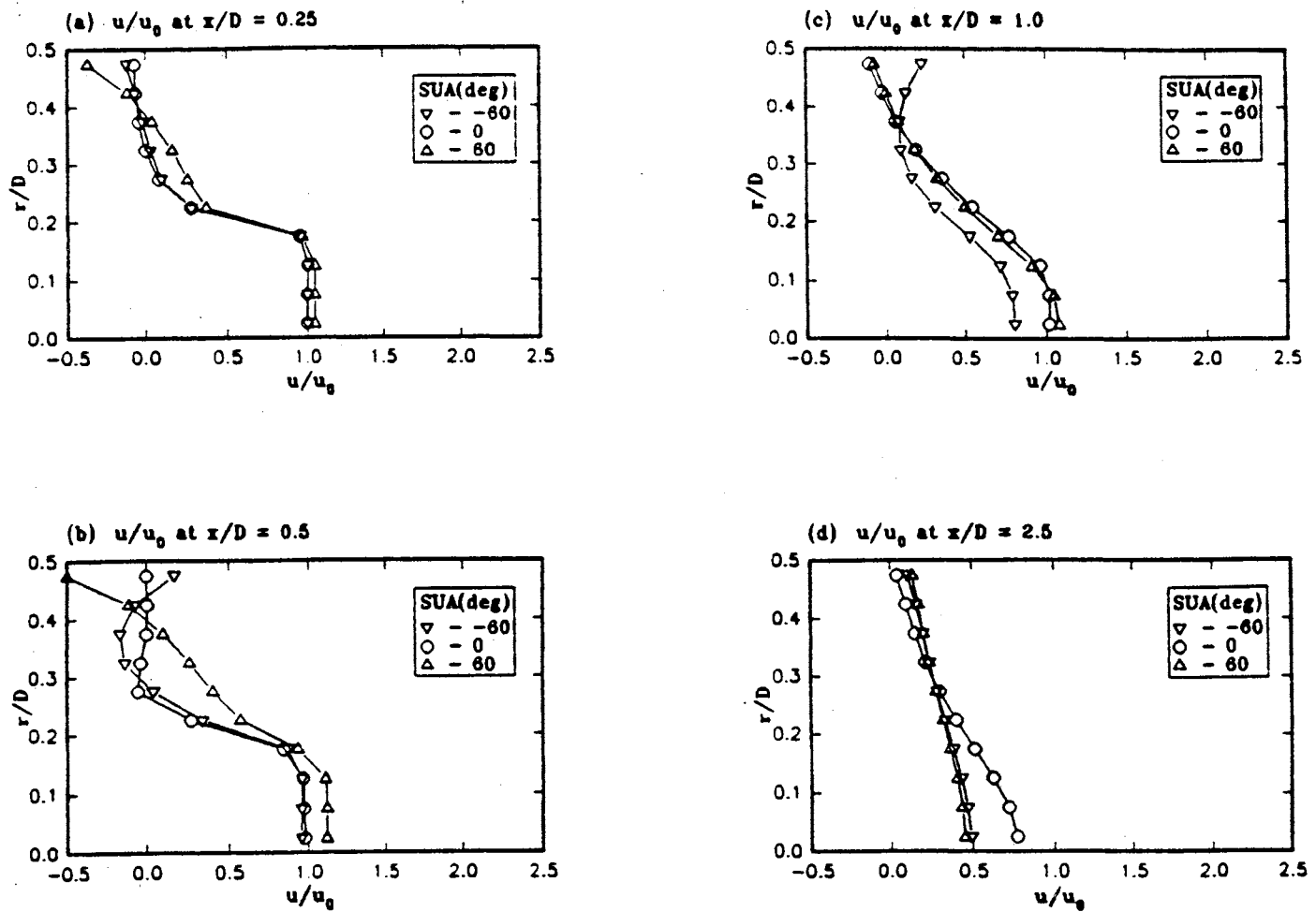
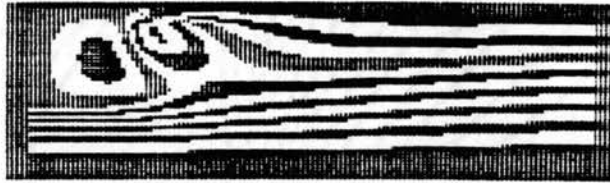


Figure 26. Effect of Secondary Upstream Angle on Axial Velocity for Nonreacting Flows

(a) SUA = -60 degrees



(b) SUA = 0 degrees



(c) SUA = 60 degrees

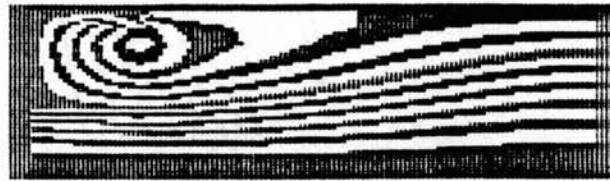


Figure 27. Effect of Secondary Upstream Angle on Streamline Patterns for Nonreacting Flows

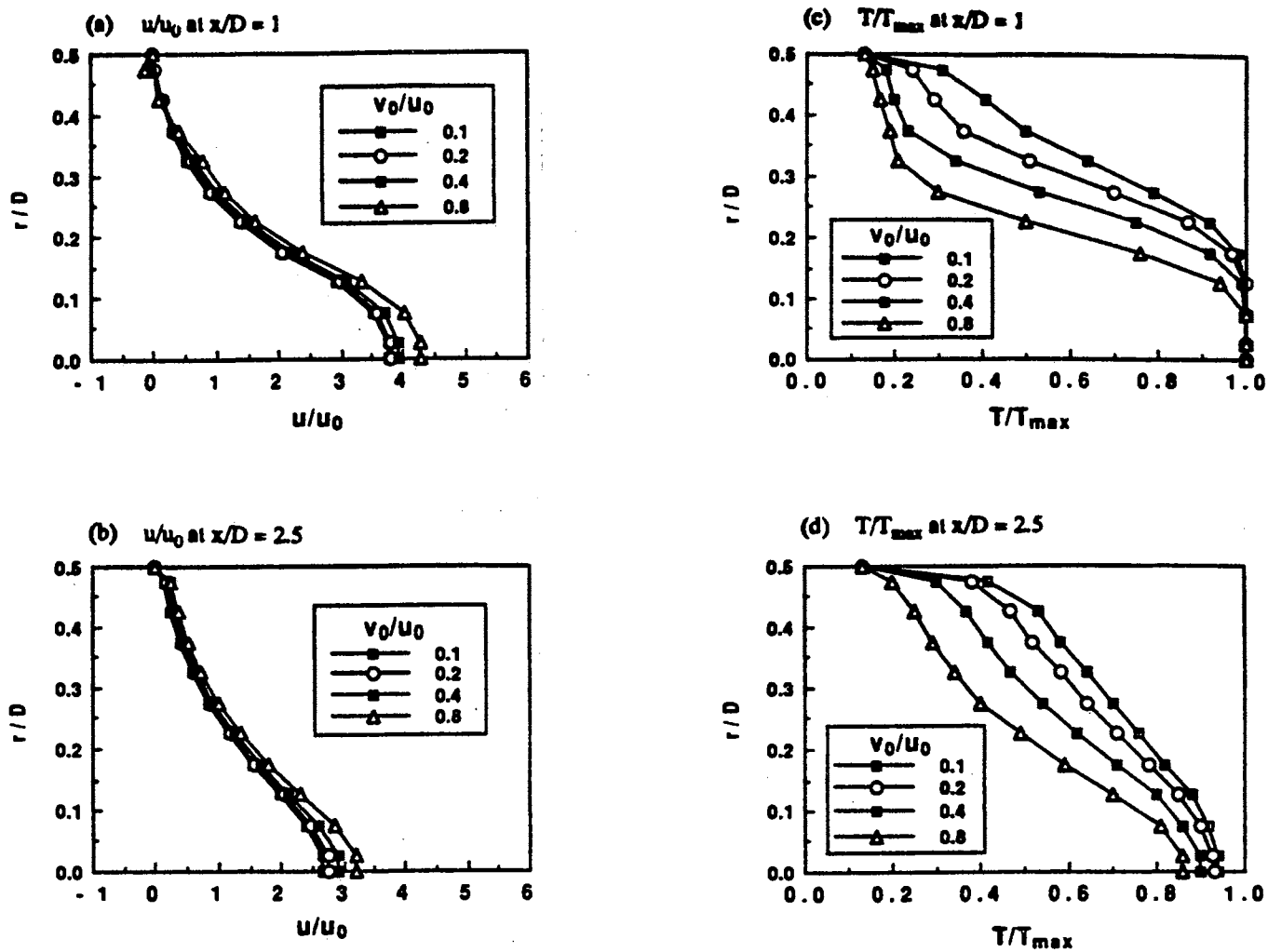
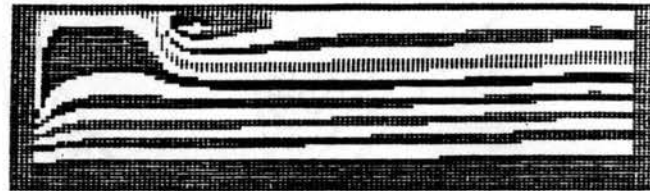


Figure 28. Effects of Secondary Injection Velocity on Axial Velocity and Temperature for Reacting Flows

(a) $v_0/u_0 = 0.1$



(b) $v_0/u_0 = 0.2$



(c) $v_0/u_0 = 0.4$



(d) $v_0/u_0 = 0.8$



Figure 29. Effects of Secondary Injection Velocity on Streamline Patterns for Reacting Flows

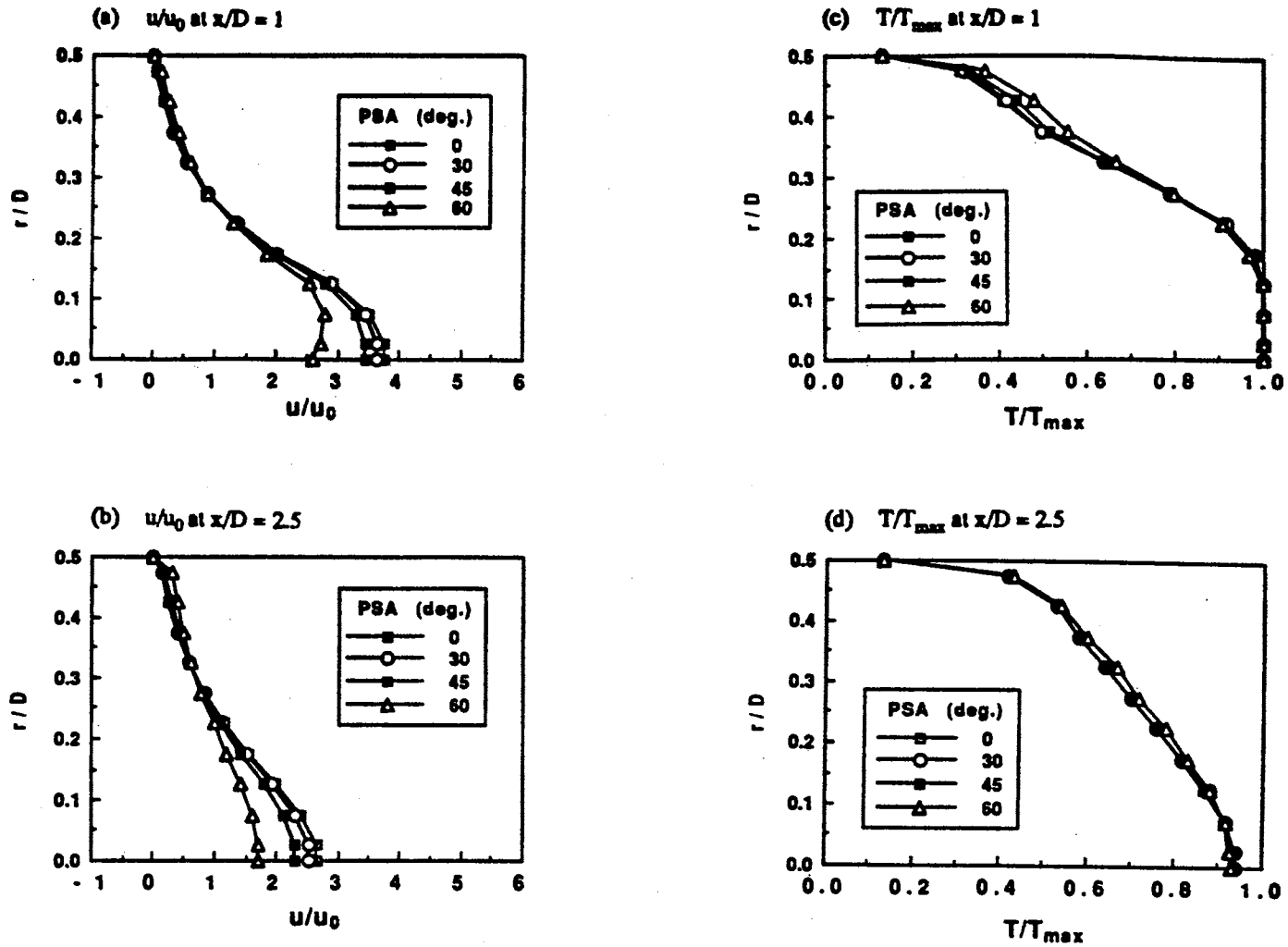


Figure 30. Effects of Primary Swirl Angle on Axial Velocity and Temperature for Reacting Flows

(a) PSA = 0 degrees



(b) PSA = 30 degrees



(c) PSA = 45 degrees



(d) PSA = 60 degrees

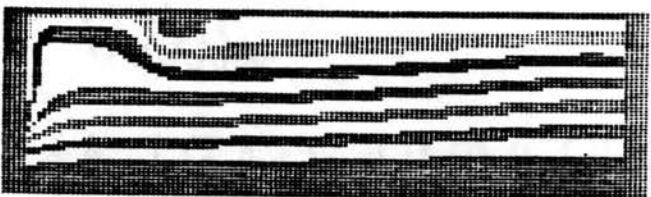


Figure 31. Effects of Primary Swirl Angle on Streamline Patterns for Reacting Flows

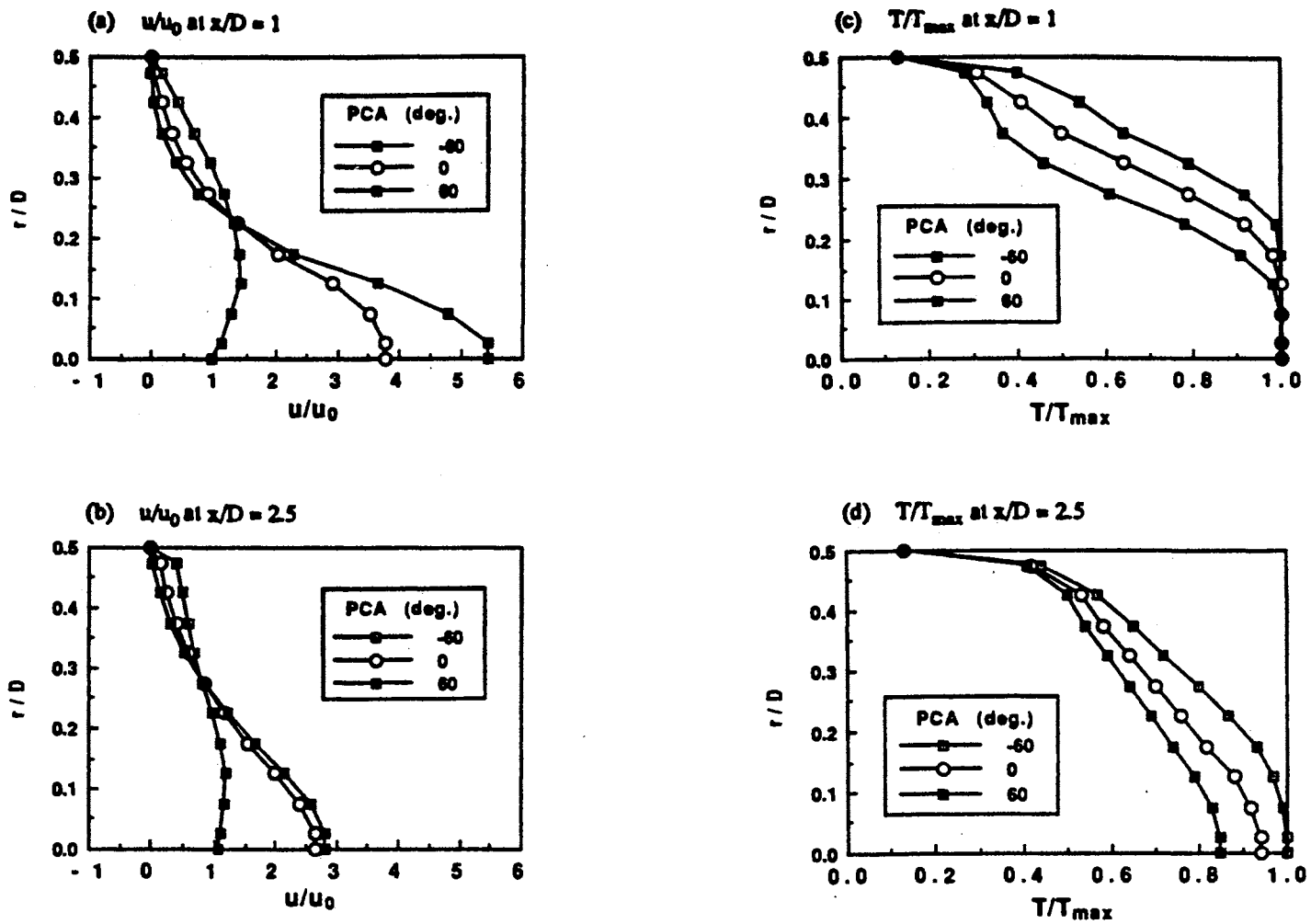


Figure 32. Effect of Primary Contraction Angle on Axial Velocity and Temperature for Reacting Flows

(a) PCA = -60 degrees



(b) PCA = 0 degrees



(c) PCA = 60 degrees



Figure 33. Effect of Primary Contraction Angle on Streamline Patterns for Reacting Flows

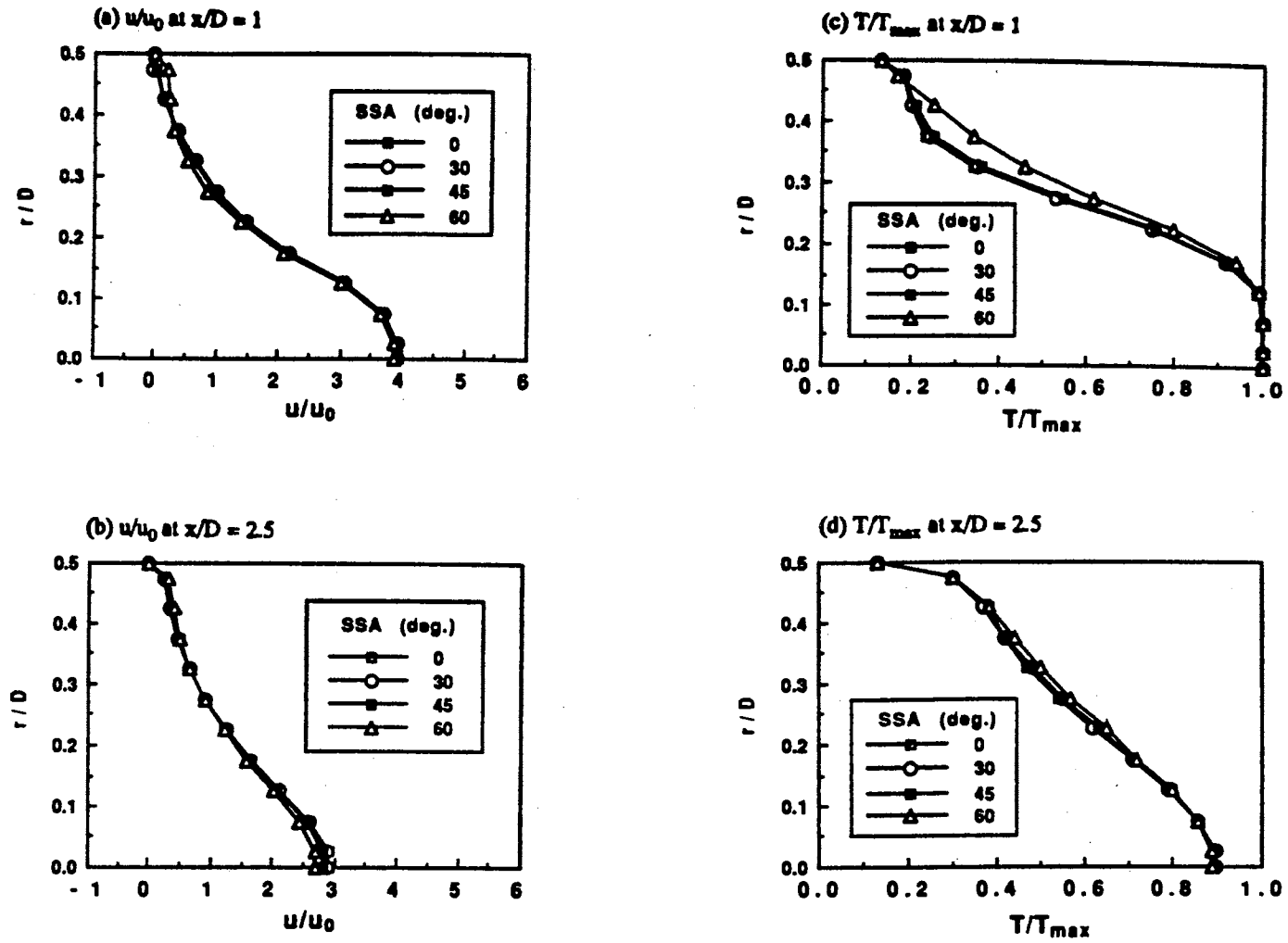


Figure 34. Effect of Secondary Swirl Angle on Axial Velocity and Temperature for Reacting Flows

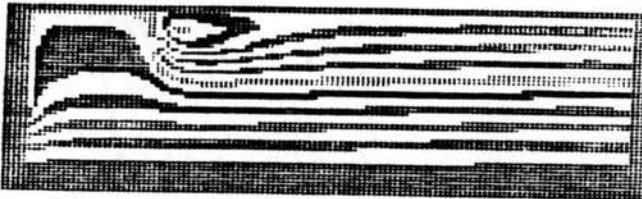
(a) SSA = 0 degrees



(b) SSA = 30 degrees



(c) SSA = 45 degrees



(d) SSA = 60 degrees



Figure 35. Effect of Secondary Swirl Angle on Streamline Patterns for Reacting Flows

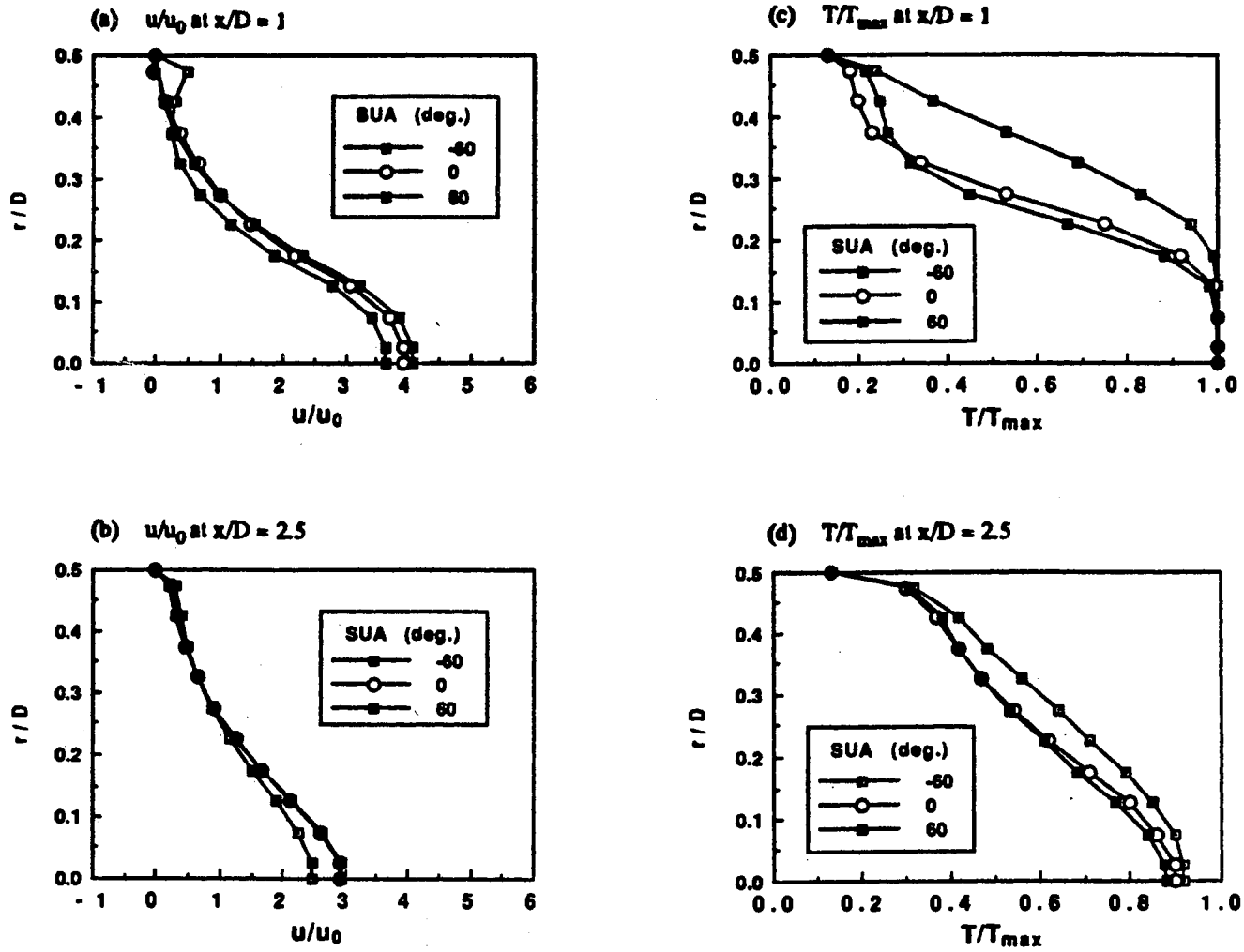


Figure 36. Effect of Secondary Upstream Angle on Axial Velocity and Temperature for Reacting Flows

(a) SUA = -60 degrees



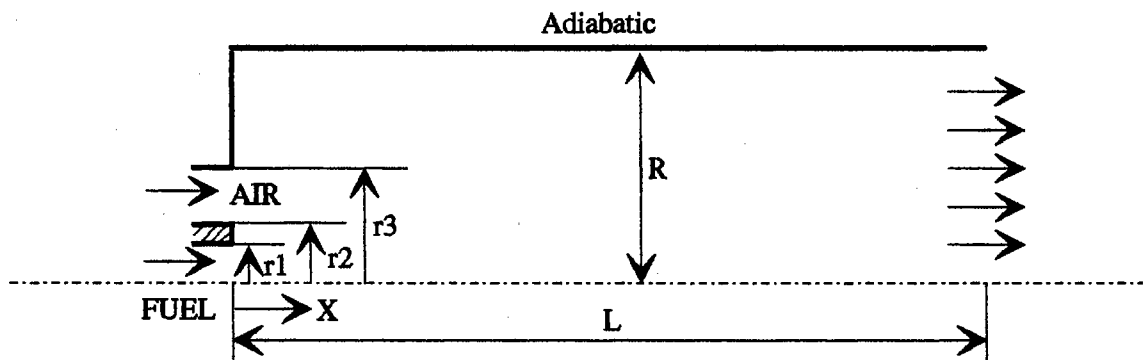
(b) SUA = 0 degrees



(c) SUA = 60 degrees



Figure 37. Effect of Secondary Upstream Angle on Streamline Patterns for Reacting Flows



$r_1 = 0.008 \text{ m}$	$U_{\text{air}} = 34.3 \text{ m/s}$
$r_2 = 0.0111 \text{ m}$	$U_{\text{fuel}} = 21.3 \text{ m/s}$
$r_3 = 0.0286 \text{ m}$	$T_{\text{air}} = 589 \text{ deg K}$
$R = 0.1016 \text{ m}$	$T_{\text{fuel}} = 300 \text{ deg K}$
$L = 1.524 \text{ m}$	$P = 94 \text{ KPa}$

Figure 38. Geometry of Axisymmetric Combustor with Coaxial Fuel and Air Jets [31]

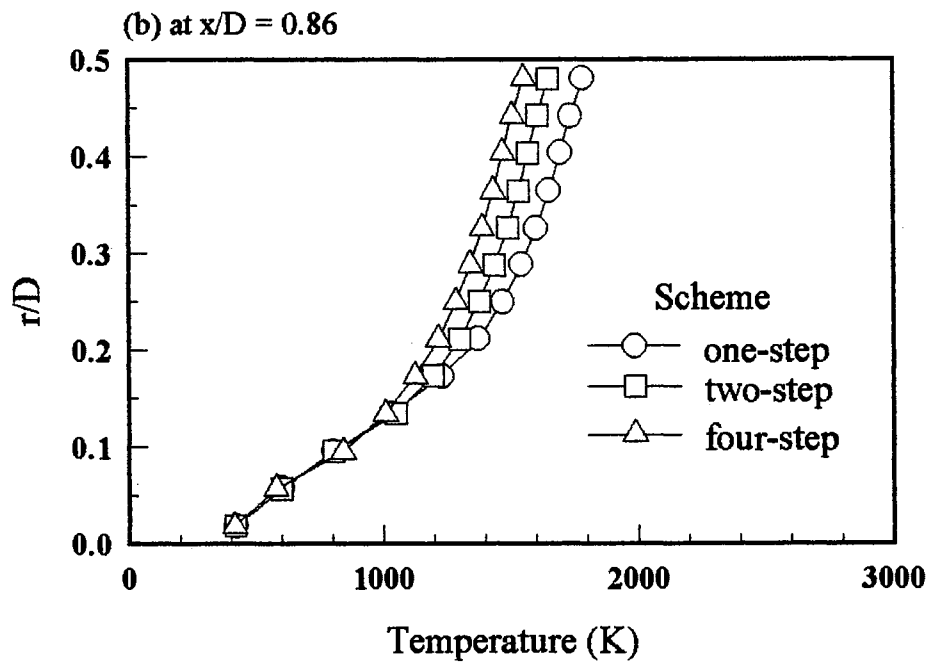
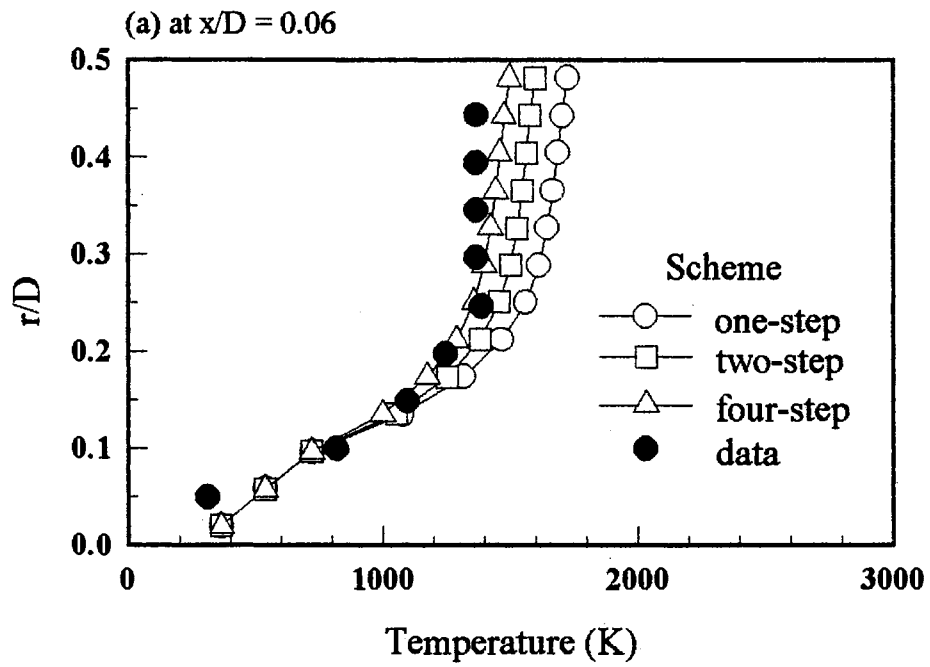


Figure 39. Temperature Profiles with Data of Lewis & Smoot [31]

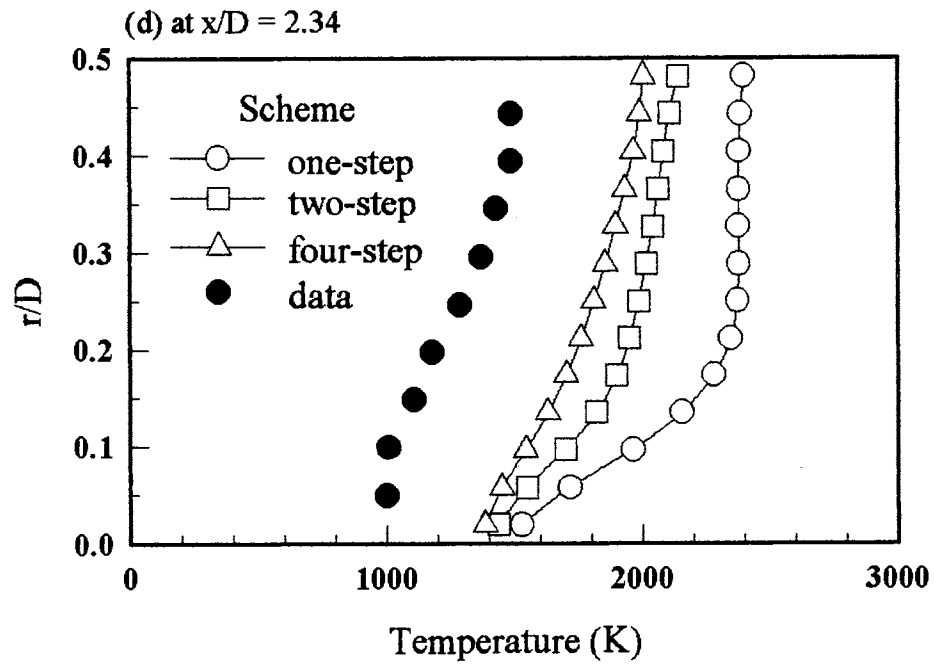
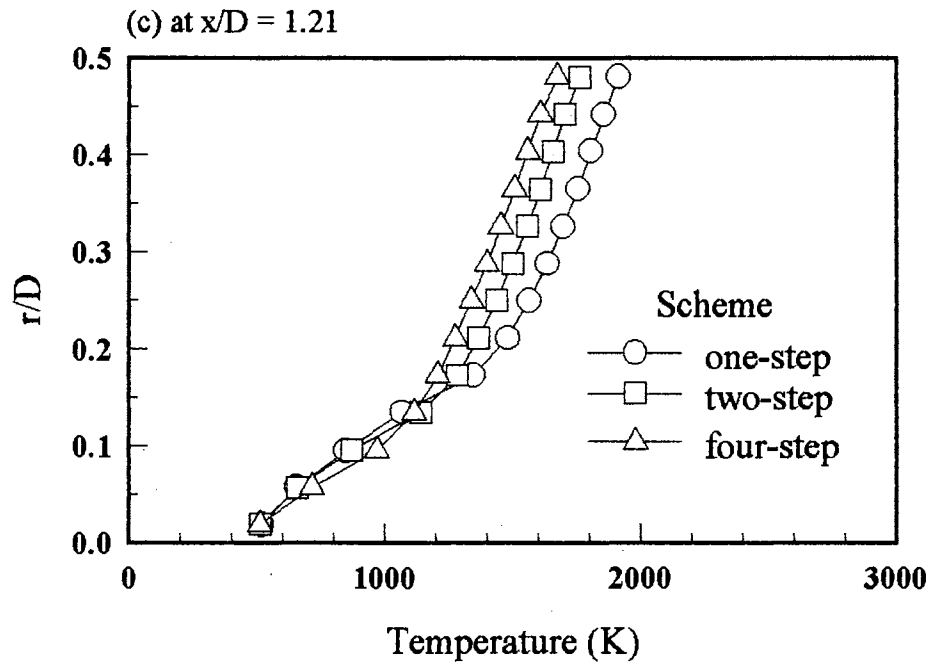


Figure 39. Continued

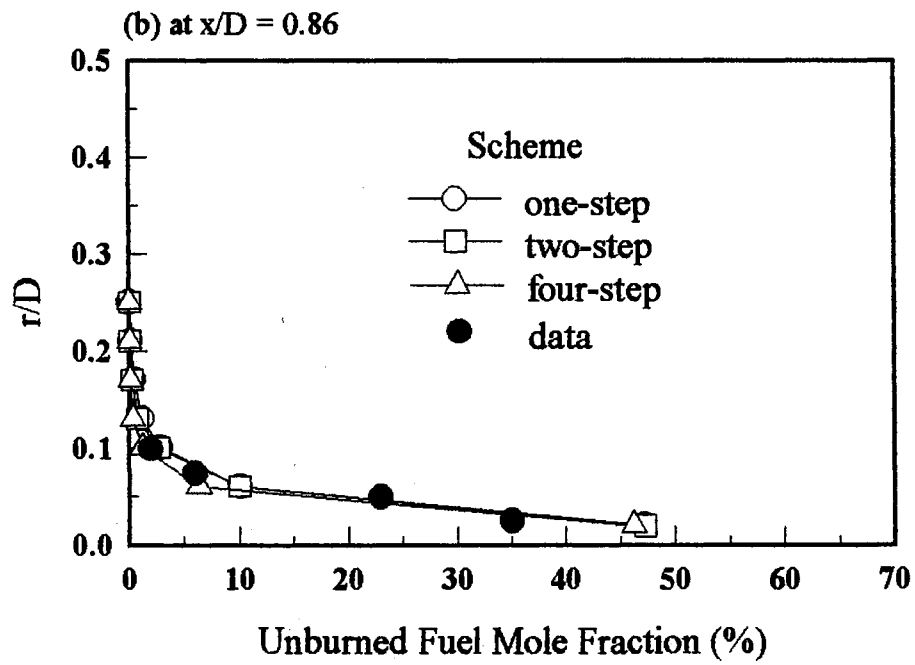
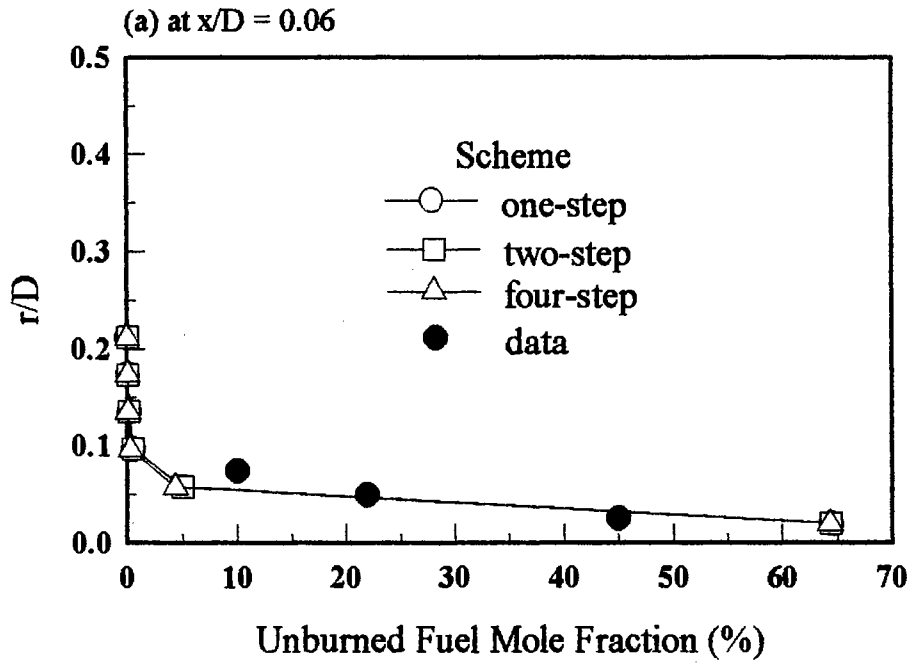


Figure 40. Unburned Fuel Profiles with Data of Lewis & Smoot [31]

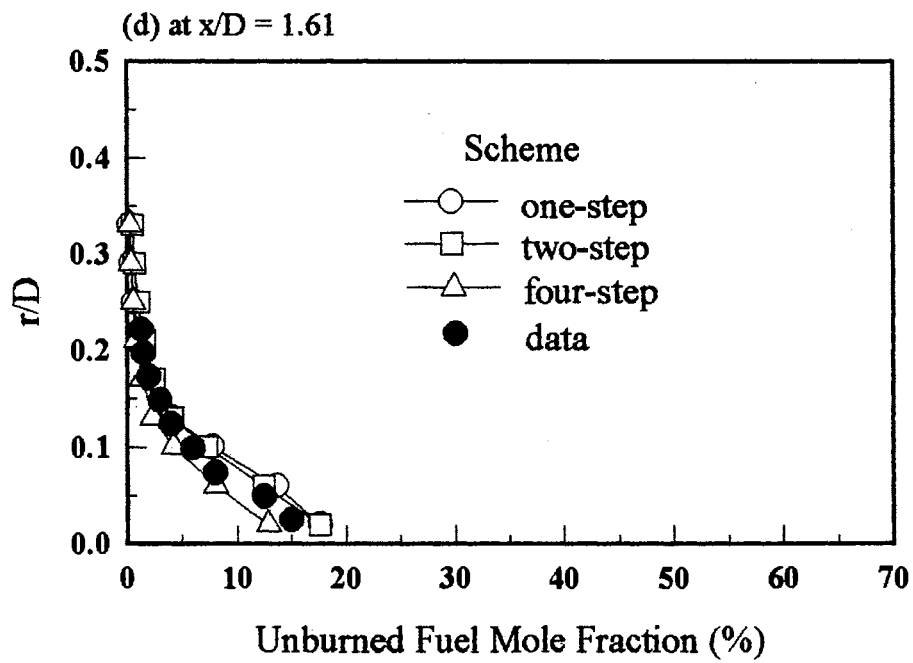
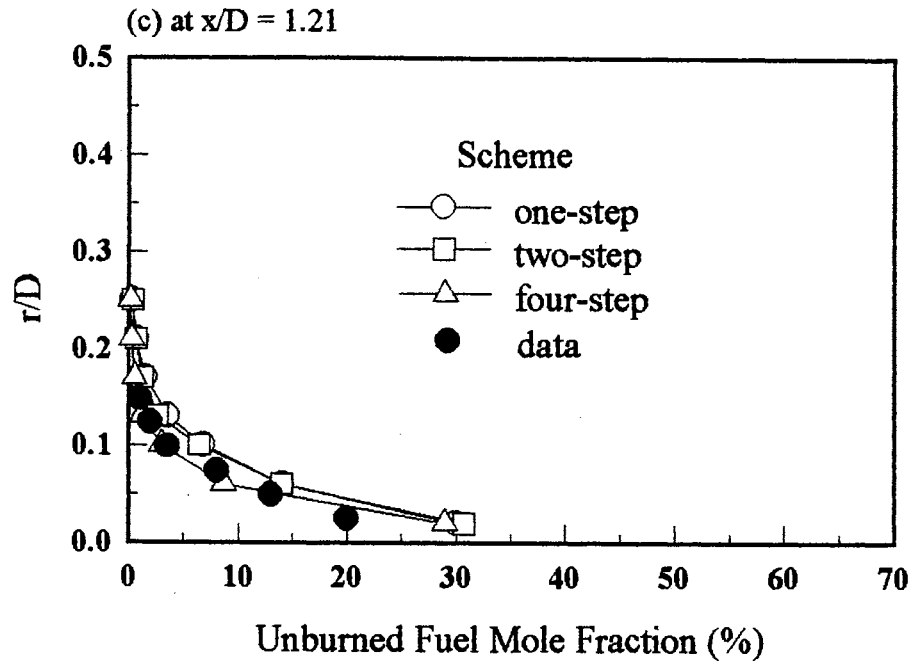


Figure 40. Continued

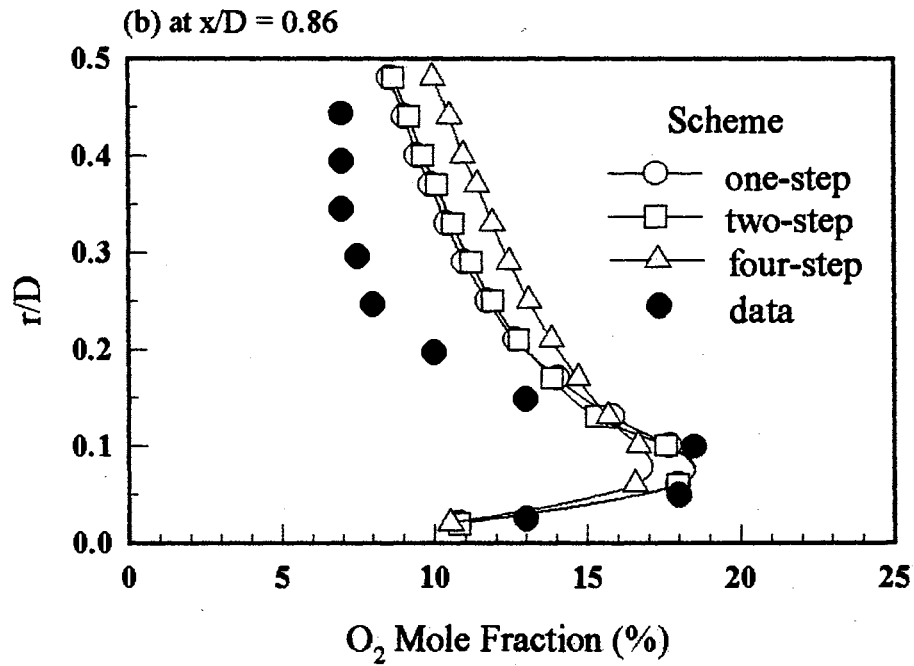
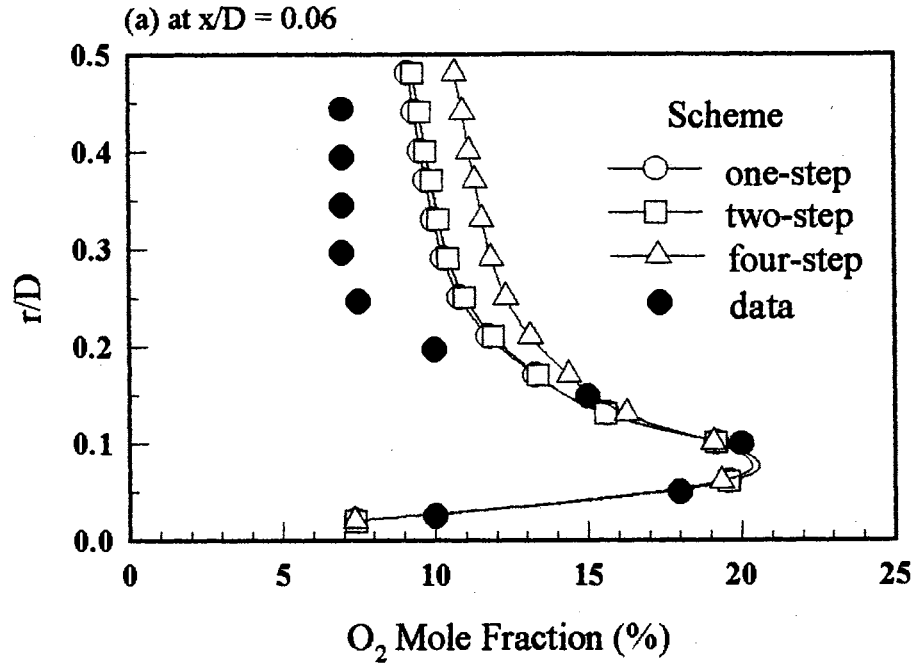


Figure 41. Oxygen Profiles with Data of Lewis & Smoot [31]

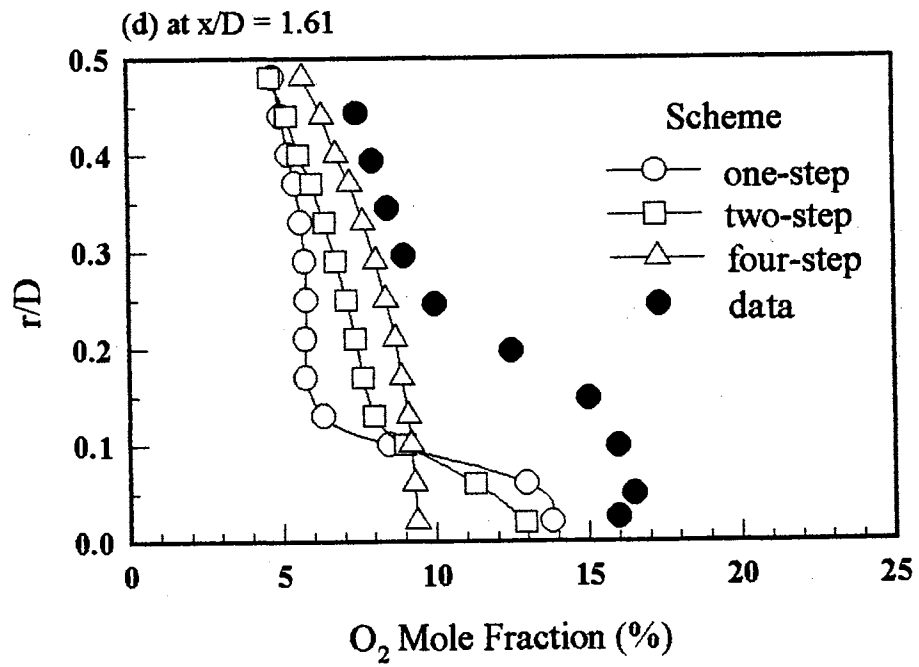
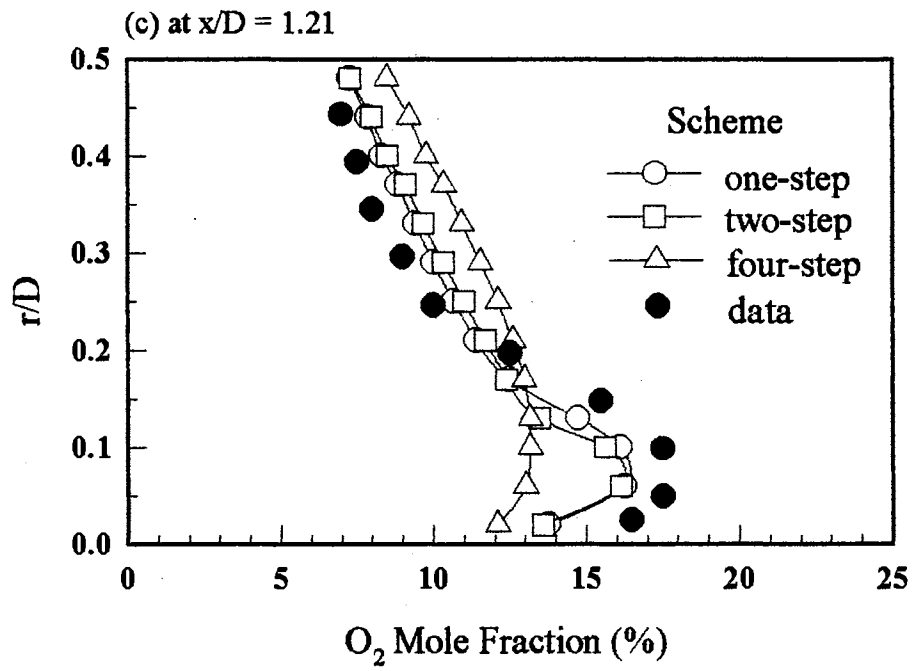


Figure 41. Continued

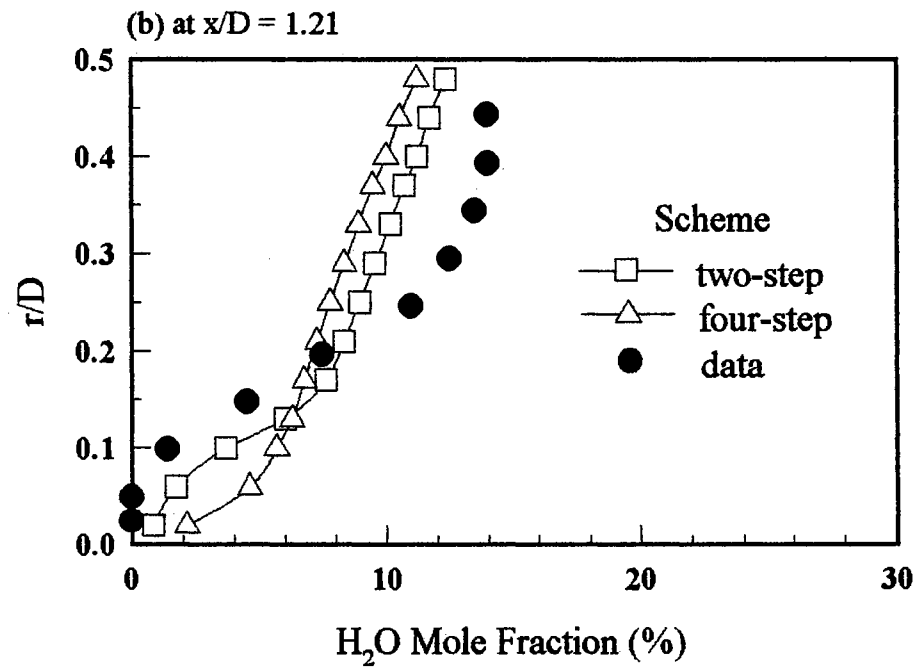
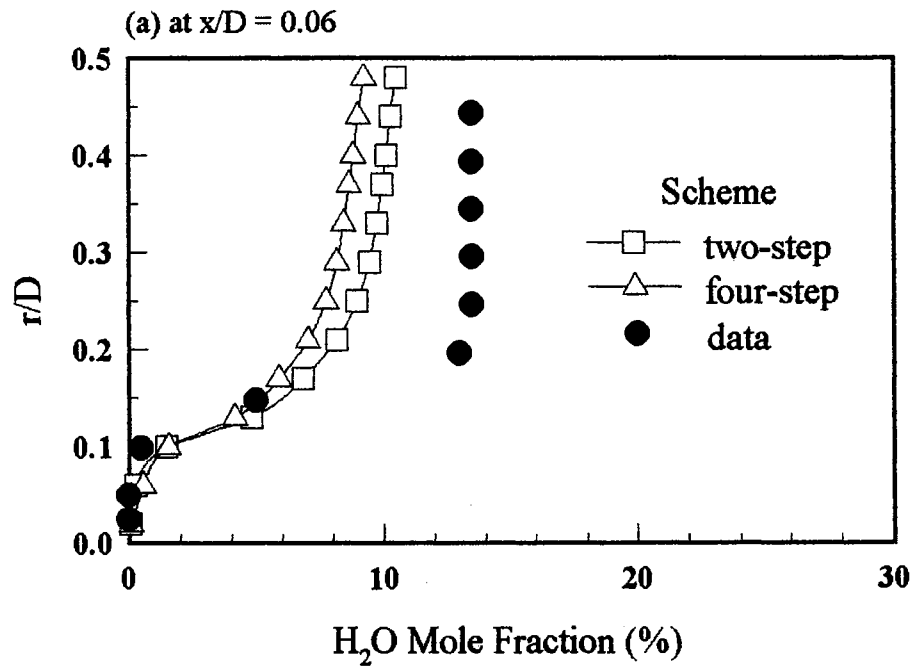


Figure 42. Water Vapor Profiles with Data of Lewis & Smoot [31]

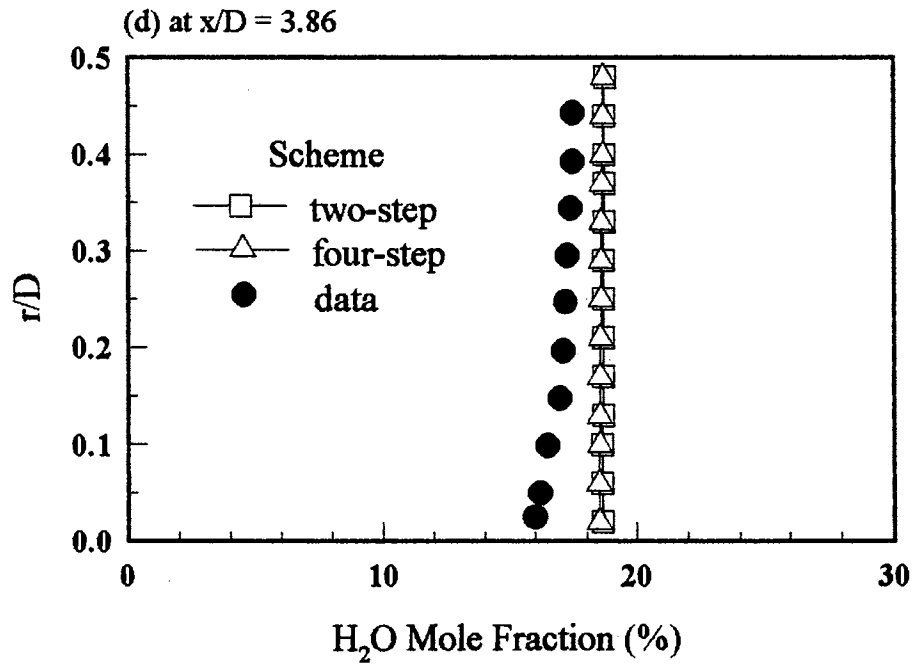
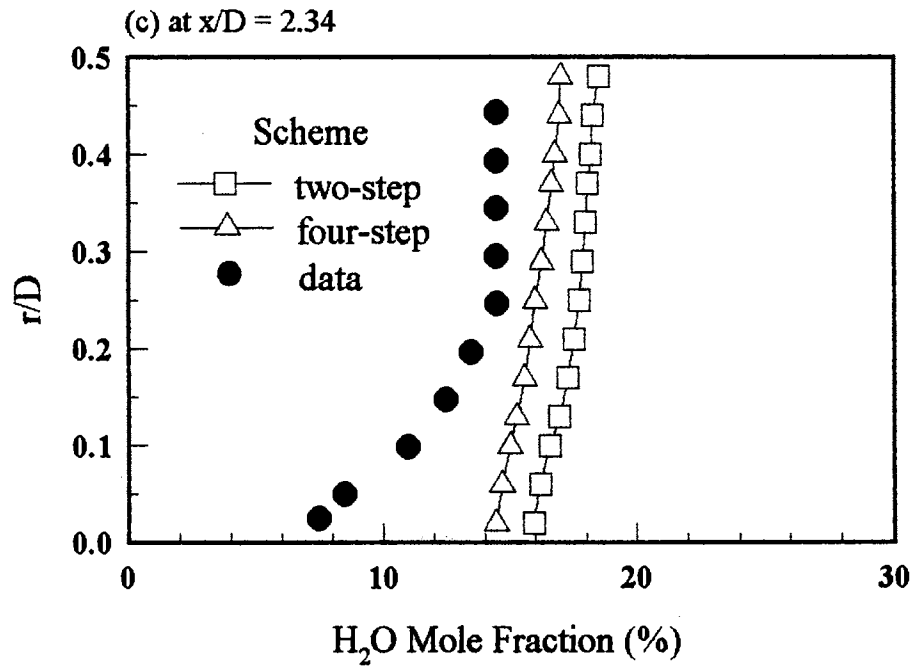


Figure 42. Continued

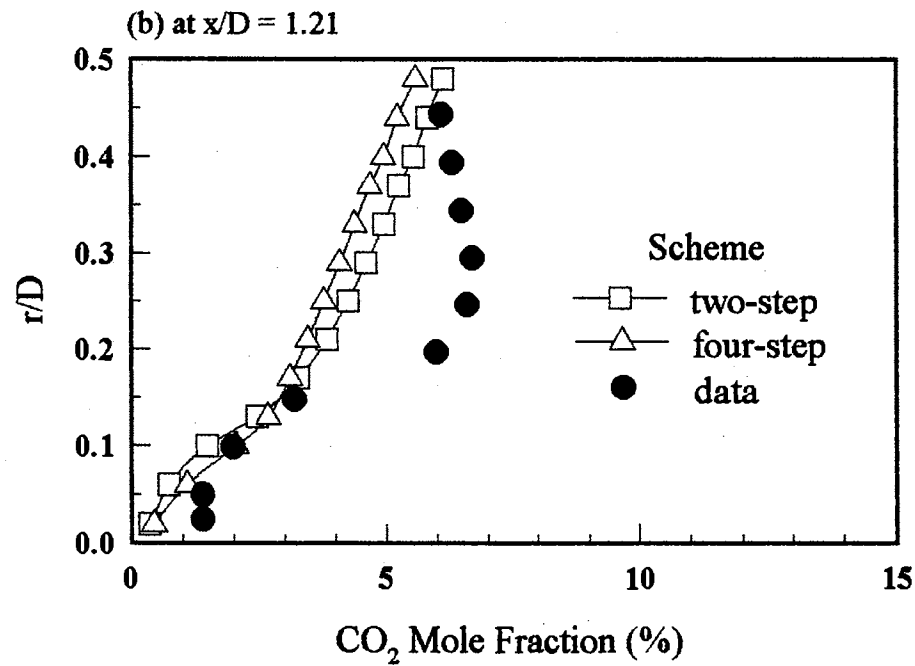
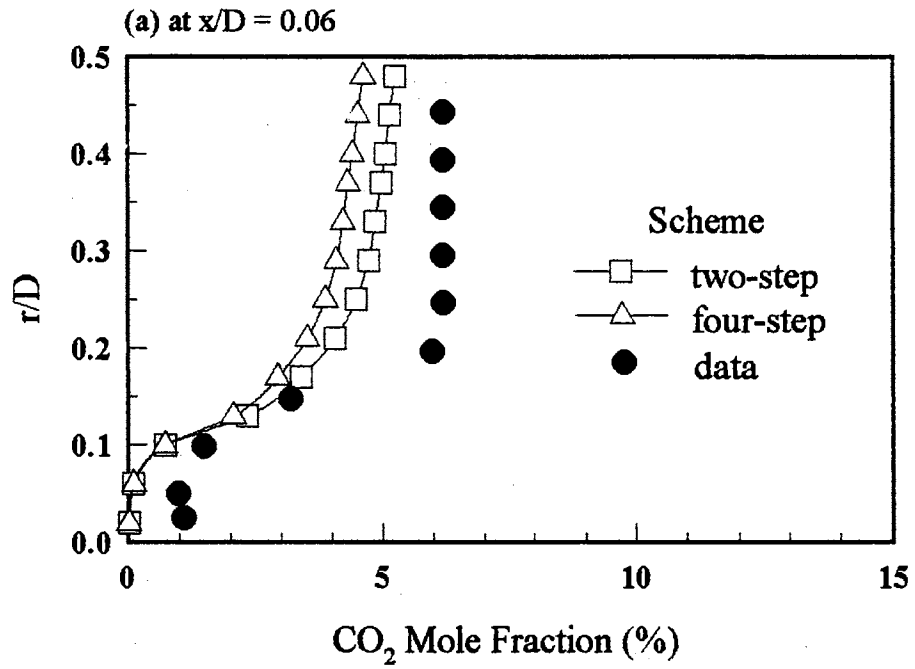


Figure 43. Carbon Dioxide Profiles with Data of Lewis & Smoot [31]

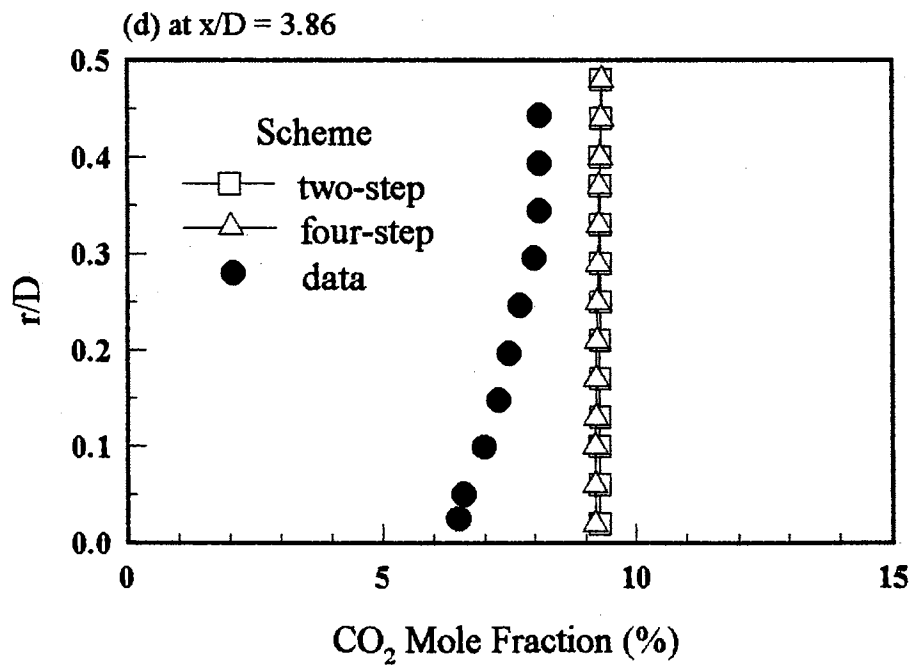
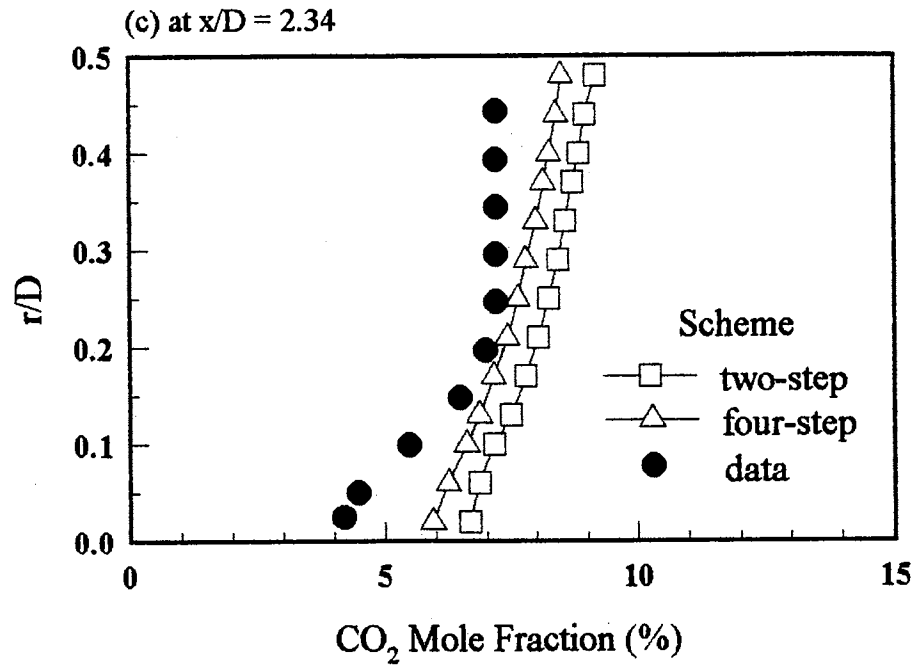


Figure 43. Continued

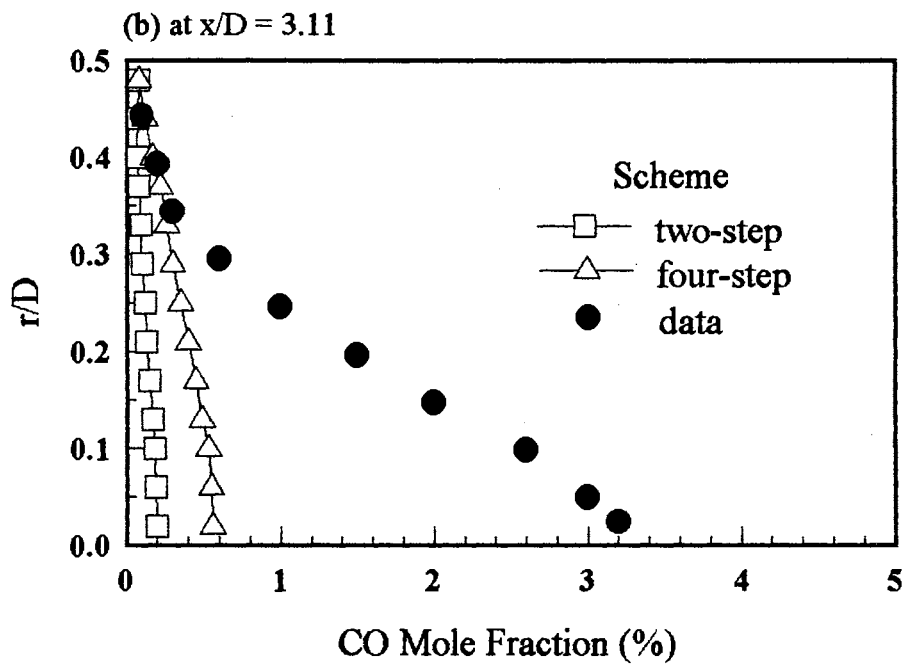
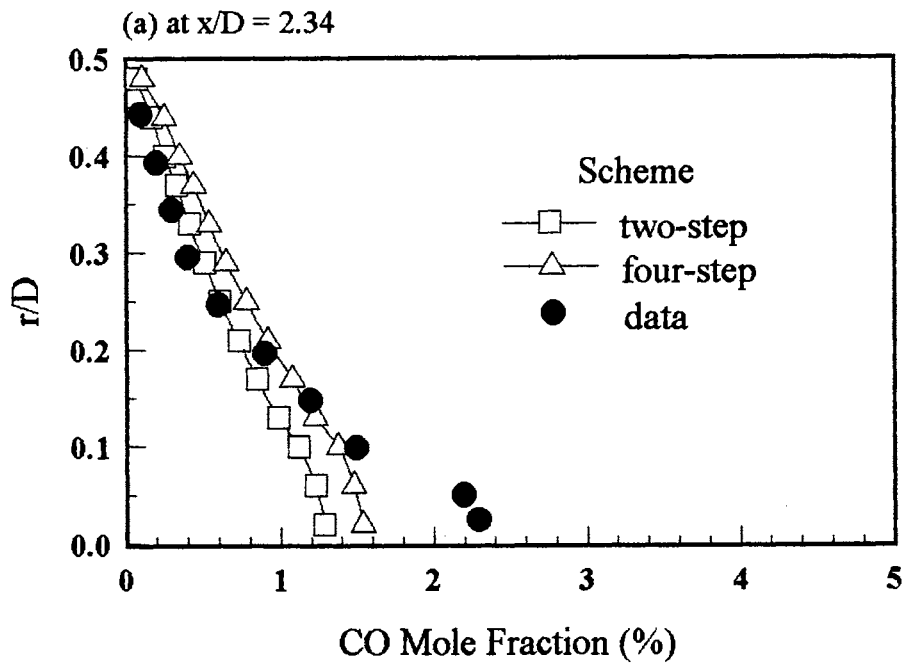


Figure 44. Carbon Monoxide Profiles with Data of Lewis & Smoot [31]

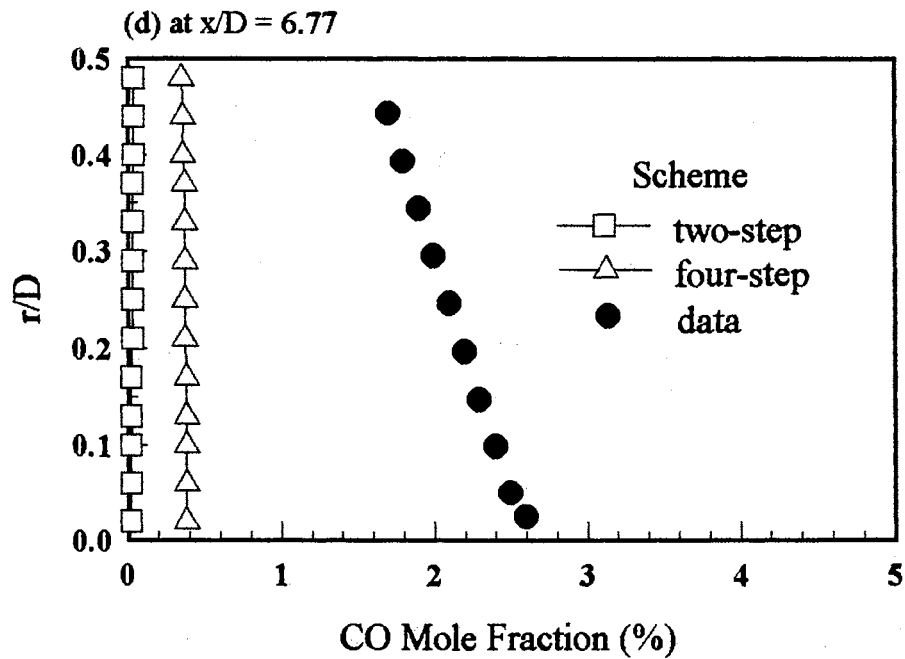
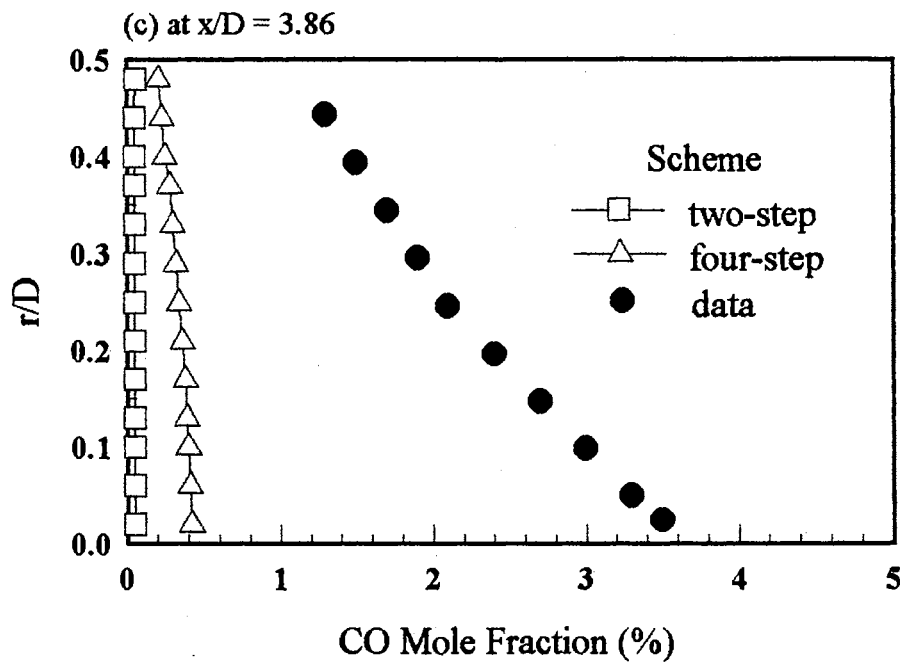


Figure 44. Continued

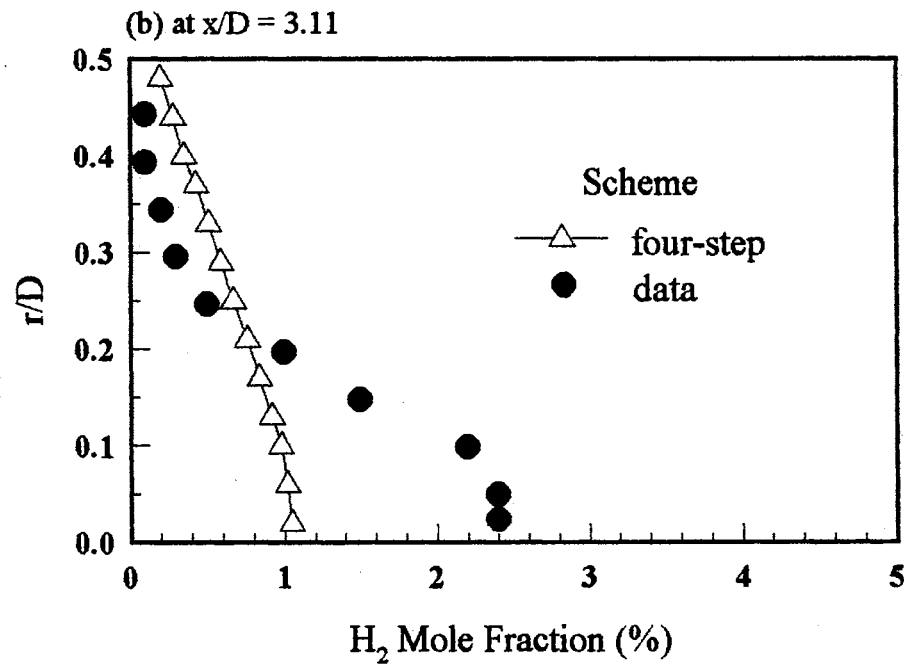
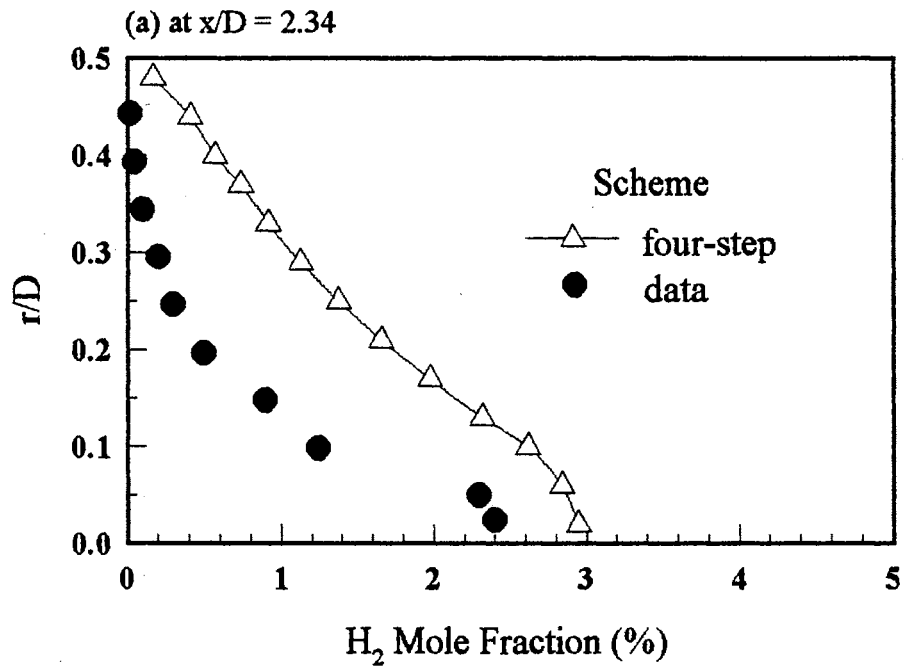


Figure 45. Hydrogen Profiles with Data of Lewis & Smoot [31]

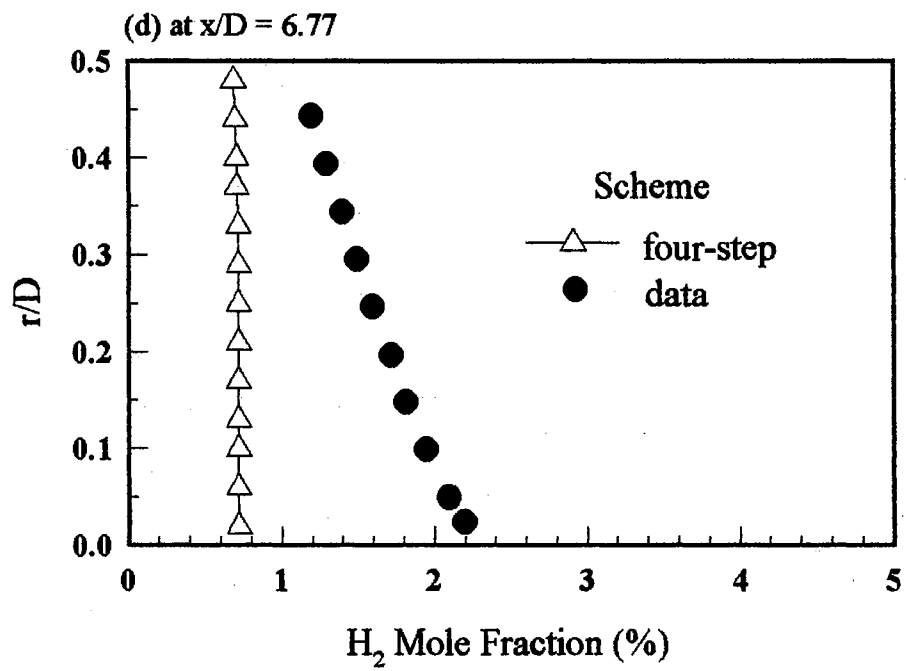
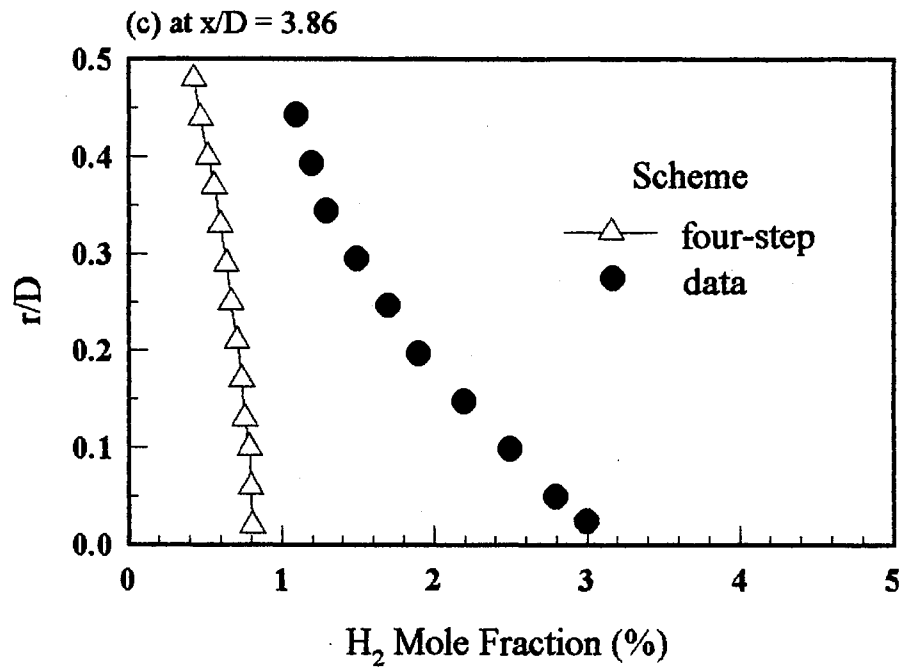
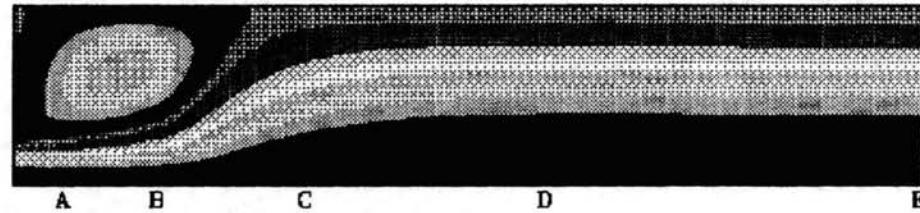


Figure 45. Continued

DIMENSIONLESS STREAM FUNCTION



One-Step Scheme (CH₄/Air) L=1.524 m
 R1=0.008 m R2=0.0111 m R3=0.0286 m
 U_{air}=34.3 m/s U_{fu}=21.3 m/s
 T_{air}=589 deg K T_{fu}=300 deg K

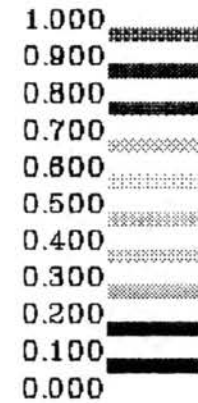
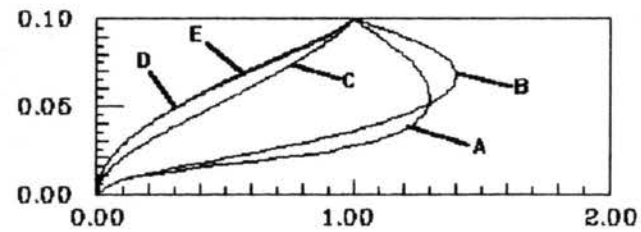
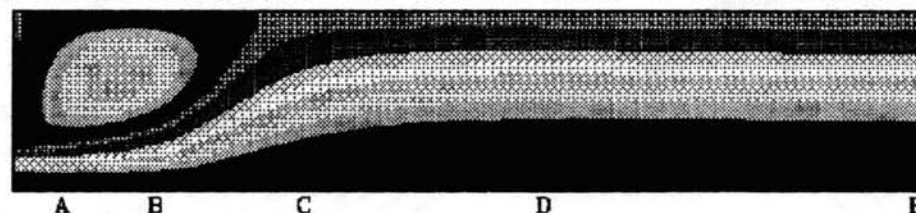


Figure 46. Streamline Patterns with One-Step Scheme

DIMENSIONLESS STREAM FUNCTION



Two-Step Scheme (CH₄/Air) L=1.524 m
 R1=0.008 m R2=0.0111 m R3=0.0286 m
 U_{air}=34.3 m/s U_{fu}=21.3 m/s
 T_{air}=589 deg K T_{fu}=300 deg K

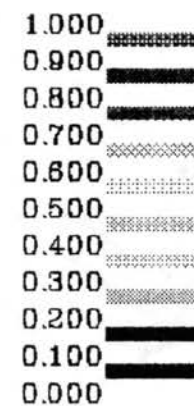
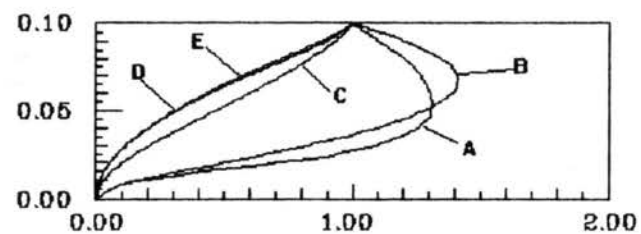
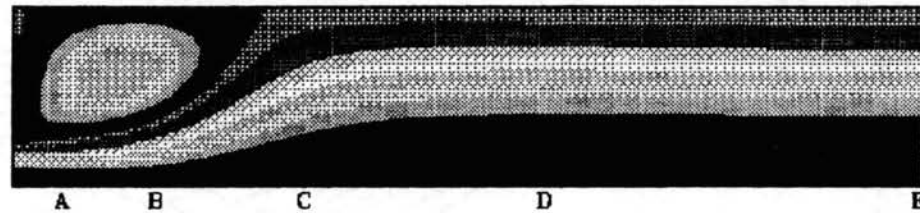


Figure 47. Streamline Patterns with Two-Step Scheme

DIMENSIONLESS STREAM FUNCTION



Four-Step Scheme (CH₄/Air) L=1.524 m
 R1=0.008 m R2=0.0111 m R3=0.0286 m
 U_{air}=34.3 m/s U_{fu}=21.3 m/s
 T_{air}=589 deg K T_{fu}=300 deg K

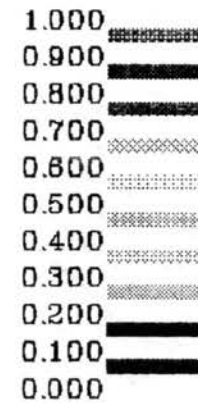
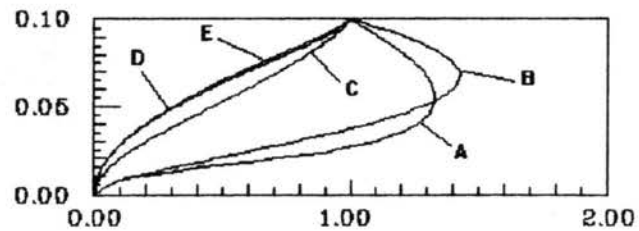
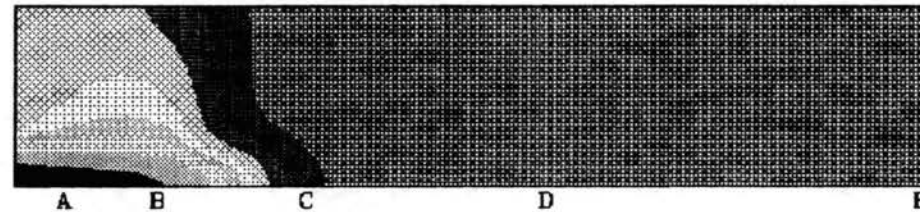


Figure 48. Streamline Patterns with Four-Step Scheme

TEMPERATURE



One-Step Scheme (CH₄/Air) L=1.524 m
R1=0.008 m R2=0.0111 m R3=0.0286 m
U_{air}=34.3 m/s U_{fu}=21.3 m/s
T_{max}=2631 deg K

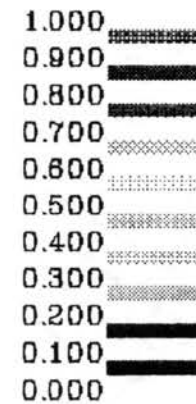
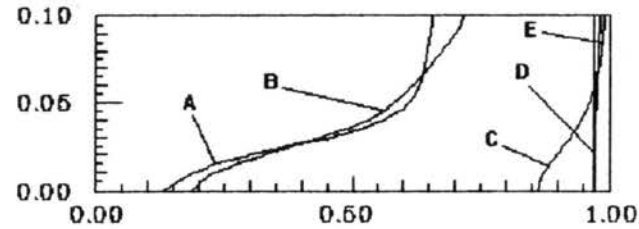
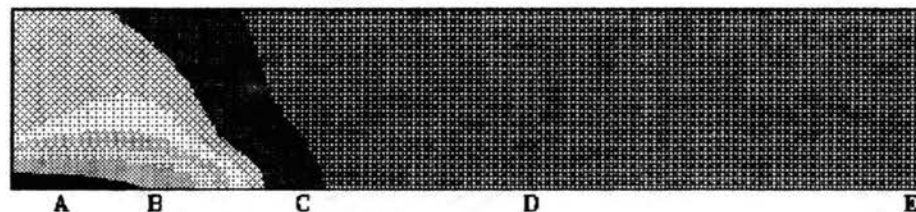


Figure 49. Temperature Contour Map with One-Step Scheme

TEMPERATURE



Two-Step Scheme (CH₄/Air) L=1.524 m
R1=0.008 m R2=0.0111 m R3=0.0286 m
U_{air}=34.3 m/s U_{fu}=21.3 m/s
T_{max}=2337 deg K

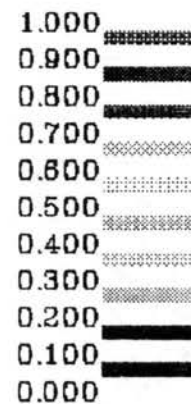
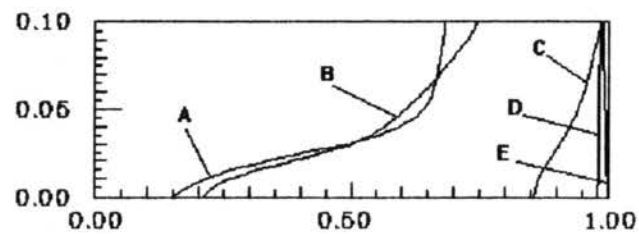
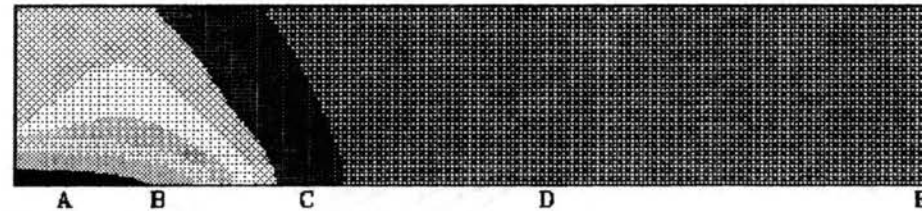


Figure 50. Temperature Contour Map with Two-Step Scheme

TEMPERATURE



Four-Step Scheme (CH₄/Air) L=1.524 m
 R1=0.008 m R2=0.0111 m R3=0.0286 m
 U_{air}=34.3 m/s U_{fu}=21.3 m/s
 T_{max}=2339 deg K

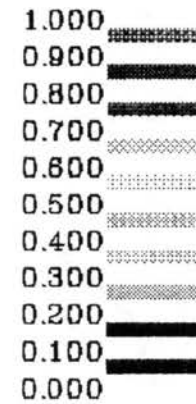
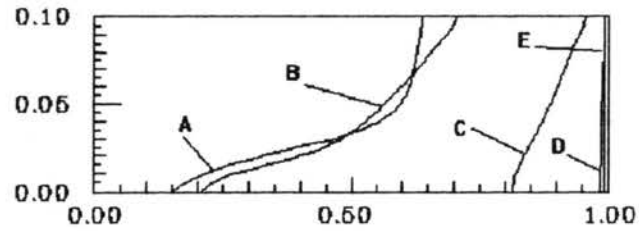


Figure 51. Temperature Contour Map with Four-Step Scheme

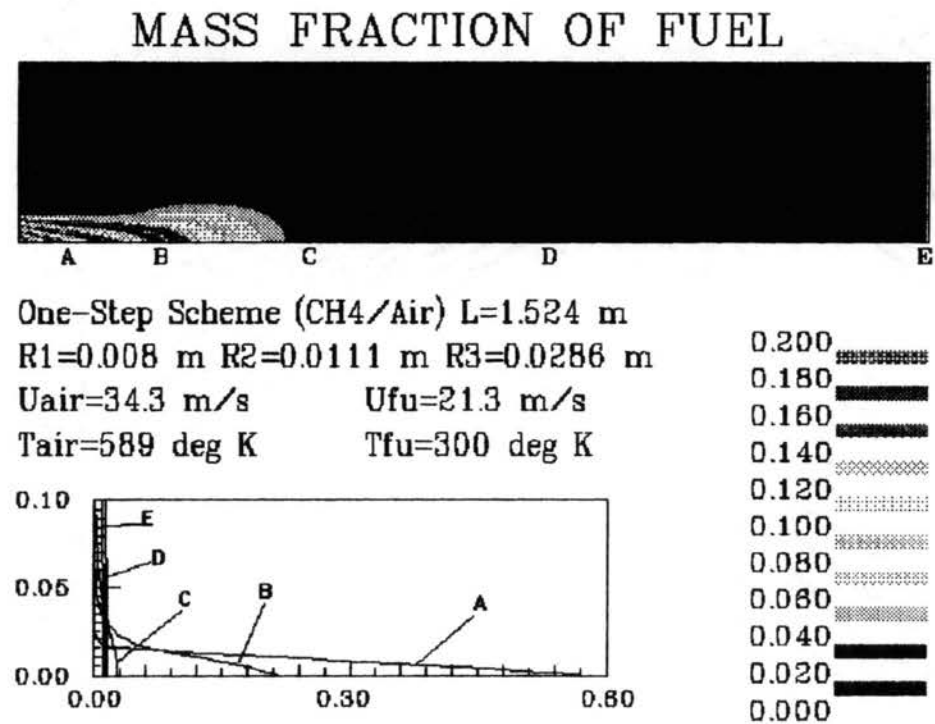


Figure 52. Unburned Fuel Mass Fraction Contour Map with One-Step Scheme

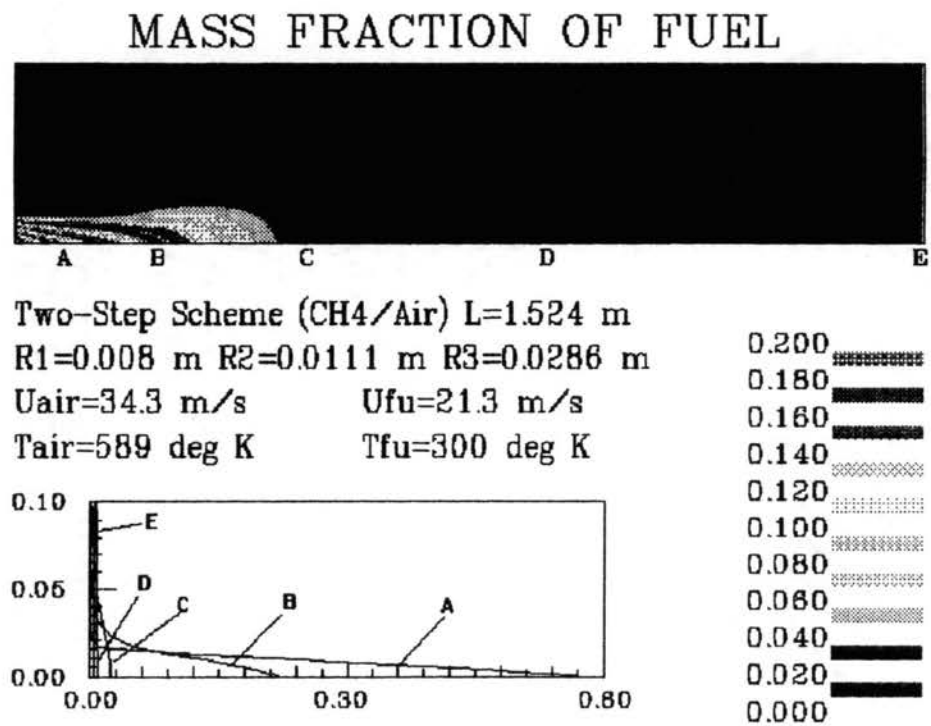
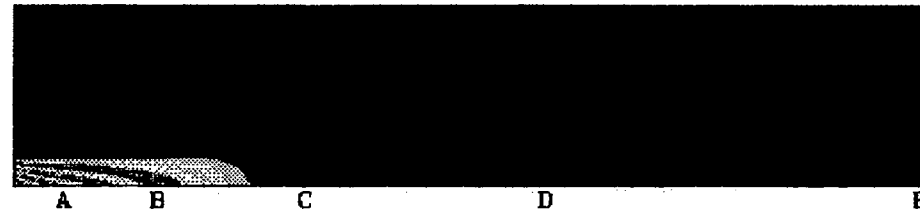


Figure 53. Unburned Fuel Mass Fraction Contour Map with Two-Step Scheme

MASS FRACTION OF FUEL



Four-Step Scheme (CH₄/Air) L=1.524 m
 R1=0.008 m R2=0.0111 m R3=0.0286 m
 U_{air}=34.3 m/s U_{fu}=21.3 m/s
 T_{air}=589 deg K T_{fu}=300 deg K

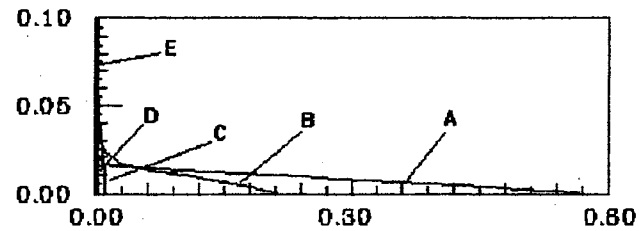
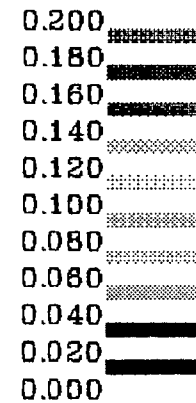


Figure 54. Unburned Fuel Mass Fraction Contour Map with Four-Step Scheme

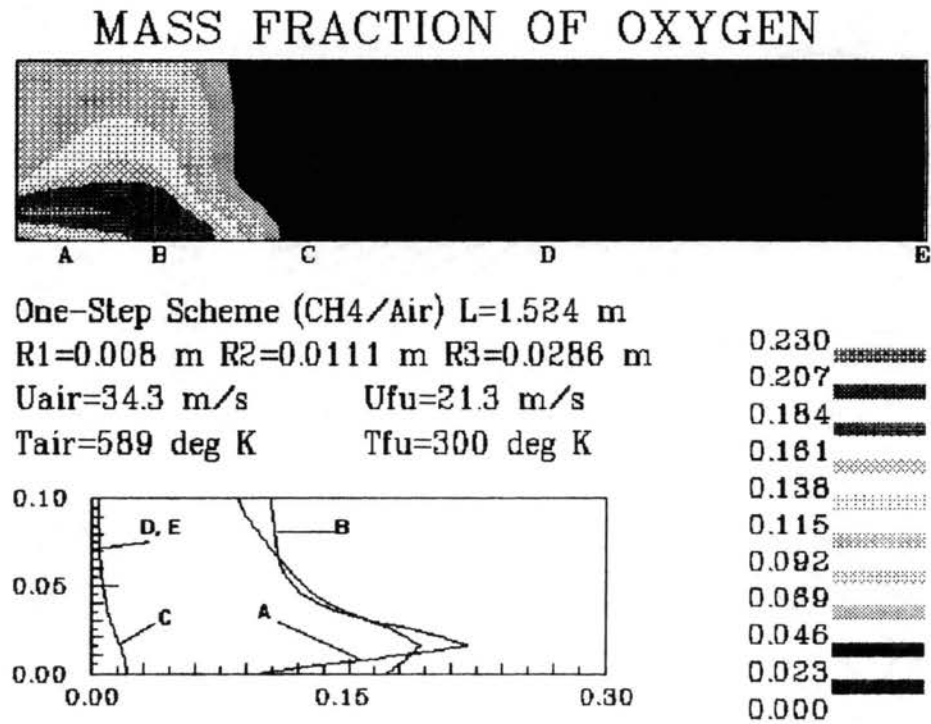
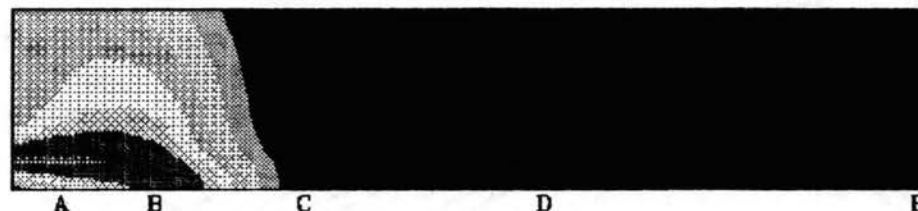


Figure 55. Oxygen Mass Fraction Contour Map with One-Step Scheme

MASS FRACTION OF OXYGEN



Two-Step Scheme (CH₄/Air) L=1.524 m
 R1=0.008 m R2=0.0111 m R3=0.0286 m
 U_{air}=34.3 m/s U_{fu}=21.3 m/s
 T_{air}=589 deg K T_{fu}=300 deg K

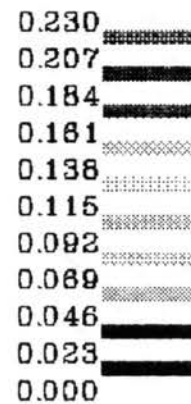
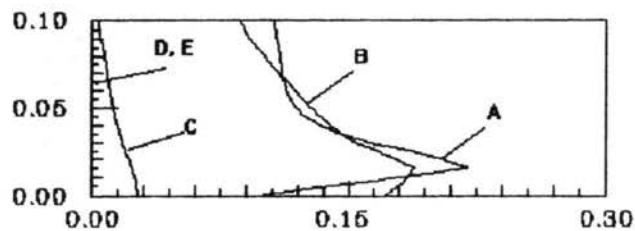
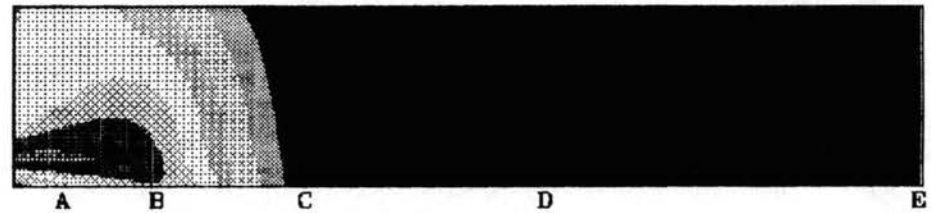


Figure 56. Oxygen Mass Fraction Contour Map with Two-Step Scheme

MASS FRACTION OF OXYGEN



Four-Step Scheme (CH₄/Air) L=1.524 m
 R1=0.008 m R2=0.0111 m R3=0.0286 m
 U_{air}=34.3 m/s U_{fu}=21.3 m/s
 T_{air}=589 deg K T_{fu}=300 deg K

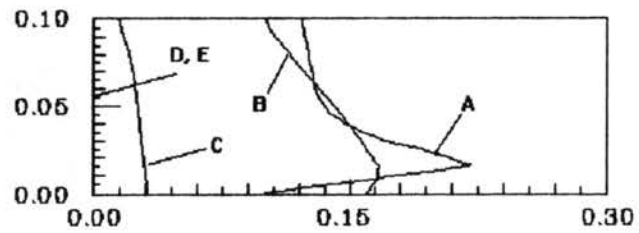
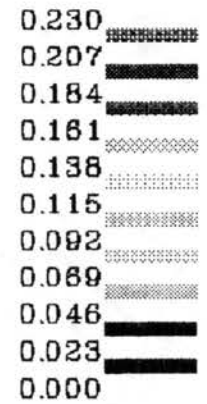
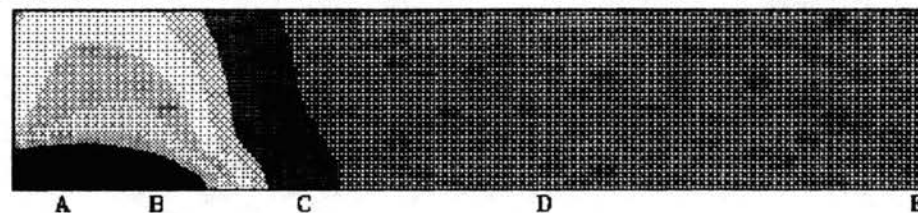


Figure 57. Oxygen Mass Fraction Contour Map with Four-Step Scheme

MASS FRACTION OF WATER VAPOR



Two-Step Scheme (CH₄/Air) L=1.524 m
 R1=0.008 m R2=0.0111 m R3=0.0286 m
 U_{air}=34.3 m/s U_{fu}=21.3 m/s
 T_{air}=589 deg K T_{fu}=300 deg K

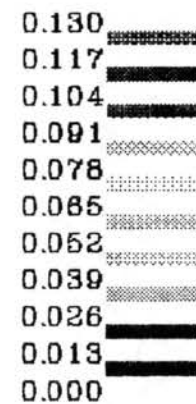
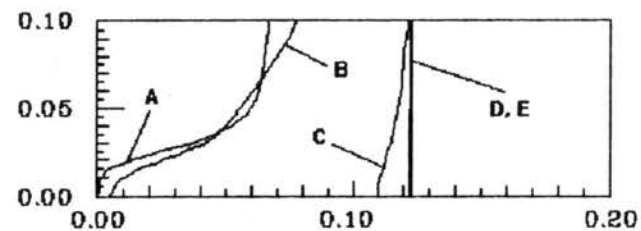
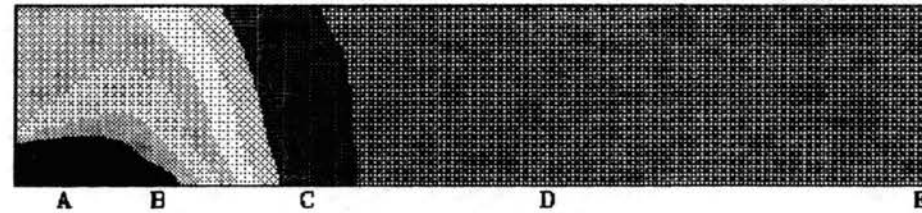


Figure 58. Water Vapor Mass Fraction Contour Map with Two-Step Scheme

MASS FRACTION OF WATER VAPOR



Four-Step Scheme (CH₄/Air) L=1.524 m
 R1=0.008 m R2=0.0111 m R3=0.0286 m
 U_{air}=34.3 m/s U_{fu}=21.3 m/s
 T_{air}=589 deg K T_{fu}=300 deg K

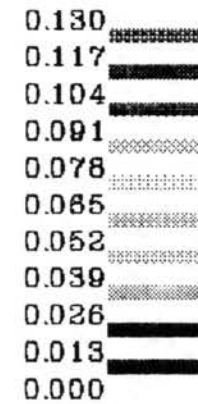
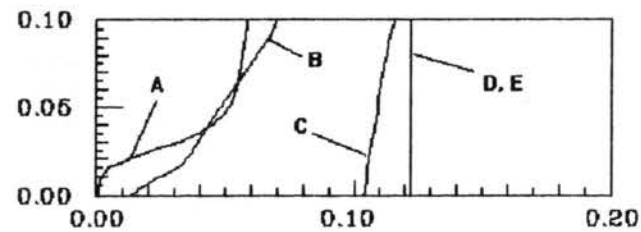
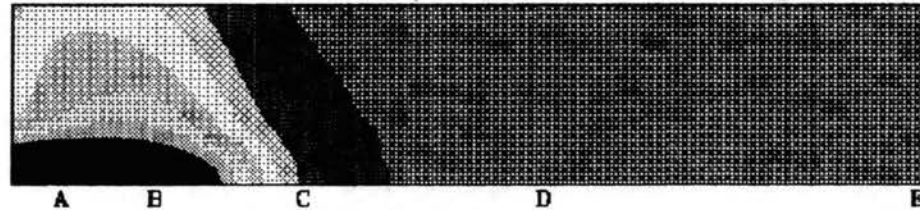


Figure 59. Water Vapor Mass Fraction Contour Map with Four-Step Scheme

MASS FRACTION OF CARBON DIOXIDE



Two-Step Scheme (CH₄/Air) L=1.524 m
 R1=0.008 m R2=0.0111 m R3=0.0286 m
 U_{air}=34.3 m/s U_{fu}=21.3 m/s
 T_{air}=589 deg K T_{fu}=300 deg K

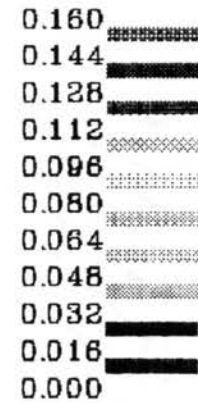
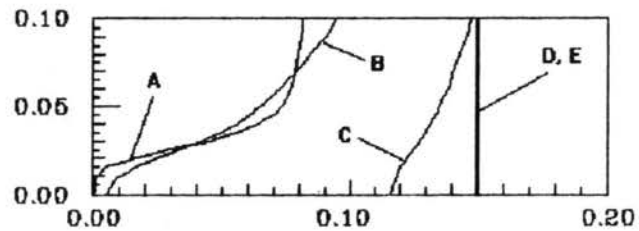
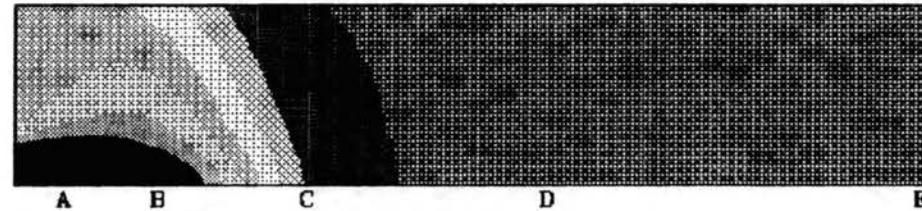


Figure 60. Carbon Dioxide Mass Fraction Contour Map with Two-Step Scheme

MASS FRACTION OF CARBON DIOXIDE



Four-Step Scheme (CH₄/Air) L=1.524 m
 R1=0.008 m R2=0.0111 m R3=0.0286 m
 U_{air}=34.3 m/s U_{fu}=21.3 m/s
 T_{air}=589 deg K T_{fu}=300 deg K

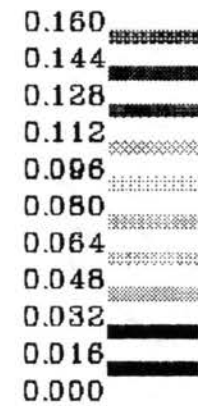
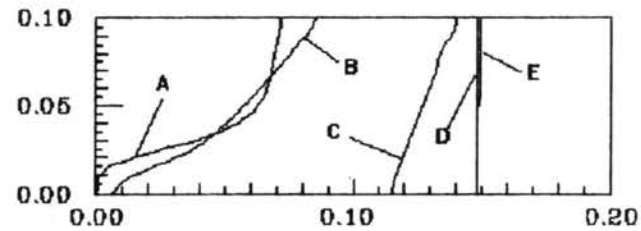


Figure 61. Carbon Dioxide Mass Fraction Contour Map with Four-Step Scheme

MASS FRACTION OF CARBON MONOXIDE



Two-Step Scheme (CH₄/Air) L=1.524 m
 R1=0.008 m R2=0.0111 m R3=0.0286 m
 U_{air}=34.3 m/s U_{fu}=21.3 m/s
 T_{air}=589 deg K T_{fu}=300 deg K

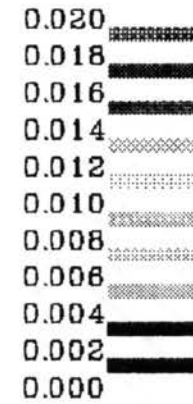
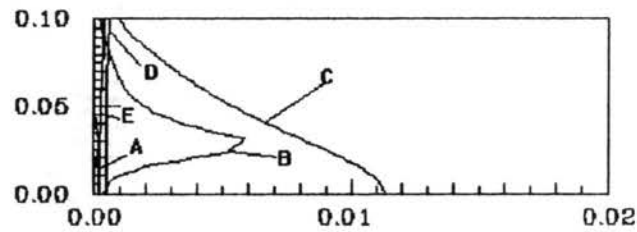
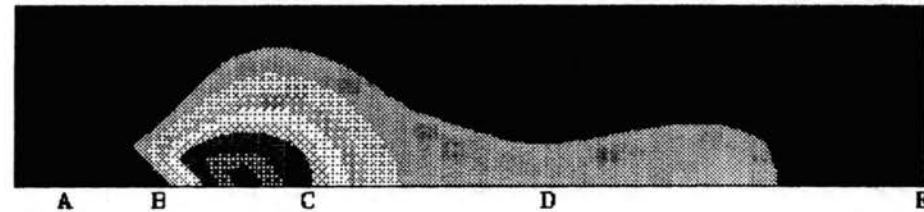


Figure 62. Carbon Monoxide Mass Fraction Contour Map with Two-Step Scheme

MASS FRACTION OF CARBON MONOXIDE



Four-Step Scheme (CH₄/Air) L=1.524 m
 R1=0.008 m R2=0.0111 m R3=0.0286 m
 U_{air}=34.3 m/s U_{fu}=21.3 m/s
 T_{air}=589 deg K T_{fu}=300 deg K

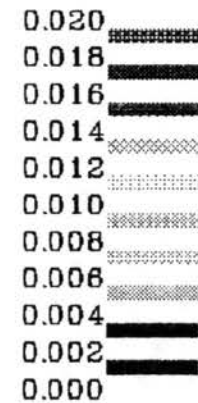
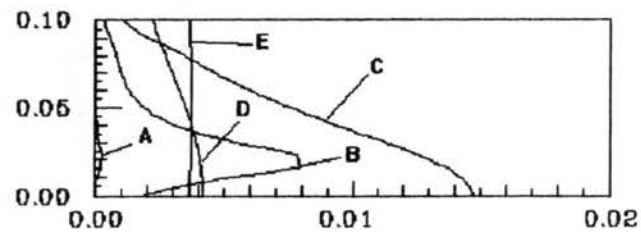


Figure 63. Carbon Monoxide Mass Fraction Contour Map with Four-Step Scheme

MASS FRACTION OF HYDROGEN

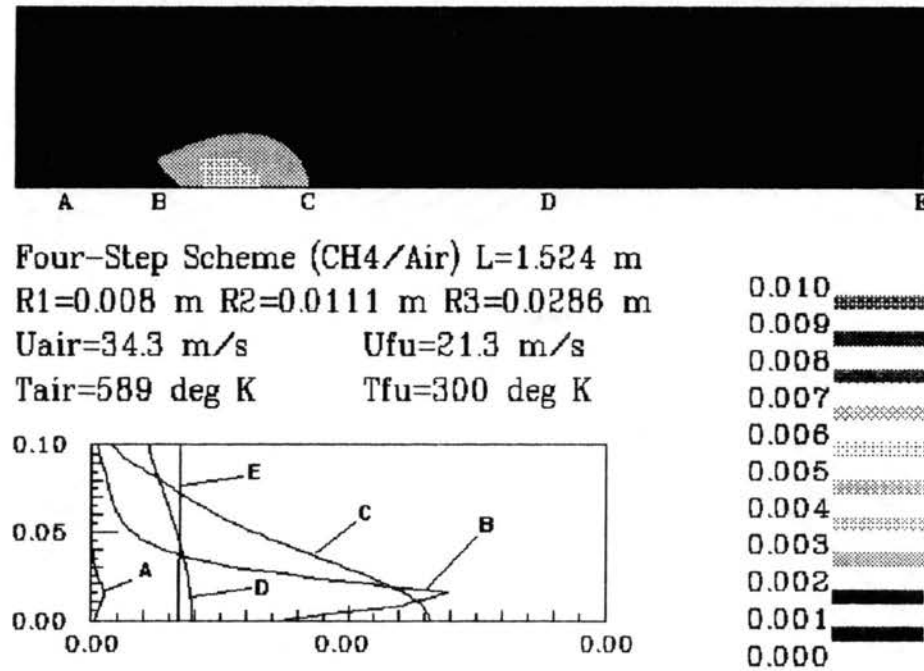


Figure 64. Hydrogen Mass Fraction Contour Map with Four-Step Scheme

APPENDIX C
TYPICAL INPUT AND OUTPUT

```

IMODEL = COMBUSTION SCHEME CONTROL CODE = ?
    0 = NO COMBUSTION - ISOTHERMAL FLOW
    1 = ONE-STEP SCHEME, THREE SPECIES
    2 = TWO-STEP SCHEME, SIX SPECIES
    4 = FOUR-STEP SCHEME, EIGHT SPECIES
1
IGCT = TOP INLET (AIR ONLY) GEOMETRY CODE = ?
    0 = NO TOP INLET
    1 = 1.0 INCH GAP
    2 = 1.6 INCH GAP
    3 = 2.1 INCH GAP
THESE GAP SIZES ARE ASSOCIATED WITH X-DIR GRID DESIGN
HERE THE GAP SIZES ARE FOR FINE GRID SYSTEM ONLY !!!!
(FOR COARSE GRID, YOU MAY GET DIFFERENT GAP SIZES)
0
PREMIXED FLAME ? (OTHERWISE DIFFUSION FLAME) Y/N
- PREMIXED FLAME -> ONE SIDE INLET ONLY - A
- DIFFUSION FLAME -> TWO SIDE INLETS, A AND B
N
WEST SIDE FLOWIN VELOCITIES (IN M/S): UIN, UINB = ?
22.3, 49.0
ENTER THE COMPOSITION OF THE HYDROCARBON FUEL - CxHy
---> X = ?, Y = ?
1, 4
ENTER THE FUEL MASS FRACTION FOR STREAM A = ?
1.0
ENTER THE TEMPERATURE OF STREAM A AT PRIMARY INLET ?
300.0
ENTER THE OXYGEN MASS FRACTION FOR STREAM B = ?
0.232
ENTER THE TEMPERATURE OF STREAM B AT PRIMARY INLET ?
589.0
SET HOT SPOTS ? Y/N
N
PRIMARY SWIRL ANGLE PSA = ? (IN DEGREES)
-FLAT SWIRL PROFILE IN STREAM A IF 1 SIDE INLET
-FLAT SWIRL PROFILE IN STREAM B ONLY IF 2 SIDE INLETS
0.0
PRIMARY CONTRACTION ANGLE PCA = ? (IN DEGREES)
-STREAM A IS CONTRACTING IF 1 SIDE INLET
-ONLY STREAM B IS CONTRACTING IF 2 SIDE INLETS
0.0
COARSE GRID IN X-DIRECTION ? (Y/N)
N
NUMBER OF ITERATIONS BETWEEN INTERMEDIATE PRINTOUT
601
MAXIMUM NUMBER OF ITERATIONS = ?
600
PRINT INITIAL FIELDS ? (Y/N)
Y
ENTER FILE NAME FOR PRINTOUT - R.OUT, CON, PRN, ETC...
MODEL1.OUT
ENTER FILE NAME FOR COLOR GRAPHICS - R.DAT, ETC...
MODEL1.DAT

```

REFINED

=====

REACTING ELLIPTIC FLOWS IN EXPANSION DOMAINS
VARIABLE DENSITY
TWO-EQUATION MODEL FOR TURBULENCE SIMULATION
ONE, TWO OR FOUR-STEP SCHEME FOR COMBUSTION SIMULATION
SECONDARY INLET - SWIRL - PRIMARY CONTRACTION
COPYRIGHT (c) 1994 BY
MINGCHUN DONG AND DAVID G. LILLEY
STILLWATER, OK 74074

Prim Swirl Angle = .0 deg, Prim Contraction Angle = .0 deg
Sec Swirl Angle = .0 deg, Top Wall Injection Angle = .0 deg
Annular Width = .0000 in

1 ITER <----- ABSOLUTE RESIDUAL SOURCE SUMS ----->						<----- FIELD VALUES AT MONITORING LOCATION (10, 5) ----->						
NO.	UMON	VMON	WMON	MASS	TKIN	FUEL	U	V	W	P	K	F
1	5.513E-01	3.076E-04	0.000E+00	2.768E+00	3.104E+02	7.664E-01	3.731E+00	1.086E-01	0.000E+00	-2.744E+02	9.023E+00	7.905E-01
100	2.094E+00	1.373E+00	0.000E+00	1.235E+00	2.281E-01	1.741E+00	3.091E+01	2.120E-01	0.000E+00	-8.323E+01	1.281E+02	3.449E-02
200	1.740E+00	1.749E+00	0.000E+00	1.099E+00	3.003E-01	5.452E-01	2.761E+01	-4.026E+00	0.000E+00	-2.477E+01	1.695E+02	1.227E-03
300	8.635E-01	1.018E+00	0.000E+00	7.093E-02	3.648E-01	1.992E-01	2.789E+01	1.279E+00	0.000E+00	2.171E+01	1.284E+02	9.849E-04
400	1.632E-01	1.262E-01	0.000E+00	7.597E-03	7.571E-02	5.419E-02	2.813E+01	1.532E+00	0.000E+00	1.207E+01	1.265E+02	1.458E-03
500	3.600E-02	1.948E-02	0.000E+00	2.212E-03	2.736E-02	2.455E-02	2.818E+01	1.512E+00	0.000E+00	1.207E+01	1.255E+02	1.441E-03
600	2.480E-02	4.990E-03	0.000E+00	5.286E-04	1.427E-02	1.726E-02	2.823E+01	1.504E+00	0.000E+00	1.209E+01	1.251E+02	1.431E-03

0	I =	25	26	27	28	29	30	31	32	33	34	35	36
	X =	.52819	.57110	.61657	.66478	.71588	.77005	.82746	.88832	.95283	1.02122	1.09370	1.17054
0 J	Y												
15	.10551	0.00E+00	0.00E+00	0.00E+00	0.00E+00	0.00E+00	0.00E+00	0.00E+00	0.00E+00	0.00E+00	0.00E+00	0.00E+00	0.00E+00
14	.09769	5.07E+00	5.74E+00	6.24E+00	6.57E+00	6.74E+00	6.78E+00	6.72E+00	6.60E+00	6.45E+00	6.29E+00	6.14E+00	5.99E+00
13	.08988	7.07E+00	7.82E+00	8.41E+00	8.85E+00	9.15E+00	9.34E+00	9.44E+00	9.46E+00	9.43E+00	9.36E+00	9.26E+00	9.15E+00
12	.08206	8.40E+00	9.08E+00	9.62E+00	1.00E+01	1.03E+01	1.06E+01	1.07E+01	1.08E+01	1.08E+01	1.09E+01	1.08E+01	1.08E+01
11	.07425	9.68E+00	1.02E+01	1.06E+01	1.10E+01	1.12E+01	1.14E+01	1.15E+01	1.16E+01	1.17E+01	1.18E+01	1.18E+01	1.18E+01
10	.06643	1.11E+01	1.14E+01	1.16E+01	1.18E+01	1.19E+01	1.20E+01	1.21E+01	1.22E+01	1.23E+01	1.24E+01	1.24E+01	1.25E+01
9	.05862	1.26E+01	1.26E+01	1.26E+01	1.26E+01	1.26E+01	1.26E+01	1.27E+01	1.27E+01	1.28E+01	1.28E+01	1.29E+01	1.30E+01
8	.05080	1.42E+01	1.40E+01	1.37E+01	1.34E+01	1.33E+01	1.32E+01	1.31E+01	1.31E+01	1.31E+01	1.32E+01	1.32E+01	1.33E+01
7	.04298	1.60E+01	1.53E+01	1.47E+01	1.42E+01	1.39E+01	1.36E+01	1.35E+01	1.34E+01	1.34E+01	1.35E+01	1.35E+01	1.36E+01
6	.03517	1.78E+01	1.67E+01	1.57E+01	1.50E+01	1.44E+01	1.41E+01	1.38E+01	1.37E+01	1.37E+01	1.37E+01	1.37E+01	1.38E+01
5	.02735	1.95E+01	1.79E+01	1.66E+01	1.56E+01	1.49E+01	1.44E+01	1.41E+01	1.39E+01	1.39E+01	1.39E+01	1.39E+01	1.40E+01
4	.01954	2.11E+01	1.90E+01	1.74E+01	1.62E+01	1.53E+01	1.47E+01	1.43E+01	1.41E+01	1.40E+01	1.40E+01	1.40E+01	1.41E+01
3	.01172	2.22E+01	1.98E+01	1.79E+01	1.66E+01	1.56E+01	1.49E+01	1.45E+01	1.42E+01	1.41E+01	1.41E+01	1.41E+01	1.42E+01
2	.00391	2.28E+01	2.02E+01	1.82E+01	1.68E+01	1.57E+01	1.50E+01	1.46E+01	1.43E+01	1.42E+01	1.41E+01	1.41E+01	1.42E+01
1	-.00391	0.00E+00	0.00E+00	0.00E+00	0.00E+00	0.00E+00	0.00E+00	0.00E+00	0.00E+00	0.00E+00	0.00E+00	0.00E+00	0.00E+00
0	I =	37	38	39	40								
	X =	1.25198	1.33831	1.42982	1.52400								
15	.10551	0.00E+00	0.00E+00	0.00E+00	0.00E+00								
14	.09769	5.87E+00	5.76E+00	5.67E+00	5.67E+00								
13	.08988	9.04E+00	8.93E+00	8.84E+00	8.84E+00								
12	.08206	1.07E+01	1.07E+01	1.06E+01	1.06E+01								
11	.07425	1.18E+01	1.18E+01	1.18E+01	1.18E+01								
10	.06643	1.25E+01	1.26E+01	1.26E+01	1.26E+01								
9	.05862	1.30E+01	1.31E+01	1.32E+01	1.32E+01								
8	.05080	1.34E+01	1.35E+01	1.36E+01	1.36E+01								
7	.04298	1.37E+01	1.38E+01	1.39E+01	1.39E+01								
6	.03517	1.39E+01	1.40E+01	1.41E+01	1.41E+01								
5	.02735	1.41E+01	1.42E+01	1.43E+01	1.43E+01								
4	.01954	1.42E+01	1.43E+01	1.44E+01	1.44E+01								
3	.01172	1.43E+01	1.44E+01	1.45E+01	1.45E+01								
2	.00391	1.43E+01	1.44E+01	1.45E+01	1.45E+01								
1	-.00391	0.00E+00	0.00E+00	0.00E+00	0.00E+00								

0	I =	25	26	27	28	29	30	31	32	33	34	35	36
	X =	.54902	.59317	.63998	.68959	.74217	.79792	.85701	.91964	.98603	1.05640	1.13100	1.21007
0 J	Y												
15		.10160	0.00E+00	0.00E+00	0.00E+00	0.00E+00	0.00E+00	0.00E+00	0.00E+00	0.00E+00	0.00E+00	0.00E+00	0.00E+00
14		.09378	1.30E-01	9.22E-02	5.79E-02	2.92E-02	7.72E-03	-6.60E-03	-1.47E-02	-1.81E-02	-1.84E-02	-1.69E-02	-1.47E-02
13		.08597	2.85E-01	2.09E-01	1.40E-01	8.29E-02	3.90E-02	8.15E-03	-1.16E-02	-2.26E-02	-2.75E-02	-2.84E-02	-2.68E-02
12		.07815	4.44E-01	3.29E-01	2.27E-01	1.42E-01	7.78E-02	3.18E-02	1.25E-03	-1.75E-02	-2.78E-02	-3.23E-02	-3.31E-02
11		.07034	5.96E-01	4.41E-01	3.08E-01	1.99E-01	1.16E-01	5.68E-02	1.71E-02	-8.09E-03	-2.30E-02	-3.10E-02	-3.42E-02
10		.06252	7.30E-01	5.38E-01	3.76E-01	2.46E-01	1.48E-01	7.89E-02	3.22E-02	2.18E-03	-1.62E-02	-2.68E-02	-3.21E-02
9		.05471	8.35E-01	6.11E-01	4.26E-01	2.80E-01	1.71E-01	9.54E-02	4.43E-02	1.13E-02	-9.26E-03	-2.15E-02	-2.81E-02
8		.04689	9.01E-01	6.52E-01	4.51E-01	2.97E-01	1.83E-01	1.05E-01	5.20E-02	1.81E-02	-3.24E-03	-1.61E-02	-2.35E-02
7		.03908	9.15E-01	6.54E-01	4.48E-01	2.94E-01	1.82E-01	1.06E-01	5.46E-02	2.18E-02	1.22E-03	-1.14E-02	-1.87E-02
6		.03126	8.65E-01	6.09E-01	4.14E-01	2.69E-01	1.67E-01	9.78E-02	5.19E-02	2.24E-02	3.89E-03	-7.49E-03	-1.43E-02
5		.02345	7.45E-01	5.16E-01	3.47E-01	2.25E-01	1.39E-01	8.19E-02	4.41E-02	2.00E-02	4.78E-03	-4.57E-03	-1.02E-02
4		.01563	5.51E-01	3.76E-01	2.50E-01	1.61E-01	1.00E-01	5.89E-02	3.20E-02	1.49E-02	4.13E-03	-2.50E-03	-6.49E-03
3		.00782	2.93E-01	1.98E-01	1.31E-01	8.43E-02	5.22E-02	3.08E-02	1.68E-02	7.95E-03	2.37E-03	-1.08E-03	-3.15E-03
2		.00000	0.00E+00	0.00E+00	0.00E+00	0.00E+00	0.00E+00	0.00E+00	0.00E+00	0.00E+00	0.00E+00	0.00E+00	0.00E+00
1		.00000	0.00E+00	0.00E+00	0.00E+00	0.00E+00	0.00E+00	0.00E+00	0.00E+00	0.00E+00	0.00E+00	0.00E+00	0.00E+00
0	I =	37	38	39	40								
	X =	1.29389	1.38274	1.47691	1.57109								
15		.10160	0.00E+00	0.00E+00	0.00E+00	0.00E+00							
14		.09378	-9.97E-03	-7.73E-03	1.63E-04	0.00E+00							
13		.08597	-2.06E-02	-1.64E-02	3.41E-04	0.00E+00							
12		.07815	-2.86E-02	-2.35E-02	5.02E-04	0.00E+00							
11		.07034	-3.26E-02	-2.76E-02	6.27E-04	0.00E+00							
10		.06252	-3.34E-02	-2.89E-02	7.09E-04	0.00E+00							
9		.05471	-3.17E-02	-2.79E-02	7.45E-04	0.00E+00							
8		.04689	-2.84E-02	-2.55E-02	7.36E-04	0.00E+00							
7		.03908	-2.43E-02	-2.20E-02	6.85E-04	0.00E+00							
6		.03126	-1.97E-02	-1.80E-02	5.97E-04	0.00E+00							
5		.02345	-1.48E-02	-1.36E-02	4.77E-04	0.00E+00							
4		.01563	-9.88E-03	-9.14E-03	3.32E-04	0.00E+00							
3		.00782	-4.94E-03	-4.58E-03	1.70E-04	0.00E+00							
2		.00000	0.00E+00	0.00E+00	0.00E+00	0.00E+00							
1		.00000	0.00E+00	0.00E+00	0.00E+00	0.00E+00							

0	I =	25	26	27	28	29	30	31	32	33	34	35	36
	X =	.54902	.59317	.63998	.68959	.74217	.79792	.85701	.91964	.98603	1.05640	1.13100	1.21007
0 J	Y												
15	.10551	0.00E+00	0.00E+00	0.00E+00	0.00E+00	0.00E+00	0.00E+00	0.00E+00	0.00E+00	0.00E+00	0.00E+00	0.00E+00	0.00E+00
14	.09769	2.62E+03	2.61E+03	2.60E+03	2.60E+03	2.59E+03	2.59E+03	2.58E+03	2.58E+03	2.57E+03	2.57E+03	2.57E+03	2.56E+03
13	.08988	2.61E+03	2.61E+03	2.60E+03	2.59E+03	2.59E+03	2.58E+03	2.58E+03	2.57E+03	2.57E+03	2.57E+03	2.56E+03	2.56E+03
12	.08206	2.60E+03	2.60E+03	2.59E+03	2.59E+03	2.58E+03	2.58E+03	2.57E+03	2.57E+03	2.57E+03	2.56E+03	2.56E+03	2.56E+03
11	.07425	2.60E+03	2.59E+03	2.59E+03	2.58E+03	2.58E+03	2.58E+03	2.57E+03	2.57E+03	2.57E+03	2.56E+03	2.56E+03	2.56E+03
10	.06643	2.59E+03	2.58E+03	2.58E+03	2.58E+03	2.58E+03	2.57E+03	2.57E+03	2.57E+03	2.56E+03	2.56E+03	2.56E+03	2.56E+03
9	.05862	2.57E+03	2.58E+03	2.58E+03	2.58E+03	2.57E+03	2.57E+03	2.57E+03	2.56E+03	2.56E+03	2.56E+03	2.56E+03	2.55E+03
8	.05080	2.56E+03	2.57E+03	2.57E+03	2.57E+03	2.57E+03	2.57E+03	2.57E+03	2.56E+03	2.56E+03	2.56E+03	2.56E+03	2.55E+03
7	.04298	2.54E+03	2.56E+03	2.56E+03	2.57E+03	2.57E+03	2.57E+03	2.56E+03	2.56E+03	2.56E+03	2.56E+03	2.55E+03	2.55E+03
6	.03517	2.52E+03	2.54E+03	2.56E+03	2.56E+03	2.56E+03	2.56E+03	2.56E+03	2.56E+03	2.56E+03	2.55E+03	2.55E+03	2.55E+03
5	.02735	2.50E+03	2.53E+03	2.55E+03	2.56E+03	2.56E+03	2.56E+03	2.56E+03	2.56E+03	2.56E+03	2.55E+03	2.55E+03	2.55E+03
4	.01954	2.48E+03	2.52E+03	2.54E+03	2.55E+03	2.56E+03	2.56E+03	2.56E+03	2.56E+03	2.56E+03	2.55E+03	2.55E+03	2.55E+03
3	.01172	2.46E+03	2.51E+03	2.54E+03	2.55E+03	2.56E+03	2.56E+03	2.56E+03	2.56E+03	2.55E+03	2.55E+03	2.55E+03	2.55E+03
2	.00391	2.45E+03	2.51E+03	2.54E+03	2.55E+03	2.56E+03	2.56E+03	2.56E+03	2.56E+03	2.55E+03	2.55E+03	2.55E+03	2.55E+03
1	-.00391	0.00E+00	0.00E+00	0.00E+00	0.00E+00	0.00E+00	0.00E+00	0.00E+00	0.00E+00	0.00E+00	0.00E+00	0.00E+00	0.00E+00
0	I =	37	38	39	40								
	X =	1.29389	1.38274	1.47691	1.57109								
15	.10551	0.00E+00	0.00E+00	0.00E+00	0.00E+00								
14	.09769	2.56E+03	2.56E+03	2.56E+03	2.56E+03								
13	.08988	2.56E+03	2.56E+03	2.56E+03	2.56E+03								
12	.08206	2.56E+03	2.56E+03	2.56E+03	2.56E+03								
11	.07425	2.56E+03	2.56E+03	2.55E+03	2.55E+03								
10	.06643	2.55E+03	2.55E+03	2.55E+03	2.55E+03								
9	.05862	2.55E+03	2.55E+03	2.55E+03	2.55E+03								
8	.05080	2.55E+03	2.55E+03	2.55E+03	2.55E+03								
7	.04298	2.55E+03	2.55E+03	2.55E+03	2.55E+03								
6	.03517	2.55E+03	2.55E+03	2.55E+03	2.55E+03								
5	.02735	2.55E+03	2.55E+03	2.55E+03	2.55E+03								
4	.01954	2.55E+03	2.55E+03	2.55E+03	2.55E+03								
3	.01172	2.55E+03	2.55E+03	2.55E+03	2.55E+03								
2	.00391	2.55E+03	2.55E+03	2.55E+03	2.55E+03								
1	-.00391	0.00E+00	0.00E+00	0.00E+00	0.00E+00								

0	I =	25	26	27	28	29	30	31	32	33	34	35	36
	X =	.54902	.59317	.63998	.68959	.74217	.79792	.85701	.91964	.98603	1.05640	1.13100	1.21007
0 J	Y												
15	.10551	0.00E+00	0.00E+00	0.00E+00	0.00E+00	0.00E+00	0.00E+00	0.00E+00	0.00E+00	0.00E+00	0.00E+00	0.00E+00	0.00E+00
14	.09769	2.45E-03	3.89E-03	5.08E-03	6.08E-03	6.94E-03	7.71E-03	8.41E-03	9.06E-03	9.69E-03	1.03E-02	1.08E-02	1.14E-02
13	.08988	3.19E-03	4.54E-03	5.67E-03	6.61E-03	7.42E-03	8.14E-03	8.80E-03	9.42E-03	1.00E-02	1.06E-02	1.11E-02	1.16E-02
12	.08206	3.90E-03	5.18E-03	6.23E-03	7.12E-03	7.88E-03	8.58E-03	9.22E-03	9.82E-03	1.04E-02	1.09E-02	1.14E-02	1.19E-02
11	.07425	4.70E-03	5.86E-03	6.81E-03	7.61E-03	8.33E-03	8.98E-03	9.60E-03	1.02E-02	1.07E-02	1.13E-02	1.17E-02	1.22E-02
10	.06643	5.63E-03	6.62E-03	7.42E-03	8.11E-03	8.75E-03	9.36E-03	9.95E-03	1.05E-02	1.11E-02	1.16E-02	1.20E-02	1.24E-02
9	.05862	6.75E-03	7.48E-03	8.07E-03	8.62E-03	9.17E-03	9.72E-03	1.03E-02	1.08E-02	1.14E-02	1.18E-02	1.23E-02	1.27E-02
8	.05080	8.09E-03	8.45E-03	8.77E-03	9.14E-03	9.57E-03	1.00E-02	1.06E-02	1.11E-02	1.16E-02	1.21E-02	1.25E-02	1.29E-02
7	.04298	9.64E-03	9.52E-03	9.50E-03	9.65E-03	9.95E-03	1.04E-02	1.08E-02	1.13E-02	1.18E-02	1.23E-02	1.27E-02	1.31E-02
6	.03517	1.14E-02	1.06E-02	1.02E-02	1.01E-02	1.03E-02	1.06E-02	1.11E-02	1.15E-02	1.20E-02	1.25E-02	1.29E-02	1.32E-02
5	.02735	1.32E-02	1.18E-02	1.09E-02	1.06E-02	1.06E-02	1.09E-02	1.12E-02	1.17E-02	1.22E-02	1.26E-02	1.30E-02	1.33E-02
4	.01954	1.50E-02	1.28E-02	1.15E-02	1.10E-02	1.09E-02	1.10E-02	1.14E-02	1.18E-02	1.23E-02	1.27E-02	1.31E-02	1.34E-02
3	.01172	1.65E-02	1.36E-02	1.20E-02	1.12E-02	1.10E-02	1.12E-02	1.15E-02	1.19E-02	1.24E-02	1.28E-02	1.32E-02	1.35E-02
2	.00391	1.73E-02	1.40E-02	1.22E-02	1.14E-02	1.11E-02	1.12E-02	1.15E-02	1.19E-02	1.24E-02	1.28E-02	1.32E-02	1.35E-02
1	-.00391	0.00E+00	0.00E+00	0.00E+00	0.00E+00	0.00E+00	0.00E+00	0.00E+00	0.00E+00	0.00E+00	0.00E+00	0.00E+00	0.00E+00
0	I =	37	38	39	40								
	X =	1.29389	1.38274	1.47691	1.57109								
15	.10551	0.00E+00	0.00E+00	0.00E+00	0.00E+00								
14	.09769	1.19E-02	1.23E-02	1.27E-02	1.27E-02								
13	.08988	1.21E-02	1.25E-02	1.28E-02	1.28E-02								
12	.08206	1.23E-02	1.27E-02	1.30E-02	1.30E-02								
11	.07425	1.26E-02	1.29E-02	1.32E-02	1.32E-02								
10	.06643	1.28E-02	1.31E-02	1.33E-02	1.33E-02								
9	.05862	1.30E-02	1.33E-02	1.35E-02	1.35E-02								
8	.05080	1.32E-02	1.34E-02	1.36E-02	1.36E-02								
7	.04298	1.34E-02	1.36E-02	1.37E-02	1.37E-02								
6	.03517	1.35E-02	1.37E-02	1.38E-02	1.38E-02								
5	.02735	1.36E-02	1.37E-02	1.38E-02	1.38E-02								
4	.01954	1.37E-02	1.38E-02	1.39E-02	1.39E-02								
3	.01172	1.37E-02	1.38E-02	1.39E-02	1.39E-02								
2	.00391	1.37E-02	1.39E-02	1.39E-02	1.39E-02								
1	-.00391	0.00E+00	0.00E+00	0.00E+00	0.00E+00								

0	I =	25	26	27	28	29	30	31	32	33	34	35	36
	X =	.54902	.59317	.63998	.68959	.74217	.79792	.85701	.91964	.98603	1.05640	1.13100	1.21007
0 J	Y												
15	.10551	0.00E+00	0.00E+00	0.00E+00	0.00E+00	0.00E+00	0.00E+00	0.00E+00	0.00E+00	0.00E+00	0.00E+00	0.00E+00	0.00E+00
14	.09769	1.38E-04	5.00E-05	2.18E-05	9.91E-06	4.49E-06	2.00E-06	8.79E-07	3.84E-07	1.68E-07	6.71E-08	2.98E-08	7.45E-09
13	.08988	5.84E-04	2.58E-04	1.25E-04	6.16E-05	3.02E-05	1.45E-05	6.85E-06	3.16E-06	1.44E-06	6.56E-07	2.91E-07	1.23E-07
12	.08206	9.17E-04	4.45E-04	2.29E-04	1.20E-04	6.25E-05	3.21E-05	1.62E-05	8.06E-06	3.95E-06	1.90E-06	9.13E-07	4.28E-07
11	.07425	1.23E-03	6.33E-04	3.37E-04	1.81E-04	9.69E-05	5.13E-05	2.69E-05	1.39E-05	7.13E-06	3.61E-06	1.82E-06	8.94E-07
10	.06643	1.57E-03	8.37E-04	4.54E-04	2.47E-04	1.33E-04	7.14E-05	3.80E-05	2.01E-05	1.06E-05	5.51E-06	2.87E-06	1.47E-06
9	.05862	1.97E-03	1.07E-03	5.85E-04	3.18E-04	1.71E-04	9.21E-05	4.93E-05	2.63E-05	1.40E-05	7.46E-06	3.96E-06	2.07E-06
8	.05080	2.45E-03	1.35E-03	7.33E-04	3.95E-04	2.12E-04	1.13E-04	6.06E-05	3.24E-05	1.74E-05	9.34E-06	5.02E-06	2.67E-06
7	.04298	3.05E-03	1.67E-03	8.98E-04	4.78E-04	2.53E-04	1.34E-04	7.15E-05	3.82E-05	2.06E-05	1.11E-05	6.01E-06	3.24E-06
6	.03517	3.78E-03	2.04E-03	1.08E-03	5.63E-04	2.94E-04	1.54E-04	8.16E-05	4.35E-05	2.34E-05	1.27E-05	6.89E-06	3.75E-06
5	.02735	4.64E-03	2.44E-03	1.26E-03	6.47E-04	3.33E-04	1.73E-04	9.07E-05	4.82E-05	2.59E-05	1.40E-05	7.64E-06	4.18E-06
4	.01954	5.55E-03	2.84E-03	1.43E-03	7.21E-04	3.66E-04	1.88E-04	9.80E-05	5.19E-05	2.78E-05	1.51E-05	8.23E-06	4.52E-06
3	.01172	6.37E-03	3.17E-03	1.57E-03	7.78E-04	3.90E-04	1.99E-04	1.03E-04	5.45E-05	2.91E-05	1.58E-05	8.61E-06	4.75E-06
2	.00391	6.87E-03	3.37E-03	1.64E-03	8.08E-04	4.03E-04	2.05E-04	1.06E-04	5.58E-05	2.98E-05	1.62E-05	8.82E-06	4.86E-06
1	-.00391	0.00E+00	0.00E+00	0.00E+00	0.00E+00	0.00E+00	0.00E+00	0.00E+00	0.00E+00	0.00E+00	0.00E+00	0.00E+00	0.00E+00
0	I =	37	38	39	40								
	X =	1.29389	1.38274	1.47691	1.57109								
15	.10551	0.00E+00	0.00E+00	0.00E+00	0.00E+00								
14	.09769	7.45E-09	1.12E-08	3.73E-09	3.73E-09								
13	.08988	5.22E-08	2.61E-08	1.49E-08	1.49E-08								
12	.08206	2.05E-07	9.69E-08	4.84E-08	4.84E-08								
11	.07425	4.47E-07	2.20E-07	1.04E-07	1.04E-07								
10	.06643	7.49E-07	3.91E-07	1.90E-07	1.90E-07								
9	.05862	1.08E-06	5.74E-07	2.98E-07	2.98E-07								
8	.05080	1.42E-06	7.60E-07	4.02E-07	4.02E-07								
7	.04298	1.75E-06	9.50E-07	5.14E-07	5.14E-07								
6	.03517	2.04E-06	1.11E-06	6.11E-07	6.11E-07								
5	.02735	2.28E-06	1.26E-06	6.93E-07	6.93E-07								
4	.01954	2.49E-06	1.36E-06	7.53E-07	7.53E-07								
3	.01172	2.62E-06	1.43E-06	7.93E-07	7.93E-07								
2	.00391	2.67E-06	1.47E-06	8.16E-07	8.16E-07								
1	-.00391	0.00E+00	0.00E+00	0.00E+00	0.00E+00								

VITA

Mingchun Dong

Candidate for the Degree of

Doctor of Philosophy

Thesis: PREDICTION OF TURBULENT SWIRLING REACTING FLOWS

Major Field: Mechanical Engineering

Biographical:

Personal Data: Born in Harbin, P. R. China, On May 9, 1963, the son of Mr. Guimin Dong and Mrs. Fengyun Xu.

Education: Graduated from the High School of Harbin Teacher's University, Harbin, P. R. China, in July, 1980; received the Bachelor of Science degree in Power Department of Harbin Institute of Technology, Harbin, P. R. China, in July, 1984; received the Master of Science degree in the School of Mechanical and Aerospace Engineering from Oklahoma State University, Stillwater, Oklahoma, in July, 1989; completed the requirements for the Doctor of Philosophy degree with a major in Mechanical and Aerospace Engineering at Oklahoma State University, in July 1994.

Professional Experience: Employed as a lecturer in the Department of Agricultural Engineering, Northeast Agricultural College, Harbin, P. R. China, from July 1984 to July 1987; employed as a graduate research and teaching assistant in the School of Mechanical and Aerospace Engineering, Oklahoma State University, from August 1989 to July 1994.

Professional Memberships: The American Society of Mechanical Engineers.